Ultra high energy muons in extensive air showers

Pickersgill, D. R.

ULTRA HIGH ENERGY MUONS IN EXTENSIVE AIR SHOWERS

by

D. R. Pickersgill, B.Sc.

A Thesis submitted to the University of Durham in accordance with the Regulations for admittance to the Degree of Doctor of Philosophy

Department of Physics
University of Durham.

January, 1973

ABSTRACT

The design of the modification required to increase the angular resolution of the Haverah Park Magnet Spectrograph is described. It is shown that the reduction in uncertainty of angular measurement achieved by the modification is characterised by a standard deviation of 0.16°, corresponding to a limit of momentum resolution of 120 GeV/c.

The momentum spectra of muons in EAS derived from the data available at the conclusion of the period of operation of the original spectrograph are presented. These spectra relate to muons falling between 150 m and 600 m from the cores of showers of primary energy within the approximate range 10^{16} eV to 10^{18} eV. The preliminary results from the modified spectrograph are also presented but they are shown to be statistically insufficient to be considered as evidence, for or against, the validity of the earlier data.

An investigation of the dependence of the momentum spectra on primary energy and shower zenith angle, originally undertaken using data available prior to the end of the period of operation of the original spectrograph, has been repeated in the light of the improved statistics and revised EAS data. In addition, other checks have been undertaken: (a) on the effect of the accuracy of core location on the momentum spectra, and (b) on the method of deriving the spectra from the data.

The data available at the conclusion of the original experiment have also been used, in conjunction with a new theoretical study of the distortion of the muon charge ratio produced by the geomagnetic field, to estimate the height of origin of muons in EAS. It is shown that measurement of this distortion cannot be used to give sufficiently accurate assessment of the height of muon production, to allow comment to be made on the nature of the primary particle or the ultra high energy interactions.

Finally, an improved analytical model of EAS is described and the results are compared with those of other workers and observation.

PREFACE

In this thesis an account is given of the work done by the author, both in Durham and at Haverah Park, during the period October 1968 to August 1971 whilst under the supervision of Dr. K. E. Turver.

At Haverah Park, Extensive Air Showers having primary energies in the range 10^{16} eV to 10^{19} eV are detected by means of arrays of water Cerenkov detectors. These array systems are operated by workers from the University of Leeds.

A modified version of the magnet spectrograph, originally designed and built by Professor G. D. Rochester and Dr. K. E. Turver in 1964, was completed in November 1969. Dr. K. E. Turver, Mr. A. C. Machin and the author were responsible for the design and construction of this modified instrument.

The routine operation of the spectrograph and the treatment of the data has been the joint responsibility of the author and his colleagues. The mechanical design of the modified spectrograph, described in Chapter 2, has been the sole responsibility of the author together with the derivation of the method of calculating the deflection of muons in the geomagnetic field, as described in Chapter 5. The work described in Chapter 6 is a continuation of that begun by Dr. K. J. Orford.

Work in which the author has been involved has been reported in the following publications: Machin et al., (1969), and Earnshaw et al., (1971a and 1971b).

Contents

Page

Page

Chapter 1

Introduction

1.1 The Cosmic Radiation

Variations with height in the electrical conductivity of the atmosphere, first noted at the beginning of the twentieth century, were explained by supposing that a highly penetrating radiation entered the atmosphere from outer space. Progress in the study of this radiation accelerated rapidly with the development of the Geiger Müller counter and the Wilson cloud chamber. In the cloud chamber cascade showers were discovered by Anderson in 1932, and shortly afterwards both positive and negative electrons were observed in such showers. This latter discovery led to the explanation of these showers in terms of two main processes: bremsstrahlung and pair-production. An anomoly arose from this explanation, however, in that the proportionality of bremsstrahlung to the inverse square of the mass of the accelerating particle implied that the penetrating component of these showers should consist of particles much heavier than the electron although the manner in which the component was absorbed ruled out the proton as a candidate. The anomoly was not resolved until 1937, when the muon was discovered.

The weak interaction of the muon with matter distinguished it from the particle predicted by Yukawa in 1935 to account for the nuclear binding force. This particle, the pion, was eventually discovered using the nuclear emulsion techniques. It was shown to be created in the high energy collisions of the primary radiation near the top of the atmosphere and to decay into a muon in flight.

Although our knowledge of elementary particles has expanded rapidly with the development of accelerator technology, the increasing complexity in the particles and resonances so far discovered demand experimental investigation at higher energies if a more complete picture is to be revealed. The highest energies involved in the collisions of the primary cosmic radiation with air nuclei far exceed those which it will be possible to achieve in the

forseeable future with accelerators. Whilst the study of these collisions is thus of importance to high energy nuclear physics it is also very relevant to astrophysics since the energy and nature of the primary particles may provide information as to their origin. The direct observation of such events is impracticable on a statistically adequate scale because of their low frequency of occurrence but information may be obtained from a study of extensive air showers, (EAS), since these are produced as the result of an interaction of a primary particle with an air nucleus and can extend over a very large area at sea level. The investigation of the properties of EAS and the clarification of the relationship between their characteristics at the level of observation and the elementary act of initiation is thus of great importance.

Because of their inert character, muons, especially those of high energy, are of potential interest in that they carry information directly from all points in the shower. Their heights of origin thus reflect the longitudinal development of the shower. Studies of this particular aspect are reported in this thesis.

The momentum spectrum of those high energy muons which originate in the early interactions of the shower may be expected to be sensitive to characteristics of the nuclear processes such as inelasticity, transverse momentum and to the mass composition of the primary particles.

1.2 Previous muon momentum spectra measurements

Orford (1968) gives a comprehensive survey of the work done by Barratt (1952), Dovzhenko (1957), Oda (1957),Bennett and Greisen (1961), Khrenov (1962), de Beer et al., (1962), and Barnavelli (1964). It is pointed out that the results obtained by these authors, with the exception of those of de Beer et al., who quote steeper spectra particularly at larger core distances, are confirmed by measurements using the Haverah Park Magnet Spectrograph. The burst spectra

reported by Orford also offer some confirmation of the momentum spectra obtained directly using the magnet spectrograph.

Recently Suga et al., (1969) have given details of measurements of the spectrum of burstsproduced in the scintillator shielding of the BASJE air shower array muon detector by muons in 1600 showers of sizes larger than 5×10^7 particles and in 50 showers larger than 5×10^8 particles. The spectrum obtained leads to a value for the slope of the integral energy spectrum from 20 GeV to 300 GeV of -2.2 ± 0.2 at a distance of 100 m and at an altitude of 5300 m. This is in substantial agreement with the results obtained with the Haverah Park spectrograph at the corresponding core distance at sea level.

1.3 High energy interactions

1.3.1 Theoretical considerations

There are gross features of high energy nuclear interactions which may be described in terms of a system with associated input and output parameters even though the processes themselves are not fully understood. By investigation of the properties of EAS it is hoped to learn more about these parameters, in particular the following:

(a) The multiplicity, that is the number of secondary particles produced in an interaction.

(b) The inelasticity, defined as the fraction of the energy of the incident particle which is radiated in the form of mesons.

(c) The mean transverse momentum of the produced mesons.

(d) The interaction mean free path for protons and pions.

1.3.2 Information from EAS

The multiplicity of the nucleon-nucleus collision is generally accepted to be related to the primary energy in a manner intermediate between the relationship predicted by a multiperipheral model, similar to that proposed by Amati et

al., (1962) and that predicted by kinematic considerations assuming that the energy radiated in the form of mesons is independent of the primary energy in the centre of mass system. Feinberg and Ivanenko (1969) have pointed out that the height of shower maximum is especially sensitive to the form of the multiplicity law used. No convincing conclusions have been reported on this problem however.

Winn et al., (1965), obtained a mean value of 0.54 for the inelasticity of nucleon-air nucleus collisions although the parameter is subject to large fluctuations. For collisions of pions with air nuclei the inelasticity appears close to unity (Azimov et al., (1964)).

The results of several experiments prior to 1961 designed to determine the value of the mean transverse momentum have been summarised by Earnshaw (1968). Since that time there have been further reports of results for the electron distribution in multicore air shower studies yielding rather large values of mean transverse momentum: Matano et al., (1967), Bakich et al., (1967) and Miyake et al., (1967). Partly on the basis of his own group's work and also by considering the frequency of events such as those observed by the above workers, Trümper suggests that there is no reason to suppose that the distribution of transverse momentum changes dramatically beyond 5 GeV/c (Böhm et al., (1967), Trümper (1969)). Present evidence from cosmic ray experiments suggests that at low energies the value of mean transverse momentum is about 0.4 GeV/c rising to approximately 0.5 GeV/c at 10^5 GeV (Kazuno (1967)). Experiments at accelerator energies indicate a constant value for the mean transverse momentum.

By comparison with many of the other quantities discussed, the mean free path for nuclear interaction of protons in air is accurately known and appears to be nearly independent of energy. For cosmic ray energies Matano et al., (1963) give a value of 80 ± 5 gm cm^{-2} and this value is supported by measurements at the highest energies available from accelerators.

1.4 Information on origin and nature of cosmic ray primaries from EAS

From a consideration of the number spectrum of air showers up to a primary energy of 10^{15} eV the constancy of the gradient indicates that the primary composition is unchanged. The observed steepening of the spectrum beyond this energy has been explained by Peters as due to the onset of a rigidity-cut-off for cosmic rays originating in our galaxy. A consequence of this explanation is that there should be an enhancement of the proportion of heavy primaries at energies above 10^{15} eV assuming that heavy primaries exist at any EAS energies. Evidence for a mixed composition at an energy of 10^{15} eV, which becomes progressively richer in heavier elements in the energy interval 3×10^{15} eV to 10^{17} eV, is, in fact, claimed by McCusker et al., (1969) from an analysis of the electron and hadron distribution in shower cores and the altitude dependence of the density spectrum. From an analysis of fluctuations of hadron energy flow at an energy of 10^{15} eV and of Cerenkov light emission at an energy of 10^{16} eV, the BASJE - MIT group find evidence for a mixed composition at both energies, (Rappaport (1969), Krieger (1969)). On the basis of a study of fluctuations in electron "size" at fixed muon "size" Vernov et al., (1969) suggest a constant chemical composition with a significant number of protons between energies 3×10^{15} eV and 2×10^{17} eV. Beyond 10^{17} eV, a study by Suga (1969) of fluctuations in muon content yields no evidence for other than a pure proton composition and Thompson et al., (1969), after analysing muon densities in inclined showers, conclude that there is little evidence for a modulated composition. Discrepancies between the momentum spectra of EAS muons obtained from the Haverah Park MkI spectrograph and predicted spectra for primary energies above 10^{17} eV have been interpreted as evidence for primary particles of mass greater than ten.

At the Budapest Conference the evidence for a change of slope of the primary intensity spectrum from about $-2{\cdot}2$ to $-1{\cdot}6$ at 10^{18} eV first reported

by Linsley, and interpreted as indicating the region in which particles of galactic origin can no longer be contained regardless of their charge, was apparently reinforced by Andrews et al., (1969(a)), Brownlee et al., (1969) and Hara et al., (1969). Recently, however, Andrews et al., (1971) have obtained results which indicate that the slope remains constant at - 2.3 up to an energy of 2×10^{19} eV. Beyond this the data are limited and allow no further conclusion. However, that any showers of primary energy above 10^{19} eV are reported by these authors is of interest in view of the proposed interaction of the primaries with the Universal 3 K black body radiation, (Greisen (1966)).

Turning finally to consideration of possible anisotropies in the arrival directions of very high energy primaries, Brownlee et al., (1969(b)) find no deviations from isotropy for 600 showers with energy greater than 10^{18} eV and 50 showers with energy greater than 10^{19} eV. From these results the authors conclude that pulsars cannot be the main cosmic ray accelerators in the energy region 10^{17} eV to 10^{18} eV. Recent work at Haverah Park by Lapikens et al., (1971) confirms earlier work by Andrews et al., (1969(a)) showing no significant anisotropy at energies up to 10^{18} eV.

1.5 Theories of the origin of cosmic radiation

The arguments in favour of supernovae within our own galaxy being the most likely sources of cosmic radiation on energetic grounds alone have been summarised by Shapiro (1962) and Ginzburg and Syrovatski (1964). In addition, Colgate (1966) suggests that supernovae should provide an acceleration mechanism to give an abundance of elements, up to iron, similar to that observed in cosmic radiation. (Beyond iron it is possible that the synthesis of heavier elements could occur through neutron capture). However, if pulsars are rapidly rotating neutron stars, as proposed by Gold (1968,1969),Ostriker and Gunn (1969) suggest that these could also provide an adequate acceleration mechanism whereby very high energy cosmic rays might be obtained. In this context it is interesting to note that calculations by Rosen (1969)

show that the final composition of the radiation emitted from a neutron star should be predominant in iron, and that the distribution in mass of the cosmic radiation should be quite different from the universal abundance.

Parker (1969) has shown that the universal model of Burbidge (1965), which postulates an intensity of radiation and density of sources in intergalactic space similar to that in galactic space, requires the energy emitted in the form of relativistic particles to be one thousand times as great as that emitted in the form of electromagnetic radiation. Since this is unlikely, a galactic model is favoured. Such a model is also favoured by Schmidt (1967). His calculations indicate that for the universe to be filled with radiation, ten per cent of the rest mass of the radiogalaxies would have to be converted into relativistic particles, which he considers improbable. By consideration of the measured ratio of electrons to protons in the galaxy and the X-ray background, Felton and Morrison (1966) conclude that at least the electronic component of the radiation must have a galactic origin. A galactic origin for cosmic rays, and their co-rotation with the solar system about the galactic centre were also deduced by Peters (1970) from considerations of the upper limit on anisotropy of directions of arrival. For the highest energy region ($> 10^{17}$ eV), however, this argument may be used to infer that since the galactic magnetic fields are thought to be unable to contain these particles they should exhibit more anisotropy than is observed. It is thus suggested that cosmic ray particles of energy 10^{17} eV and above may be extragalactic in origin. Beyond 10^{20} eV, however, it has been postulated by Greisen (1966), that the $p - \gamma$ interaction of the primaries with the photons of the universal 3K black body radiation should effectively cut off any extragalactic contribution to the primary flux.

Chapter 2

The Haverah Park Spectrograph

2.1 Introduction

2.1.1 General

The general design consideration and constructional details of the Haverah Park Magnet Spectrograph have been dealt with elsewhere, Earnshaw et al., (1967). A resumé of these and a description of the basic apparatus, which has remained unchanged throughout the recent modification programme, is given in this introduction. The modification reported here concerns the improvements to the spectrograph's flash tube array necessary to increase the momentum resolution to beyond 150 GeV/c, so that the original results from the spectrograph might be investigated with greater accuracy. These results indicated more high momentum muons at large distances from the core than was expected from then accepted theoretical models.

Section 2.2.1 is concerned with the principles and considerations governing the redesigning of the instrument, whilst section 2.2.2 describes some problems arising in the use of flash tubes as track delineators, and Section 2.2.3 describes the mechanical design of the modified spectrograph. In Section 2.2.4 the accuracy of location of the flash tube array is discussed, and the high voltage pulsing system used is described in section 2.2.5. Finally, certain aspects of the Haverah Park EAS array which relate to the accuracy of location of shower cores, are discussed in Section 2.3.

2.1.2 Resumé of the details of the original instrument

The original Haverah Park spectrograph, constructed in 1964, and referred to hereafter as the Mk1 spectrograph, had a momentum resolution of 60 GeV/c. This was achieved using a solid iron magnet having an induction of 1·46 Wb m^{-2} and neon flash tubes of internal diameter 1·6 cm

filled to a pressure of 600 mm Hg as track delineators. In each arm of the spectrograph there were arranged 7 layers of 2 m long flash tubes at the extremity of the arm, and 7 layers of 1·2 m long tubes nearest the magnet. 60% of the flash tubes were located in accurately machined mountings and were measured to an accuracy of ± 0·2 mm. The remaining 40% rested on top of the accurately located tubes so that knowledge of their position was marginally less precise.

2.1.3 The magnet

This is of the "Picture Frame" type and has been fully described by Walton (1966). Measurements made by Walton (1966) indicate that a current of 13·5 A produces an induction of 1·46 ± 0·06 Wb m^{-2} in the useful regions of the magnet. Recent measurements made by the author using (i) a fluxmeter directly, and (ii) an X - Y plotter to measure the value of the "instantaneous voltage" - "time" integral, and hence the flux of induction, N, using the relationship $\int dN = \int e dt$, have confirmed this value.

2.2 Development of the Mk2 Spectrograph

2.2.1 Design considerations

For the Haverah Park Magnet spectrograph the r.m.s. value of the total angular scattering, σ, in the trajectory of a muon is given by:

$$\sigma^2 = \sigma^2_{c.s.} + \sigma^2_m$$

where σ_m is the r.m.s.angular uncertainty in track measurement and $\sigma_{c.s.}$ is the r.m.s. angular Coulomb scattering. At all momenta, for the Haverah Park magnet, σ_{cs} is one third of the magnetic deflection. As a consequence of this, if the maximum detectable momentum (m.d.m.) is defined as that momentum corresponding to an angular deflection of σ, then at the m.d.m.

$$\sigma \simeq \sqrt{\frac{9}{8}}\,\sigma_m$$

Thus at the limit of resolution the inaccuracy in the measured magnetic deflection of muons is dominated by the contribution from the angular uncertainty in track measurement. It may be seen, therefore, that an improvement in the resolution is possible by reducing σ_m until it no longer makes a dominating contribution to σ. Alternatively the same result can be achieved by increasing the magnet thickness. This increases the "induction-path-length" integral in direct proportion to the thickness and σ_{cs} in proportion to the square root of the thickness, so that the net effect is to reduce the Coulomb scattering: magnetic deflection ratio. For example, a three-fold improvement in momentum resolution by this method requires the magnet thickness to be increased by a factor of 2·9. However, since increasing the accuracy in track location is simpler than increasing the magnet thickness, this method of improving the resolution of the spectrograph has been adopted here. Nevertheless, it should be noted that any future improvement of the spectrograph resolution must involve an increase in the magnetic deflection of the muon. This will necessitate an increase in magnet thickness since the magnet is already operated under conditions of near saturation.

A design study was undertaken to choose the optimum method of attaining the desired improvement in track measurement accuracy. For this, as a theoretical measure of the accuracy of track location of a flash tube array, the "mean corridor width", $\bar{w}$, as defined by Rastin (1964) was taken. This term is defined as the mean distance between adjacent tube edges when all the tubes of an array are projected onto a single plane. Thus, assuming that $\sigma_{m_1}/\sigma_{m_2} = \bar{w}_1/\bar{w}_2$, the condition for a threefold improvement in track location accuracy is

$$\frac{\bar{w}_1}{\bar{w}_2} = 3 \quad \ldots\ldots\ldots\ldots\ldots\ldots 2.1$$

Where σ_{m_1} is the r.m.s. angular error in measurement for the Mk1 spectrograph

σ_{m_2} is the r.m.s. angular error in measurement for the Mk2 spectrograph.

$\bar{w}_1$ is the mean corridor width of the Mk1 spectrograph

$\bar{w}_2$ is the mean corridor width in the Mk2 spectrograph.

Following Rastin, for a given flash tube internal efficiency, η, of 100% then for $\frac{\Delta}{\Gamma} < 0{\cdot}8$, we have;

$$\bar{w} = \frac{\Gamma}{N+1} \quad \ldots\ldots\ldots\ldots\ldots\ldots 2.2$$

Where Δ = internal flash tube diameter

Γ = distance apart of tube centres

N = number of layers of tubes in array.

Approximation 2.2 may be modified to take into account the fact that for practical flash tubes, η is less than 100%. Assuming that $\bar{w}$ is inversely proportioned to η we may write:

$$\bar{w} = \frac{\Gamma}{\left(\frac{N \times \eta}{100}\right) + 1} \quad \ldots\ldots\ldots\ldots\ldots\ldots 2.3$$

For the Mk1 spectrograph Γ = 1·9 cms and N = 7, so that taking η as 90% and noting that for N < 9, $\bar{w}$ is underestimated by about 25% (Rastin, (1964)), we obtain, $\bar{w}_1 \simeq 0{\cdot}38$ cm.

Thus, from 2.1 the value of $\bar{w}_2$ required for a threefold improvement in momentum resolution is $\bar{w}_2 \simeq 0{\cdot}1$ cm.

From approximation 2.2 it may be seen that to obtain the desired value of $\bar{w}$, if the pitch, and hence the diameter, of the tubes is small, the number of layers may also be small. However, since a constant large area is covered in this case, the total number of tubes required does not necessarily have to be smaller and it is consequently not possible to obtain an optimum value of tube diameter from these considerations. The choice of the tube diameter is therefore governed by three factors:

(a) the desirability of reducing the number of layers and hence the Coulomb

scattering in the electrodes and glass, (b) consideration of the amount of space available, and (c) the ease of manufacture of the flash tubes. The smallest satisfactory internal diameter is found to be approximately 7 mm. Below 7 mm the efficiency of a flash tube decreases rapidly even if the gas pressure is high, (Coxell and Wolfendale, (1960)), and it is very difficult to maintain the mechanical strength necessary for tubes of length 2 m.

The smallest practical value of pitch for tubes of 7 mm internal diameter was found to be 1·1 cm and insertion of this value into approximation 2.3 gives a value for the number of layers of such tubes to give the required resolution improvement as ten. The basic specification for the Mk2 spectrograph is therefore:-

Internal diameter of neon flash tubes	= 7 mm
Number of flash tube trays in each arm	= 2
Number of layers of flash tubes in each tray	= 10

2.2.2 Neon flash tube detectors

The neon flash tube detector which was introduced by Conversi (1955), and developed by Wolfendale and co-workers, has been used with success in the Mk1 spectrograph. Because of its relatively low cost, simplicity of operation, reliability and the ease with which large areas may be covered, it was chosen for the Mk2 spectrograph in preference to other detectors, for example, spark chambers.

For the application considered in this thesis, a delay of approximately 15 μsec was necessary after the arrival of an air shower until the flash tubes could be pulsed. This ensured that the EAS array electronics were not affected by the high voltage pulsing system. It was therefore important to have a knowledge of the flash tube efficiency-time delay characteristics. The work of Coxell and Wolfendale (1960) indicates that at the same pressure of Neon the efficiency-time delay curve for small diameter tubes drops away much more rapidly than for large diameter tubes; probably because for a given high voltage pulse shape, the electrons in the gas reach the tube walls

FIGURE 2.1 The variation of the efficiency of the 7 mm i.d. flash tubes with the time delay between the passage of a muon and the application of the high voltage pulse. The measurements are from tests made on the flash tubes in-situ in the Mk. 2 spectrograph.

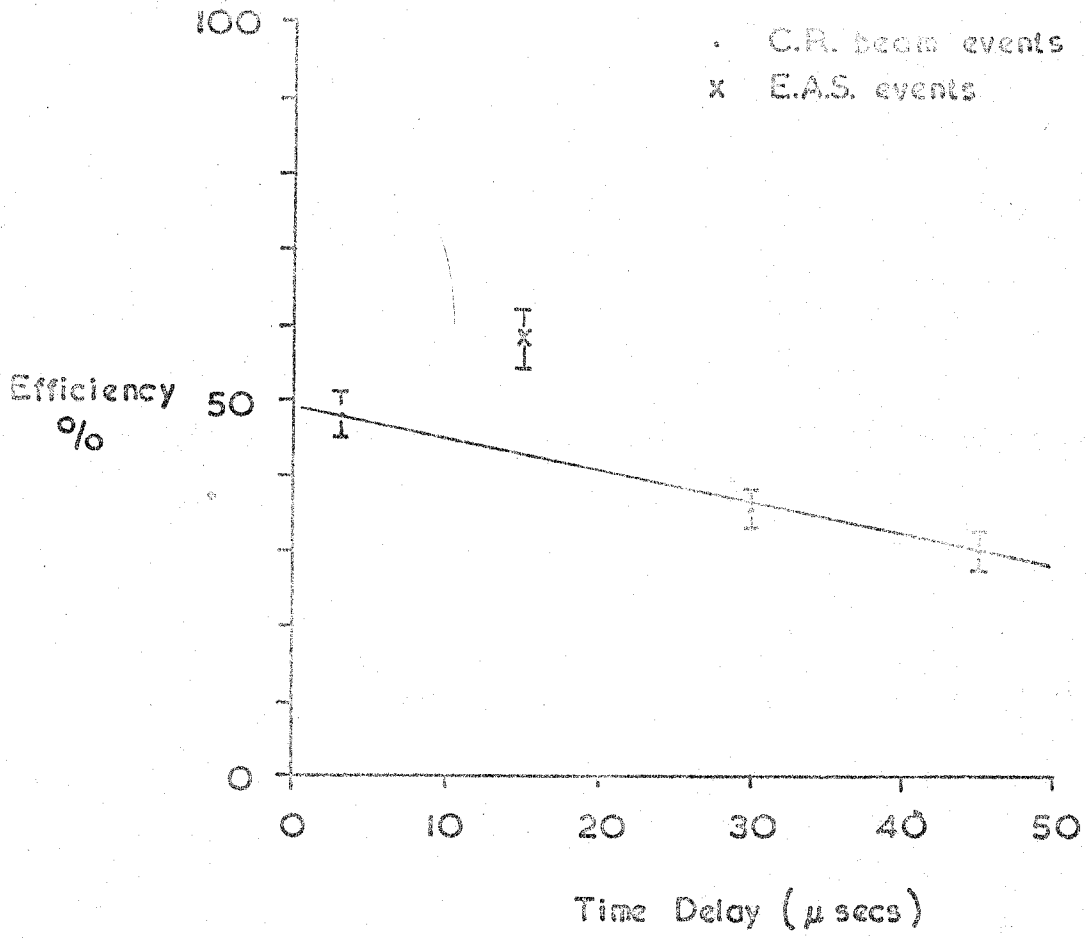
100
50
0
Efficiency %
· C.R. beam events
x E.A.S. events
0
10
20
30
40
50
Time Delay (μ secs)

before an electron cascade can be initiated. This effect can be compensated for by increasing the gas pressure in approximately inverse proportion to the diameter of the tubes, and, in the Mk2 flash tubes the pressure of Neon is 2·4 atmospheres as opposed to 1·0 atmosphere for the Mk1 tubes.

In order to have an experimental knowledge of the actual efficiency-time delay and efficiency-field characteristics of small diameter tubes a small array of 10 layers of tubes with electrodes every 3 layers was constructed. The results of this test were satisfactory, giving values for efficiency of the array(that is the average of the number of tubes flashed in a track) as 58% at a time delay of 15 μsec corresponding to an internal efficiency of 90%. When the same type of tests were made on the full size trays, with a similar electrode arrangement, it was found that a significantly larger field was required to produce the same efficiencies, and that the layers nearest the pulsed electrode were more efficient than the layers next to the earth electrode. A remedy which enabled the applied voltage to be reduced to a level which did not cause random discharges to the sides of the flash tube trays was the insertion of extra electrodes. In the final form there was one electrode between each layer of flash tubes. The results of the efficiency tests on the modified trays are shown in Figure 2.1.These efficiency tests were made using a Geiger counter telescope to select muons from the cosmic ray beam. It is interesting to note, however, that in normal running, with EAS muons, the efficiency has been found to be somewhat higher (again see Figure 2.1). An explanation of this may be obtained by considering the theoretical values for the energy loss due to ionisation for cosmic ray beam muons, for which the mean energy is approximately 1 GeV, and for EAS muons, for which the mean energy is approximately 5 GeV. In the latter case the energy loss due to ionisation is higher since it is further up the "log rise" section of the energy loss curve. Evidence in

FIGURE 2.2 The front and side elevations of the Mk. 2 Haverah Park Magnet Spectrograph.

HAVERAH PARK SPECTROGRAPH MK II

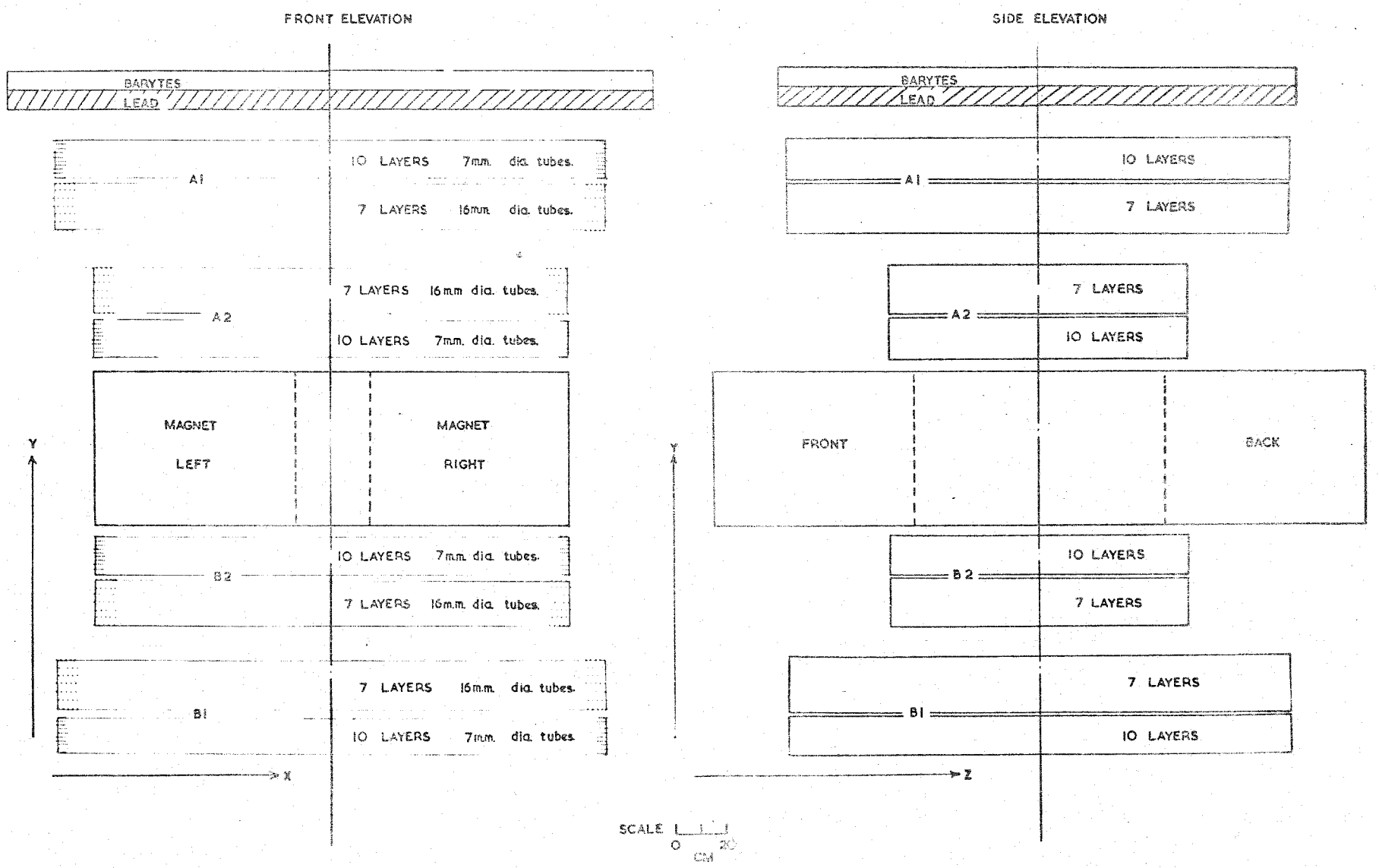

support of the theory that flash tube efficiencies at time delays above a few microseconds reflect relatively small changes in ionisation loss, has recently been presented by Diggory et al., (1971). Furthermore, work by the author (internal report, University of Durham, 1968) has also shown that when the pulse repetition rate is high, greater than about one per ten minutes, the efficiency of flash tubes in an array is diminished. It is postulated that some charging up of the glass occurs, thus providing a clearing field sweeping electrons to the walls. Confirmation of this effect has been obtained and an explanatory theory outlined by Stubbs and Breare (1969). Whilst the effect is not important from the point of view of normal operation of the spectrograph, the event rate being of the order of one per hour, it may be a partial explanation of the relatively low efficiencies obtained in Geiger counter telescope test runs.

Specification of Neon Flash Tubes

Glass	Soda
Internal dia.	7·00 ± ·17 mm
External dia.	9·78 ± 0·14 mm
Straightness	1 part in 1000
Gas pressure	2·4 ats.
Gas content (approx)	98% Ne, 2% He

2.2.3 Mechanical design and construction of the flash tube trays

To obtain approximately the same acceptance characteristics as for the Mk1 spectrograph, the 7 mm tubes were positioned as shown in Figure 2.2 - the number of layers and their spacing having been determined as outlined in Section 2.2.1. The space left by this arrangement in between the banks of 7 mm tubes was filled with 16 mm tubes from the Mk1 spectrograph to aid track recognition and separation.

FIGURE 2.3 (a) The shape of the location grooves for the 7 mm i.d. flash tube used in the Mk. 2 spectrograph.

(b) The profile of the spacers used for separating the 7 mm i.d. flash tubes.

(a)

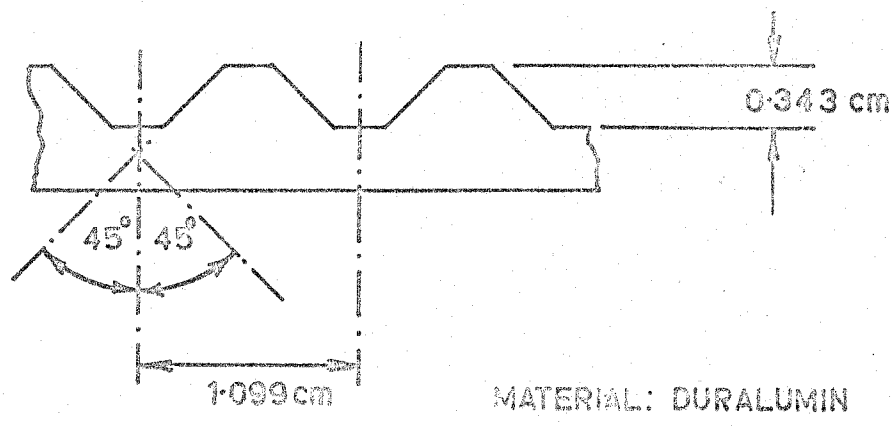

MATERIAL: DURALUMIN

(b)

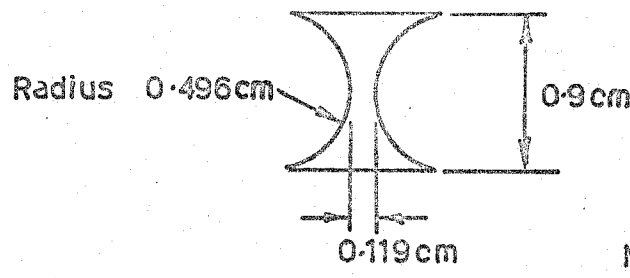

MATERIAL: DARVIC

The basic requirement of the tray design was that the 7 mm tubes should be positioned as accurately as possible (to within 0.05 mm). Several methods of locating the tubes were considered including that developed by the University of Nottingham group, who used a drilled face plate at the front and back of the tray. This particular idea was rejected, in spite of its many advantages, on the grounds that each hole has to be individually reamed out to match the exact diameter of a particular tube, an excessively time consuming process. The method adopted was based on an earlier practice of laying the tubes in "vee" shaped slots accurately milled in duralumin bar positioned at the front and back of the trays (Figure 2.3). The 16 mm tubes were positioned in a similar manner.

A 1 m long 7 mm internal diameter tube supported at its ends was found to have a typical sag under its own weight of 5·0 mm. However, as all the 7 mm tubes were "hot rolled" during manufacture, parallelism was maintained in spite of sagging, and it may be shown that a vertical displacement of 5·0 mm has little effect on track location accuracy. In the case of the 2 m long 7 mm internal diameter tubes, the sag under the same conditions was typically 1 cm, an amount which could not be tolerated and which was prevented by inserting accurately machined tufnol spacers in between each layer of flash tubes. This remedy was not without problems however, since it was found that the friction between the tubes and the tufnol was such that when tubes were slightly displaced, they remained so. To eliminate all possibility of movement, spacers to fit in between each tube were manufactured from "Darvic". These ensured that the tubes remained parallel to one another to within the allowable tolerance of 1 part in 1000.

For reasons of economy, only half the total number of 7 mm tubes was painted black. To minimise light leakage from tube to tube and the associated spurious discharges, the tubes were loaded so that painted tubes alternated with unpainted ones, and the electrodes were painted with a

FIGURE 2.4 The basic circuit diagrams of the high voltage pulsing units used for: (a) the 16 mm i.d. flash tubes, (b) the 7 mm i.d. flash tubes.

(a)

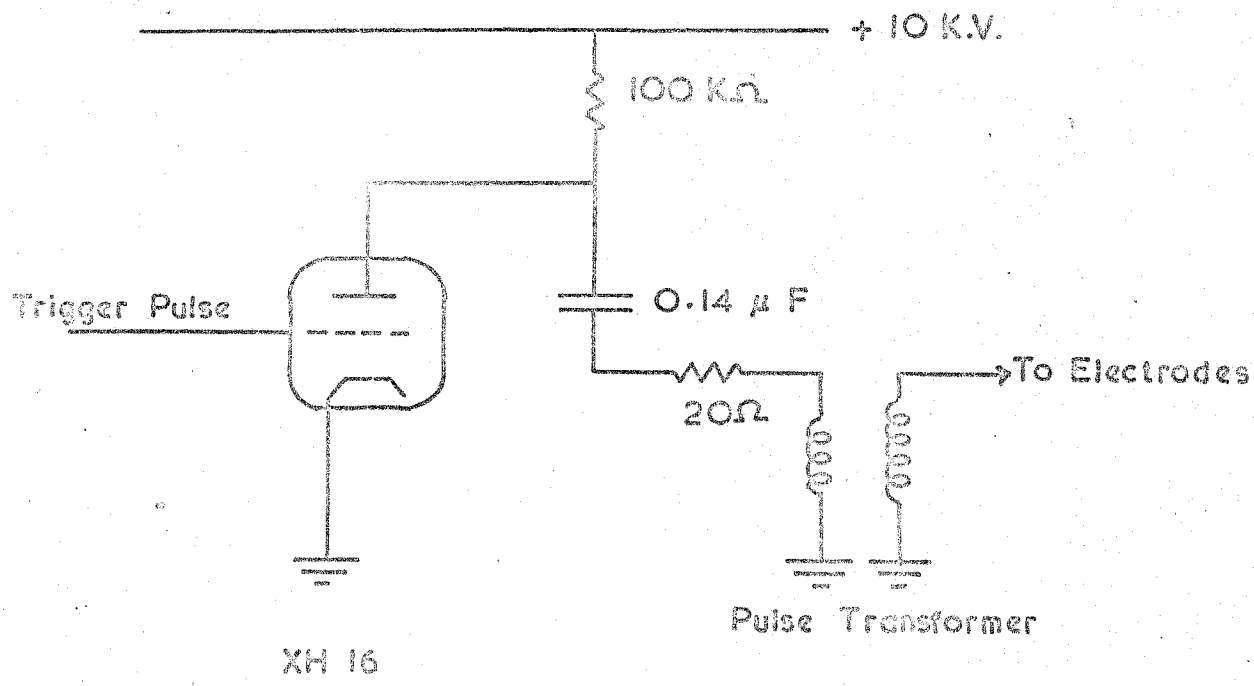
+ 10 K.V.
100 KΩ
Trigger Pulse
0.14 μ F
To Electrodes
20Ω
Pulse Transformer
XH 16

(b)

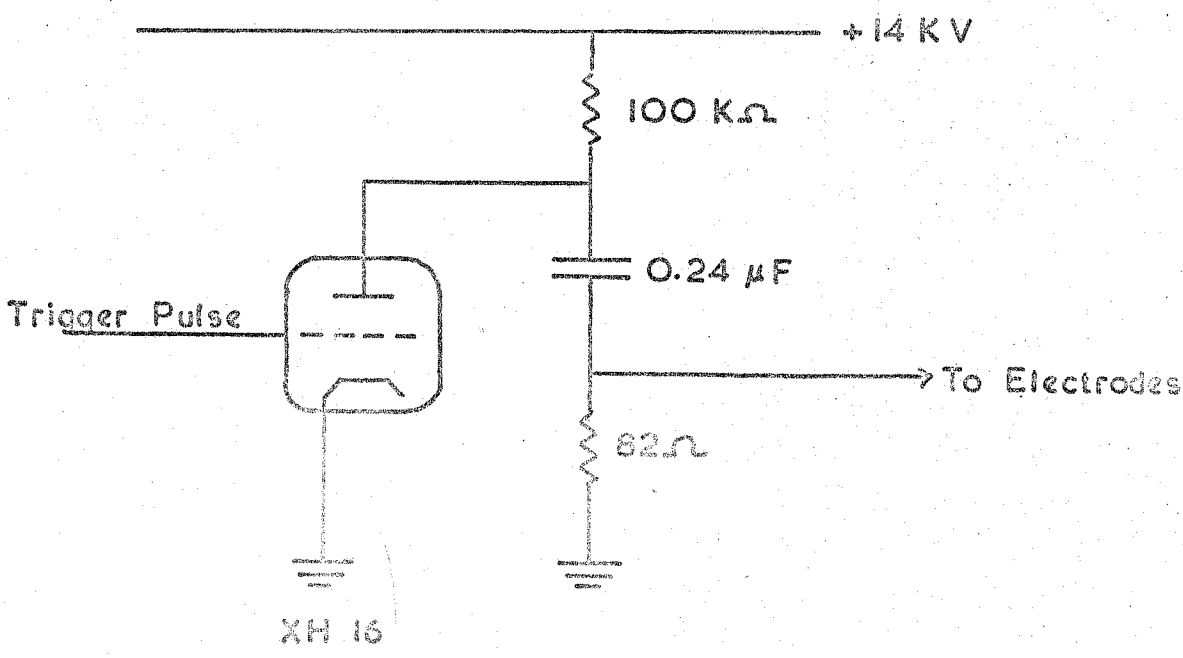
+ 14 K V
100 KΩ
0.24 μF
Trigger Pulse
To Electrodes
82Ω
XH 16

non-reflective matt-black paint. In practice these measures proved satisfactory.

To prevent sparks occurring from the edges of the electrodes, these were bound with thick insulating tape, and perspex positioners were attached to the electrodes to prevent them from being displaced and touching the metal framework of the tray.

2.2.4 The accuracy of location of flash tubes

To ensure that the flash tubes were parallel to the magnet edge, the distances of the centres and ends of the tubes from a plane defined by three plumb lines, known to be parallel to the magnet, were measured, and any appropriate adjustments made. In this way the distances of the centres of particular tubes from the magnet edge were found to within ± 0·2 mm. The locating grooves were machined during manufacture to a tolerance of 0·01 mm over 200 slots, with a tolerance of 0·005 mm on any individual pitch. The resulting estimated uncertainty in the location of the centre of any 7 mm flash tube was therefore ± 0·21 mm.

2.2.5 The pulsing system

The high voltage pulsing units are shown diagrammatically in Figure 2.4. Originally both units used pulse transformers so that extremely high voltage power supplies might be dispensed with, thus bypassing the attendent difficulties of insulation and switching. Unfortunately, the use of a pulse transformer impaired the rise time of the output pulse and the efficiency of the 7 mm flash tubes was found to be very low when such a pulse was applied. Because of this, the pulsing system eventually used for these tubes had a single RC pulse forming network which improved the rise time considerably, and enabled high efficiencies to be obtained.

FIGURE 2.5 A plan view of the Haverah Park EAS arrays.

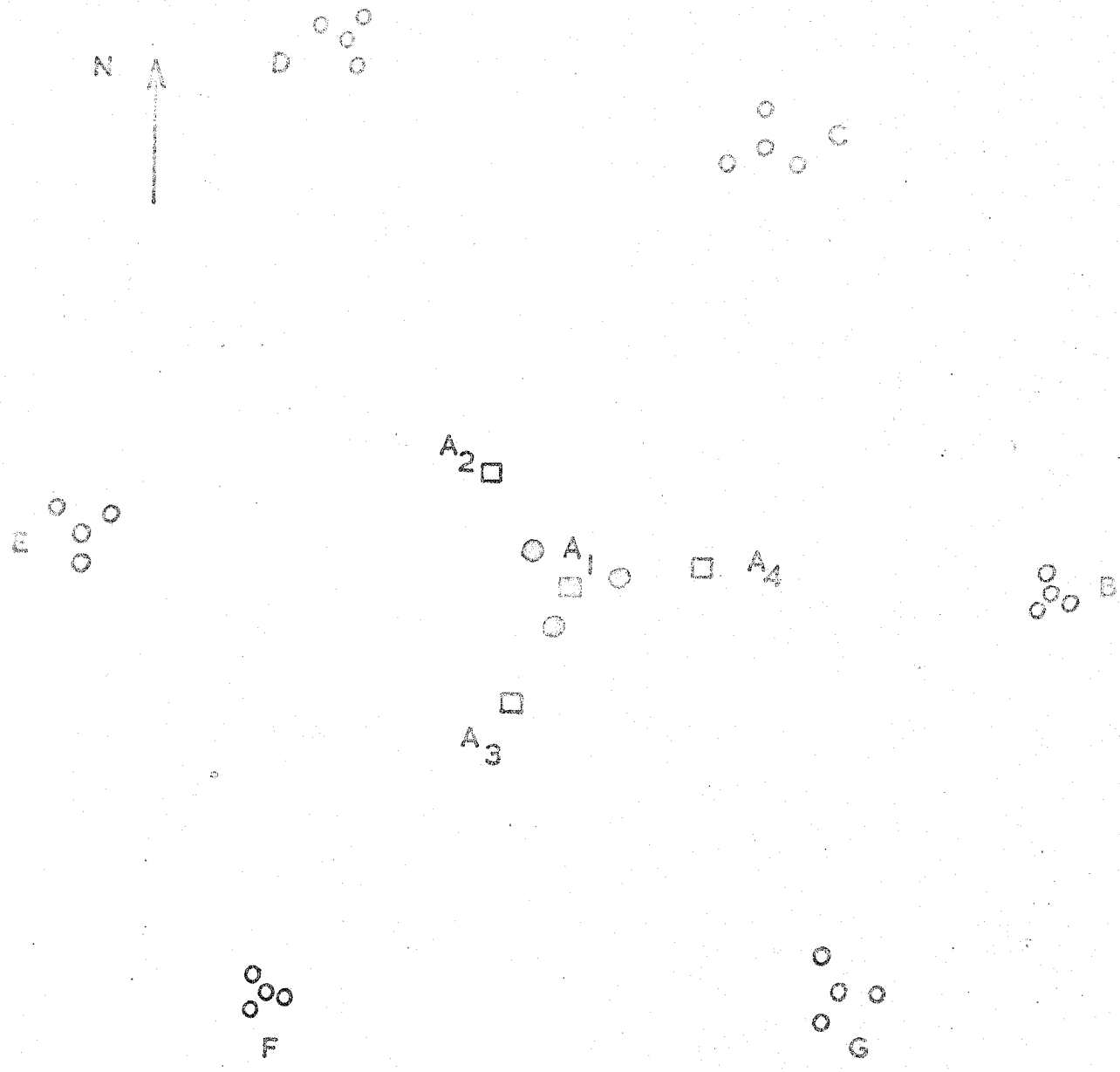
N
A
D
C
A2
E
A1
A4
B
A3
F
G
500m ARRAYS
CENTRAL DETECTOR
2 Km ARRAYS
150m ARRAYS

2.3 The Haverah Park EAS arrays

2.3.1 General

A description of the arrays has been given in detail elsewhere (Wilson et al.,(1963), Tennent (1967)), and the basic arrangement is shown in Figure 2.5.

The size, direction and location of axes of showers are obtained from Cerenkov detector energy-loss samples and time of arrival information.

The analysis of showers relating to the present work has involved the assumption that the lateral distribution of the Cerenkov response between 500 m and 1000 m from the shower core is sufficiently well represented by a power law. In this analysis the exponent and constant of proportionality of this law has been iteratively optimised. During the period of the present experiment, the method of assessing the shower primary energy has evolved. Initially a quantity, E_{100}, defined as the energy lost by those particles in a shower between 100 m and 1000 m from its core passing through 120 cm of water, was used to obtain the shower size using the relationship given by Suri (1966):

$$Ne \propto E_{100}^{1.195}$$

The primary energy was determined from E_{100} by a comparison of shower rate, or by detailed calculation of the development of the shower. Recently, however, it has been found that for large showers a more reliable parameter is the particle density at 500 m from the core, ρ_{500} (Hillas et al., (1969)). Since the particle density at this large distance from the core reaches its maximum later than for the total shower, it is less likely to be subject to fluctuations in the shower development. In addition, for 120 cm water Cerenkov detectors, the signal at 500 m has been shown to be proportional to primary energy,but approximately independent of primary mass, within the energy range 10^{17} - 10^{19} eV.

2.3.2 Accuracy of core location

The confidence which may be placed in the results of the Mk1 spectrograph depends not only on the accuracy of the momentum measurement, but also on the precision of the determination of the shower core location. Recently extra Cerenkov detectors of area 9 m^2 have been added at each of the 150 m array sites and operated in coincidence with the 500 m array. Thus three additional energy loss samples have been available for use in the analysis of showers having zenith angles less than 20° and recorded energy-loss less than or equal to 0·11 GeV m^{-2} at each of the 500 m detectors. (Andrews et al.,(1969b). The increase in accuracy of core location afforded by the extra detectors enabled these workers to justify the earlier method of analysis involving the assumption of a power law structure function, and at the same time to investigate the uncertainty in the location of shower cores. This uncertainty was studied at two shower sizes using a computer simulation of showers and also using real showers. For both real and simulated showers analysed with 500 m densities alone, 70% had a shift in core position of less than 35 m, which is in good agreement with Tennent (1967) who gives the overall uncertainty as 30 m for vertical showers within the 500 m array. For showers for which both 150 m and 500 m densities were available, 65% of the simulated showers had a shift of less than 20 m, whilst for real showers,66% of the cores shifted by 25 m or less and only 6% by greater than 50 m. A significant further observation from this work was that larger shifts in core position tended to be tangential. This is reassuring from the point of view of the analysis of the spectrograph data, although the consequences of some systematic uncertainty in location must be considered when interpreting the results of both the Mk1 and Mk2 experiments.

Chapter 3

The analysis of the Spectrograph data

3.1 Introduction

The problem of measuring the momentum spectrum of muons using the Haverah Park solid iron spectrograph reduced to its simplest elements, involves two stages:

(a) the recording of a muon track and the consequent measurement of a spectrum of deflections of muons in the magnet, and

(b) the conversion of this deflection spectrum into a momentum spectrum.

In the experiments using the Mk1 and Mk2 spectrographs, events have been recorded photographically. For the former, the flashed tubes along a particular track were identified by projection of the negative onto a master print. In contrast, the system used for tube identification in Mk2 spectrograph events involves the use of a transparent overlay. A detailed description of this method is given in Section 3.2.1.

The best estimate of a muon track in the Mk1 experiment was found by using a simulator on which the appropriate tubes could be marked and the position of the track decided by eye. For the Mk2 data, however, because of the difficulty in manufacturing a sufficiently accurate simulator, this method has been reserved for checking the results of a computer programme, briefly described in Section 3.2.2., which decides the best track in accordance with certain programmed criteria.

The magnetic deflection of a muon of given momentum in an iron magnet for a given field depends on the induction-path length integral, the coulomb scattering and the energy loss in the magnet and detectors. The accuracy with which this deflection can be measured depends on the design of the track delineating system, the accuracy with which it is constructed, and the method of track fitting. In converting a deflection spectrum to a momentum spectrum all these factors must be taken into account. A description of the method of

conversion used in the present work is given in Section 3.3.

3.2 Treatment of the Mk2 data

3.2.1 Data retrieval

During normal operation of the spectrograph each air shower trigger signal from the 500 m array causes a high voltage pulse to be applied to the flash tubes and an image of the flashed tubes, together with the solar time, to be recorded on film.

The processed films are scanned for individual events which have complete tracks in both A and B trays, (see Figure 2.2) and which appear to relate to one muon traversing the instrument. Those frames which are selected according to these broad criteria are enlarged to the exact size of a transparent overlay and then printed. This overlay is produced from a high quality photograph of the front of the spectrograph taken using the normal recording camera, and on it each tube end is represented by a point, and each of the eight fiducial lamps by an accurate outline. Prints produced in this way then undergo a further scrutiny, termed "first classification", in the process of which the usable tracks are marked. The sequence of steps in this classification is as follows:

(a) Initial selection is made of those "half tracks", that is tracks in one arm of the spectrograph which could possibly connect up in the magnet, taking into consideration the possibility of lateral scattering.

(b) Each and every one of these half tracks must then satisfy the following criteria:

  (i) More than one tube per tray per track must have flashed.

  (ii) The extremities of the track must be contained within the tray limits. If any doubt arises the track is retained for computer track fitting in which acceptance criteria can be more accurately applied.

(iii) Where more than two tracks are indicated in the upper arm, the track under consideration must not differ in direction from the majority by more than 20°. This is a safeguard to minimise the number of unassociated cosmic ray beam muons selected.

(c) Flashed tubes which are obviously caused by "knock-on" electrons or delta rays are marked to reduce the danger of confusion during the enumeration process. Where the distinction between correct and spurious tubes is not so obvious a simulator is available to aid discrimination. This simulator consists of a high quality, enlarged photograph of a small section of the trays in each arm. By marking the flashed tubes on this photograph an estimate of the "best" track may be made by aligning a cursor by eye.

Consideration of the available air shower information normally follows the "first classification". The following information is obtained from the analysis of showers carried out at Leeds University:-

(a) The zenith angle, θ, of the shower core. If this exceeds 40° the event is rejected.

(b) The core distance. This is noted on the enlarged print.

(c) Whether the shower is fully analysed. If not, the event is rejected.

The enumeration procedure for events which remain involves the identification of the flashed tubes in a given track, and the punching onto cards of the reference numbers of these tubes as data for the track fitting programme. The successful execution of this programme gives the following basic information:

(a) The computed incident angle, Ψ_o, of the muon.

(b) The computed deflection, $\Delta\Psi$, suffered by the muon.

(c) Whether the muon trajectory remained within the prescribed acceptance limits.

(d) The computed separation of the half tracks in the mid plane of the magnet, Δx_m.

The use of this information to decide on the acceptability of the event is termed "second classification" and in this the criteria are as follows:-

(i) If Ψ_o is greater than 30^o the event is rejected as being in the region where the simplifications involved in deriving the acceptance function are not valid and the necessary corrections are large and unreliable.

(ii) If $\Delta\Psi$ is greater than 16^o the event is rejected for the same reasons as in (i).

(iii) If any pair of a number of close tracks in the A and B trays could probably relate to one muon on the basis of all other criteria, rejection of the event is enforced.

3.2.2 Computer Track Fitting

Machin (1972) has investigated various methods of fitting linear trajectories to the flashed tubes in the Mk2 visual detector array. The method deemed most suitable on the basis of this work involved finding the track having the maximum path length within the flash tubes. The computer programme written to find this consisted of the following four main sections. The combined function of the first three sections is to find an approximation to the track and to form a starting point for the final section in the following way.

(a) The top and bottom flashed tubes in the array are used to define a line.

(b) Non-flashed tubes traversed by this line are found and the coordinates of the nearest gap found.

(c) A "least squares" fit is then made to all the flashed tube coordinates (or gap coordinates in the case of a non-flashed tube).

(d) The line found in this way is then rotated through steps in angle and moved in stages of lateral position over a limited range. For each step the path length within the tubes is calculated. The trial giving the maximum path length is taken as the best fit.

FIGURE 3.1 The angular convention used to define a muon trajectory.

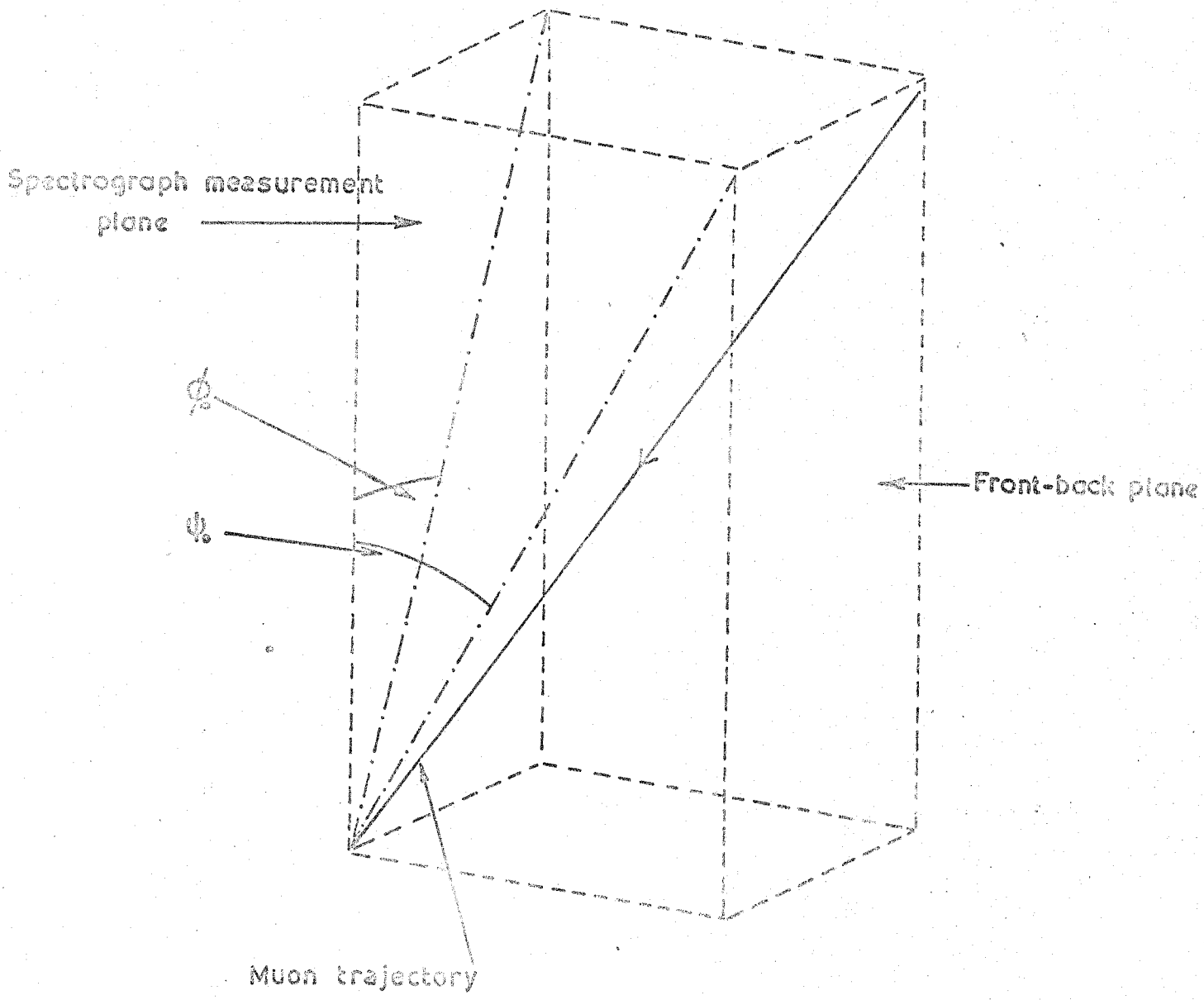
Spectrograph measurement plane
ϕ_2
ψ_2
Front-back plane
Muon trajectory

The resulting linear trajectories for the top and bottom trays are given in the form $y = mx + c$ and this information enables the angle of deflection, $\Delta\Psi$, and the lateral separation of the tracks in the mid-plane of the magnet Δx_m to be calculated.

3.3 The method of converting an observed deflection spectrum into a momentum spectrum and of estimating the uncertainty involved

3.3.1 Basic method

Several methods of converting an observed deflection spectrum into a momentum spectrum have been suggested (Rand (1962), Rochester et al., (1965), and Aurela (1967)). The method used here has been developed and fully described by Orford (1968). In brief, the outline of the method is as follows:

The probability that a positive or negative muon of momentum p incident at Ψ_o, ϕ_o (see Figure 3.1) enters the spectrograph and passes into the deflection interval $|\Delta\Psi|$ to $|\Delta\Psi + \delta\Delta\Psi|$ regardless of the sign of deflection is:

$$w(p,\Delta\Psi)d\Delta\Psi = \int_{-40^\circ}^{+40^\circ} \int_{-30^\circ}^{+30^\circ} M(\Psi_o)N(\phi_o)A(\Psi_o,\phi_o,\Delta\Psi)G(p,\Delta\Psi,\Delta\Psi_m)d\Psi_o\, d\phi_o\, d\Delta\Psi$$

Where - $M(\Psi_o)$ and $N(\phi_o)$ are the observed distributions of showers in Ψ_o and ϕ_o

$A(\Psi_o,\phi_o,\Delta\Psi)$ is the probability that a positive or negative muon, incident in a direction specified by Ψ_o,ϕ_o and undergoing a deflection of absolute value $\Delta\Psi$, will be accepted by the spectrograph.

G is a function representing the probability of a muon, of positive or negative charge, being deflected from $\Delta\Psi_m$ to $\Delta\Psi$ by measurement noise and multiple coulomb scattering.

$\Delta\Psi_m$ is the most probable magnetic deflection taking into account energy loss in the magnet.

If the differential momentum spectrum under investigation is denoted by $S(p)dp$ then the corresponding deflection spectrum in the form of a histogram is represented by

$$N(\Delta\Psi_j) = \int_{\Delta\Psi_j}^{\Delta\Psi_{j+1}} \int_0^{\infty} S(p)\, w(p,\Delta\Psi)\, dp\, d\Delta\Psi$$

In practice a mean value of $w(p,\Delta\Psi)$ for the interval $\Delta\Psi_j$ to $\Delta\Psi_{j+1}$, is calculated for a set of momentum values p_i. Thus, a matrix of "weighting factors" w_{ij} is obtained. The population of an interval in the deflection spectrum is then given by:

$$N(\Delta\Psi_j) = \sum_i S(p_i)\, \Delta p\, w_{ij}$$

By using an iterative technique, the form of the differential spectrum giving the best fit to the data may be derived. If O_j is the observed population of the deflection interval $\Delta\Psi_j$ to $\Delta\Psi_{j+1}$ and $S(p)_n$ is the nth trial spectrum, which gives a predicted population $E_{j(n)}$, the (n+1)th spectrum is given by

$$S(p_i)_{n+1}\, \Delta p = \frac{\sum_j S(p_i)_n\, \Delta p\, w_{ij}\, O_j/E_{j(n)}}{\sum_j w_{ij}}$$

3.3.2 The derivation of the weighting factors

The weighting factors are derived by numerical integration of the function $w(p,\Delta\Psi)$, as defined in Section 3.3.1, over the interval $\Delta\Psi_j$ to $\Delta\Psi_{j+1}$ for different values of momentum. The component function, $G(p, \Delta\Psi, \Delta\Psi_m)$ represents the angular distribution of deflection due to coulomb scattering and measurement noise. When considered for one sign of muon charge and unfolded about $\Delta\Psi = 0$, $G(p,\Delta\Psi, \Delta\Psi_m)$ is a gaussian function of $\Delta\Psi$ having a most probable value of $\Delta\Psi_m$. The assumption of a gaussian form for the angular deflection distribution due to multiple coulomb scattering alone is based on the work of Eyges (1948) who gave the following expression for the standard deviation of the function

$$\sigma_{c.s.} = \left[\frac{E_s^2 \cdot s}{2 \cdot p \cdot (p - q \cdot s)}\right]^{\frac{1}{2}}$$

FIGURE 3.2 The angular convention and formulae used for the computation, taking into account momentum dependent energy loss, of the deflection of a muon in the spectrograph magnet.

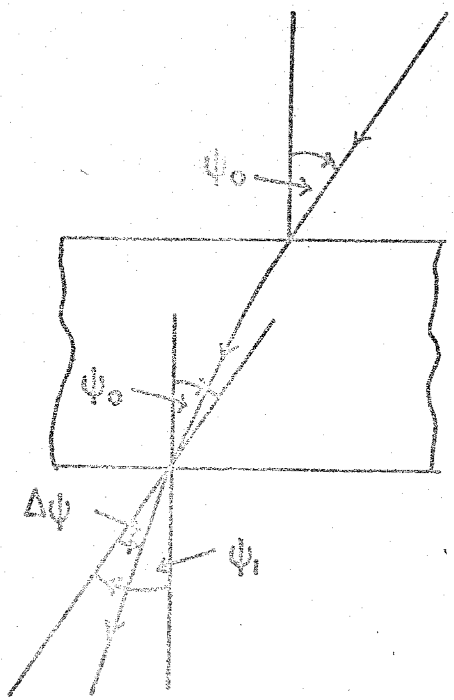

$$\sin\psi_1 = \sin\psi_0 - \frac{\Delta\ell \times 300 \times B}{P}$$

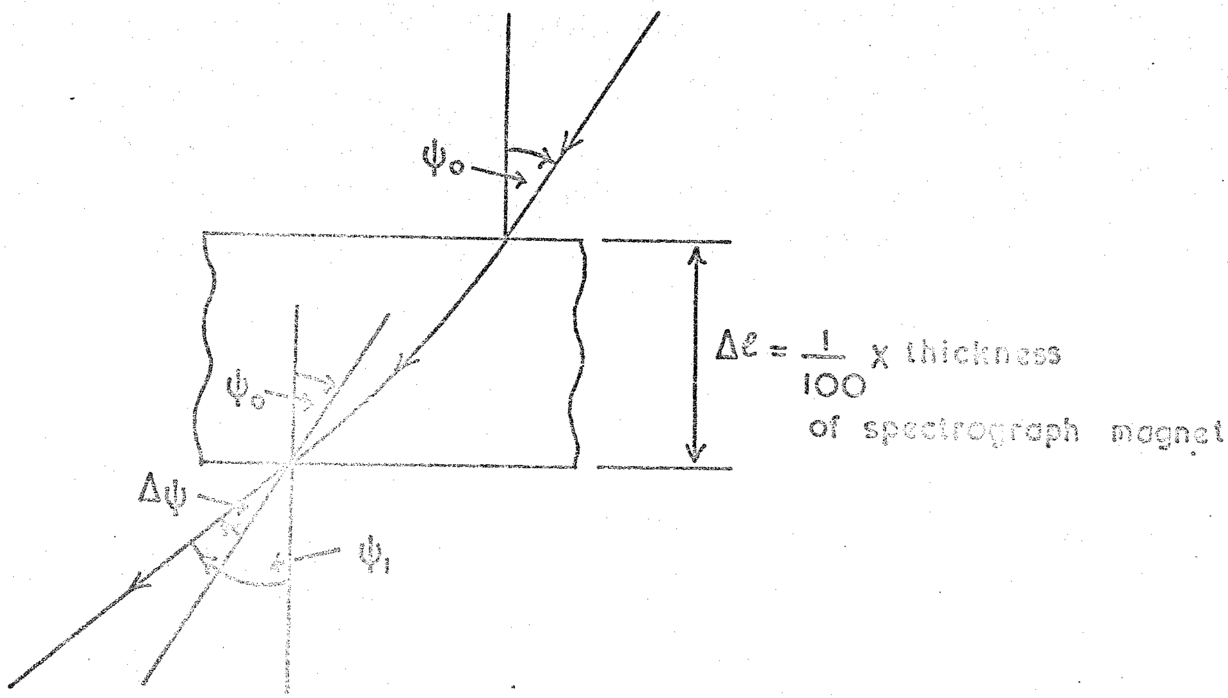

$$\sin\psi_1 = \sin\psi_0 + \frac{\Delta\ell \times 300 \times B}{P}$$

$\Delta\ell$ is in cms

P (momentum) is in eV/c

B (induction) is in gauss

where p is the momentum in eV/c, E_s is a constant having the dimensions of energy and has the value of 21 x 10^6 eV, q is the energy loss due to ionisation in eV per radiation length, and s, in radiation lengths, is the potential path length when no scattering material is present.

To take account of the measurement noise another gaussian function is assumed having a standard deviation σ_m which is measured experimentally (Section 3.4.1). The total standard deviation of the function G is then found by quadratic addition of σ_{cs} and σ_m.

The expression given by Rastin (1964) relating the most probable magnetic deflection, $\Delta\Psi_m$, to the momentum, p, in a solid magnet taking into account energy loss is:

$$p = \frac{\ell k\left(1 - \frac{\varepsilon^2}{k^2}\right)}{\exp\left\{\frac{\varepsilon}{k}(\Psi_o - \Psi_1)\right\} \cdot \left(\sin\Psi_1 + \frac{\varepsilon}{k}\cos\Psi_1\right) - \left(\sin\Psi_o + \frac{\varepsilon}{k}\cos\Psi_o\right)} \qquad \ldots\ldots\ldots 3.1$$

where p is in eV/c, ℓ is the thickness of the magnet in cms, k is a constant given by 300 x B, where B is the induction in gauss and ε is the specific energy loss due to ionisation in eV/cm. Ψ_o is as defined previously and Ψ_1 is the emergent angle measured from the vertical in the same plane as Ψ_o.

The introduction into Equation 3.1 of an energy loss ε, which is dependent on momentum, p, is not simple. To investigate the effect of such a dependence a relatively elementary method has been used. The magnet is considered to be divided into a hundred layers. For an angle of incidence of Ψ_o on the first layer, the angle of emergence, Ψ_1, together with the path length, was calculated for a positively charged muon using the formulae given in Figure 3.2. For each layer the angle of incidence was considered to be equal to the angle of emergence from the previous layer and the incident momentum be the momentum possessed by the muon in the previous layer minus

TABLE 3.1(a) The deflection in the spectrograph magnet. of a positively charged muon possessing a given incident momentum. The incident direction is defined by the angles "PSI" (Ψ_o) and "PHI" (ϕ_o). "PATH" is the total path length in the iron.

MOM(GEV/C)= 10.0

PSI	PHI	DEFLN.	PATH
0	0	1.602	60.8
0	10	1.603	61.7
0	20	1.608	64.7
0	30	1.615	70.2
0	40	1.628	79.3
10	0	1.632	61.8
10	10	1.634	62.8
10	20	1.639	65.8
10	30	1.646	71.4
10	40	1.659	80.7
20	0	1.720	65.0
20	10	1.722	66.0
20	20	1.728	69.2
20	30	1.735	75.1
20	40	1.750	84.8
30	0	1.853	70.6
30	10	1.855	71.9
30	20	1.861	75.4
30	30	1.868	81.8
30	40	1.885	92.4
40	0	2.161	80.5
40	10	2.163	81.8
40	20	2.171	85.7
40	30	2.185	93.0
40	40	2.209	105.2

MOM(GEV/C)= 20.0

PSI	PHI	DEFLN.	PATH
0	0	0.781	60.8
0	10	0.781	61.7
0	20	0.782	64.6
0	30	0.784	70.1
0	40	0.787	79.3
10	0	0.794	61.8
10	10	0.794	62.7
10	20	0.795	65.7
10	30	0.797	71.3
10	40	0.800	80.6
20	0	0.835	64.8
20	10	0.835	65.8
20	20	0.836	69.0
20	30	0.838	74.8
20	40	0.841	84.6
30	0	0.909	70.5
30	10	0.910	71.5
30	20	0.911	75.0
30	30	0.913	81.4
30	40	0.917	92.0
40	0	1.035	79.9
40	10	1.036	81.1
40	20	1.037	85.0
40	30	1.040	92.2
40	40	1.046	104.3

MOM(GEV/C)= 30.0

PSI	PHI	DEFLN.	PATH
0	0	0.516	60.8
0	10	0.517	61.7
0	20	0.517	64.6
0	30	0.518	70.1
0	40	0.519	79.3
10	0	0.525	61.7
10	10	0.525	62.7
10	20	0.525	65.7
10	30	0.526	71.3
10	40	0.527	80.6
20	0	0.551	64.8
20	10	0.551	65.8
20	20	0.552	68.9
20	30	0.552	74.8
20	40	0.554	84.5
30	0	0.599	70.4
30	10	0.600	71.4
30	20	0.600	74.9
30	30	0.601	81.2
30	40	0.603	91.8
40	0	0.681	79.7
40	10	0.681	80.9
40	20	0.682	84.8
40	30	0.683	92.0
40	40	0.685	104.0

MOM(GEV/C)= 40.0

PSI	PHI	DEFLN.	PATH
0	0	0.386	60.7
0	10	0.386	61.7
0	20	0.386	64.6
0	30	0.386	70.1
0	40	0.387	79.3
10	0	0.392	61.7
10	10	0.392	62.7
10	20	0.392	65.7
10	30	0.393	71.3
10	40	0.393	80.6
20	0	0.411	64.7
20	10	0.411	65.7
20	20	0.412	68.9
20	30	0.412	74.7
20	40	0.413	84.5
30	0	0.447	70.3
30	10	0.447	71.4
30	20	0.447	74.8
30	30	0.448	81.2
30	40	0.449	91.8
40	0	0.507	79.6
40	10	0.507	80.8
40	20	0.508	84.7
40	30	0.508	91.9
40	40	0.510	103.9

MOM(GEV/C)= 50.0

PSI	PHI	DEFLN.	PATH
0	0	0.308	60.7
0	10	0.308	61.7
0	20	0.308	64.6
0	30	0.308	70.1
0	40	0.309	79.3
10	0	0.313	61.7
10	10	0.313	62.7
10	20	0.313	65.7
10	30	0.313	71.3
10	40	0.314	80.6
20	0	0.326	64.7
20	10	0.328	65.7
20	20	0.328	68.9
20	30	0.328	74.7
20	40	0.329	84.5
30	0	0.356	70.3
30	10	0.357	71.4
30	20	0.357	74.8
30	30	0.357	81.1
30	40	0.358	91.7
40	0	0.404	79.5
40	10	0.404	80.8
40	20	0.404	84.6
40	30	0.405	91.8
40	40	0.406	103.8

MOM(GEV/C)= 15.0

PSI	PHI	DEFLN.	PATH
0	0	1.050	60.8
0	10	1.051	61.7
0	20	1.052	64.7
0	30	1.056	70.1
0	40	1.061	79.3
10	0	1.068	61.8
10	10	1.069	62.7
10	20	1.071	65.3
10	30	1.074	71.3
10	40	1.080	80.7
20	0	1.124	64.9
20	10	1.124	65.9
20	20	1.126	69.0
20	30	1.130	74.9
20	40	1.136	84.7
30	0	1.226	70.6
30	10	1.227	71.7
30	20	1.230	75.1
30	30	1.234	81.5
30	40	1.241	92.1
40	0	1.399	80.1
40	10	1.400	81.3
40	20	1.404	86.2
40	30	1.409	92.5
40	40	1.419	104.6

MOM(GEV/C)= 25.0

PSI	PHI	DEFLN.	PATH
0	0	0.622	60.8
0	10	0.622	61.7
0	20	0.623	64.6
0	30	0.624	70.1
0	40	0.625	79.3
10	0	0.632	61.7
10	10	0.632	62.7
10	20	0.633	65.7
10	30	0.634	71.3
10	40	0.636	80.6
20	0	0.664	64.8
20	10	0.664	65.8
20	20	0.665	68.9
20	30	0.666	74.8
20	40	0.668	84.6
30	0	0.723	70.4
30	10	0.723	71.5
30	20	0.724	74.9
30	30	0.725	81.3
30	40	0.728	91.9
40	0	0.821	79.8
40	10	0.822	81.0
40	20	0.823	84.9
40	30	0.825	92.1
40	40	0.828	104.1

MOM(GEV/C)= 35.0

PSI	PHI	DEFLN.	PATH
0	0	0.442	60.8
0	10	0.442	61.7
0	20	0.442	64.6
0	30	0.443	70.1
0	40	0.443	79.3
10	0	0.449	61.7
10	10	0.449	62.7
10	20	0.449	65.7
10	30	0.450	71.3
10	40	0.451	80.6
20	0	0.471	64.7
20	10	0.471	65.7
20	20	0.471	68.9
20	30	0.472	74.8
20	40	0.473	84.5
30	0	0.512	70.3
30	10	0.512	71.4
30	20	0.513	74.8
30	30	0.513	81.2
30	40	0.515	91.8
40	0	0.581	79.6
40	10	0.582	80.8
40	20	0.582	84.7
40	30	0.583	91.9
40	40	0.584	103.9

MOM(GEV/C)= 45.0

PSI	PHI	DEFLN.	PATH
0	0	0.342	60.7
0	10	0.342	61.7
0	20	0.343	64.6
0	30	0.343	70.1
0	40	0.344	79.3
10	0	0.348	61.7
10	10	0.348	62.7
10	20	0.348	65.7
10	30	0.348	71.3
10	40	0.349	80.6
20	0	0.365	64.7
20	10	0.365	65.7
20	20	0.365	68.9
20	30	0.366	74.7
20	40	0.366	84.5
30	0	0.397	70.3
30	10	0.397	71.4
30	20	0.397	74.8
30	30	0.397	81.2
30	40	0.398	91.7
40	0	0.450	79.5
40	10	0.450	80.8
40	20	0.450	84.7
40	30	0.451	91.8
40	40	0.452	103.8

TABLE 3.1(b) As for Table 3.1(a) but for a muon of negative charge.

MOM(GEV/C)= 10.0				MOM(GEV/C)= 20.0				MOM(GEV/C)= 30.0				MOM(GEV/C)= 40.0				MOM(GEV/C)= 50.0			
PSI	PHI	DEFLN.	PATH	PSI	PHI	DEFLN.	PATH	PSI	PHI	DEFLN.	PATH	PSI	PHI	DEFLN.	PATH	PSI	PHI	DEFLN.	PATH
0	0	-1.602	60.8	0	0	-0.781	60.8	0	0	-0.516	60.8	0	0	-0.386	60.7	0	0	-0.308	60.7
0	10	-1.603	61.7	0	10	-0.781	61.7	0	10	-0.517	61.7	0	10	-0.386	61.7	0	10	-0.308	61.7
0	20	-1.608	64.7	0	20	-0.782	64.6	0	20	-0.517	64.6	0	20	-0.386	64.6	0	20	-0.308	64.6
0	30	-1.615	70.2	0	30	-0.784	70.1	0	30	-0.518	70.1	0	30	-0.386	70.1	0	30	-0.308	70.1
0	40	-1.628	79.3	0	40	-0.787	79.3	0	40	-0.519	79.3	0	40	-0.387	79.3	0	40	-0.309	79.3
10	0	-1.624	61.5	10	0	-0.793	61.6	10	0	-0.524	61.6	10	0	-0.392	61.7	10	0	-0.313	61.7
10	10	-1.625	62.5	10	10	-0.793	62.6	10	10	-0.524	62.6	10	10	-0.392	62.6	10	10	-0.313	62.6
10	20	-1.630	65.5	10	20	-0.794	65.6	10	20	-0.525	65.6	10	20	-0.392	65.6	10	20	-0.313	65.6
10	30	-1.637	71.1	10	30	-0.796	71.1	10	30	-0.526	71.2	10	30	-0.392	71.2	10	30	-0.313	71.2
10	40	-1.651	80.3	10	40	-0.799	80.4	10	40	-0.527	80.5	10	40	-0.393	80.5	10	40	-0.314	80.5
20	0	-1.701	64.3	20	0	-0.830	64.5	20	0	-0.549	64.5	20	0	-0.410	64.6	20	0	-0.328	64.6
20	10	-1.703	65.3	20	10	-0.831	65.5	20	10	-0.549	65.5	20	10	-0.411	65.6	20	10	-0.328	65.6
20	20	-1.707	68.4	20	20	-0.832	68.6	20	20	-0.550	68.7	20	20	-0.411	68.7	20	20	-0.328	68.7
20	30	-1.716	74.3	20	30	-0.834	74.5	20	30	-0.551	74.5	20	30	-0.411	74.5	20	30	-0.328	74.6
20	40	-1.730	83.9	20	40	-0.837	84.2	20	40	-0.552	84.3	20	40	-0.412	84.3	20	40	-0.329	84.3
30	0	-1.847	69.5	30	0	-0.901	69.8	30	0	-0.596	69.9	30	0	-0.445	70.0	30	0	-0.356	70.0
30	10	-1.849	70.6	30	10	-0.902	70.9	30	10	-0.596	71.0	30	10	-0.445	71.1	30	10	-0.356	71.1
30	20	-1.854	74.0	30	20	-0.903	74.3	30	20	-0.597	74.4	30	20	-0.446	74.5	30	20	-0.356	74.5
30	30	-1.865	80.3	30	30	-0.905	80.6	30	30	-0.598	80.7	30	30	-0.446	80.8	30	30	-0.356	80.8
30	40	-1.882	90.7	30	40	-0.909	91.2	30	40	-0.600	91.3	30	40	-0.447	91.4	30	40	-0.357	91.4
40	0	-2.092	78.2	40	0	-1.020	78.7	40	0	-0.674	78.9	40	0	-0.504	79.0	40	0	-0.402	79.1
40	10	-2.094	79.4	40	10	-1.020	79.9	40	10	-0.674	80.1	40	10	-0.504	80.2	40	10	-0.402	80.3
40	20	-2.101	83.2	40	20	-1.022	83.8	40	20	-0.675	84.0	40	20	-0.504	84.1	40	20	-0.402	84.1
40	30	-2.114	90.2	40	30	-1.025	90.9	40	30	-0.676	91.1	40	30	-0.505	91.2	40	30	-0.403	91.3
40	40	-2.136	102.0	40	40	-1.030	102.7	40	40	-0.679	103.0	40	40	-0.506	103.1	40	40	-0.404	103.2

MOM(GEV/C)= 15.0				MOM(GEV/C)= 25.0				MOM(GEV/C)= 35.0				MOM(GEV/C)= 45.0			
PSI	PHI	DEFLN.	PATH	PSI	PHI	DEFLN.	PATH	PSI	PHI	DEFLN.	PATH	PSI	PHI	DEFLN.	PATH
0	0	-1.050	60.8	0	0	-0.622	60.8	0	0	-0.442	60.8	0	0	-0.342	60.7
0	10	-1.051	61.7	0	10	-0.622	61.7	0	10	-0.442	61.7	0	10	-0.342	61.7
0	20	-1.052	64.7	0	20	-0.623	64.6	0	20	-0.442	64.6	0	20	-0.343	64.6
0	30	-1.056	70.1	0	30	-0.624	70.1	0	30	-0.443	70.1	0	30	-0.343	70.1
0	40	-1.061	79.3	0	40	-0.625	79.3	0	40	-0.443	79.3	0	40	-0.344	79.3
10	0	-1.065	61.6	10	0	-0.631	61.6	10	0	-0.448	61.6	10	0	-0.348	61.7
10	10	-1.066	62.5	10	10	-0.631	62.6	10	10	-0.448	62.6	10	10	-0.348	62.6
10	20	-1.068	65.5	10	20	-0.632	65.6	10	20	-0.449	65.6	10	20	-0.348	65.6
10	30	-1.071	71.1	10	30	-0.633	71.2	10	30	-0.449	71.2	10	30	-0.348	71.2
10	40	-1.076	80.4	10	40	-0.635	80.4	10	40	-0.450	80.5	10	40	-0.349	80.5
20	0	-1.116	64.4	20	0	-0.661	64.5	20	0	-0.470	64.6	20	0	-0.364	64.6
20	10	-1.117	65.4	20	10	-0.661	65.5	20	10	-0.470	65.5	20	10	-0.364	65.6
20	20	-1.119	68.6	20	20	-0.662	68.7	20	20	-0.470	68.7	20	20	-0.365	68.7
20	30	-1.122	74.4	20	30	-0.663	74.5	20	30	-0.471	74.5	20	30	-0.365	74.6
20	40	-1.128	84.1	20	40	-0.666	84.2	20	40	-0.472	84.3	20	40	-0.366	84.3
30	0	-1.211	69.7	30	0	-0.718	69.9	30	0	-0.510	70.0	30	0	-0.395	70.0
30	10	-1.212	70.8	30	10	-0.718	71.0	30	10	-0.510	71.0	30	10	-0.395	71.1
30	20	-1.214	74.2	30	20	-0.719	74.4	30	20	-0.510	74.5	30	20	-0.396	74.5
30	30	-1.219	80.5	30	30	-0.720	80.7	30	30	-0.511	80.8	30	30	-0.396	80.8
30	40	-1.226	91.0	30	40	-0.723	91.2	30	40	-0.512	91.3	30	40	-0.397	91.4
40	0	-1.371	78.5	40	0	-0.812	78.8	40	0	-0.577	79.0	40	0	-0.447	79.0
40	10	-1.372	79.7	40	10	-0.812	80.1	40	10	-0.577	80.2	40	10	-0.447	80.3
40	20	-1.375	83.6	40	20	-0.813	83.9	40	20	-0.577	84.0	40	20	-0.448	84.1
40	30	-1.380	90.7	40	30	-0.815	91.0	40	30	-0.578	91.2	40	30	-0.448	91.3
40	40	-1.389	102.5	40	40	-0.818	102.9	40	40	-0.580	103.1	40	40	-0.449	103.2

FIGURE 3.3 The acceptance function for the measurement plane, $A(\Psi_o, \Delta\Psi)$, and the back-front plane, $B(\phi_o)$, of the Mk. 2 spectrograph.

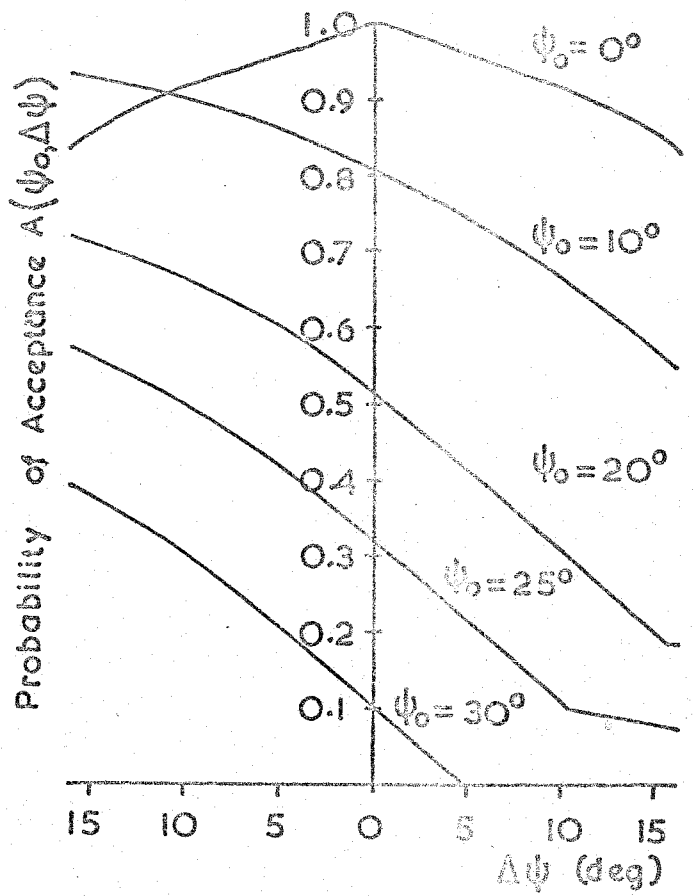
Probability of Acceptance A(ψ0,Δψ)
1.0
0.9
0.8
0.7
0.6
0.5
0.4
0.3
0.2
0.1
ψ0 = 0°
ψ0 = 10°
ψ0 = 20°
ψ0 = 25°
ψ0 = 30°
15
10
5
0
5
10
15
Δψ (deg)

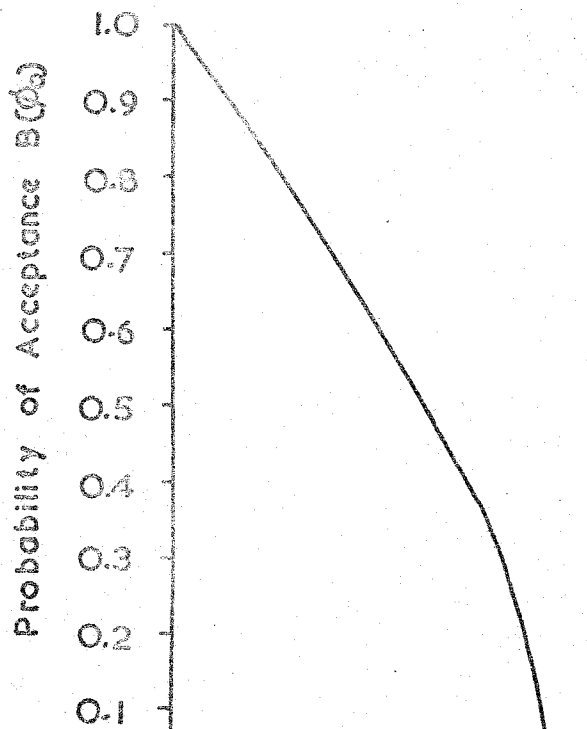
Probability of Acceptance B(φ3)
1.0
0.9
0.8
0.7
0.6
0.5
0.4
0.3
0.2
0.1
0
10
20
30
40
φ3 (deg)

that lost due to ionisation along the computed track length. The procedure was repeated for all layers using the formula for energy loss due to ionisation in iron given by Sternheimer (1959). The final angle of emergence and total path length was calculated for both positive and negative muons for several incident directions and values of momenta. The results agreed well with those obtained using Equation 3.1. Typical values of deflection and path length calculated by the method are given in Table 3.1.

The acceptance function, $A(\Psi, \phi, \Delta\Psi)$, is defined in Section 3.3.1 and has been calculated by a method similar to that described by Orford (1968). This involves calculating the acceptance function for the spectrograph measurement plane and for the front-back plane. The total acceptance for a given value of Ψ_o and ϕ_o is then the product of these two functions.

In calculating the acceptance function for the Mk2 spectrograph the imposed limits of Ψ_o were $\pm 30^\circ$, and of ϕ_o, $\pm 40^\circ$. Beyond these values the simplifications made in calculating the acceptance function are no longer valid and corrections are very unreliable. Figure 3.3 shows the respective functions for the two planes for various values of Ψ_o and ϕ_o. The method of calculation assumes no scattering in the iron of the magnet so that for the front-back plane a slight inaccuracy is introduced. Earnshaw (1968) estimates that for the Mk1 instrument this simplification involves a 5% increase in muon densities at 1 GeV/c, a 1% rise at 10 GeV/c, and no effect at 100 GeV/c. The functions for the present instrument are very similar to those for the Mk1 instrument and it is expected that the effects of the simplification will be very much the same.

Because of known rapid variation of light intensity with the angle at which a flash tube is viewed there will be a finite probability that flashed tubes at the edges of the trays and at the top of A1 and bottom B1 will not be recorded on the film. Thus tracks in the middle of the trays will be preferentially

accepted. The way in which this modifies the acceptance function has been investigated by Orford (1968) for the Mk1 spectrograph, and it was found that in general the number of apparent flashed tubes in a track decreases by 20% in going from the middle of the tray to the edges. In the analysis of the Mk2 data the films have been very carefully scrutinised for possible tracks at the edges of the trays, and all the evidence indicates that the probability of missing a track is negligible. However, when a statistically adequate sample of events becomes available it will be possible to make a quantitative estimate of the probability of completely missing a track in relation to the number of flashed tubes in it.

3.4 Noise estimation

3.4.1 Introduction

An attempt to fit a straight line through the tubes which have been caused to flash by the passage of a muon is subject to uncertainty because of:

(a) the location accuracy, finite diameter, and number of the tubes,

(b) the probability of "knock-on" electrons and delta rays causing a tube to flash,

(c) coulomb scattering in the glass walls of the flash tubes and in the electrodes, and

(d) distortion of the muon's trajectory through the magnet due to coulomb scattering. Thus the resultant measured angular deflection is the result of the deflection in the magnetic field together with the above effects.

Scattering in the magnet is dealt with in the Section 3.3.2 and we are concerned here with the consideration of the effects of (a), (b) and (c). The probability distribution for the angular deflections due to (a) and (c) are assumed to be gaussian, and the estimation of the respective standard deviations is dealt with in Section 3.4.2. Although the contribution of (b) to the measurement noise is considered to be very small it is expected to be

FIGURE 3.4 The distribution in angular deflection of EAS muons traversing the magnet hole in the Mk. 2 spectrograph.

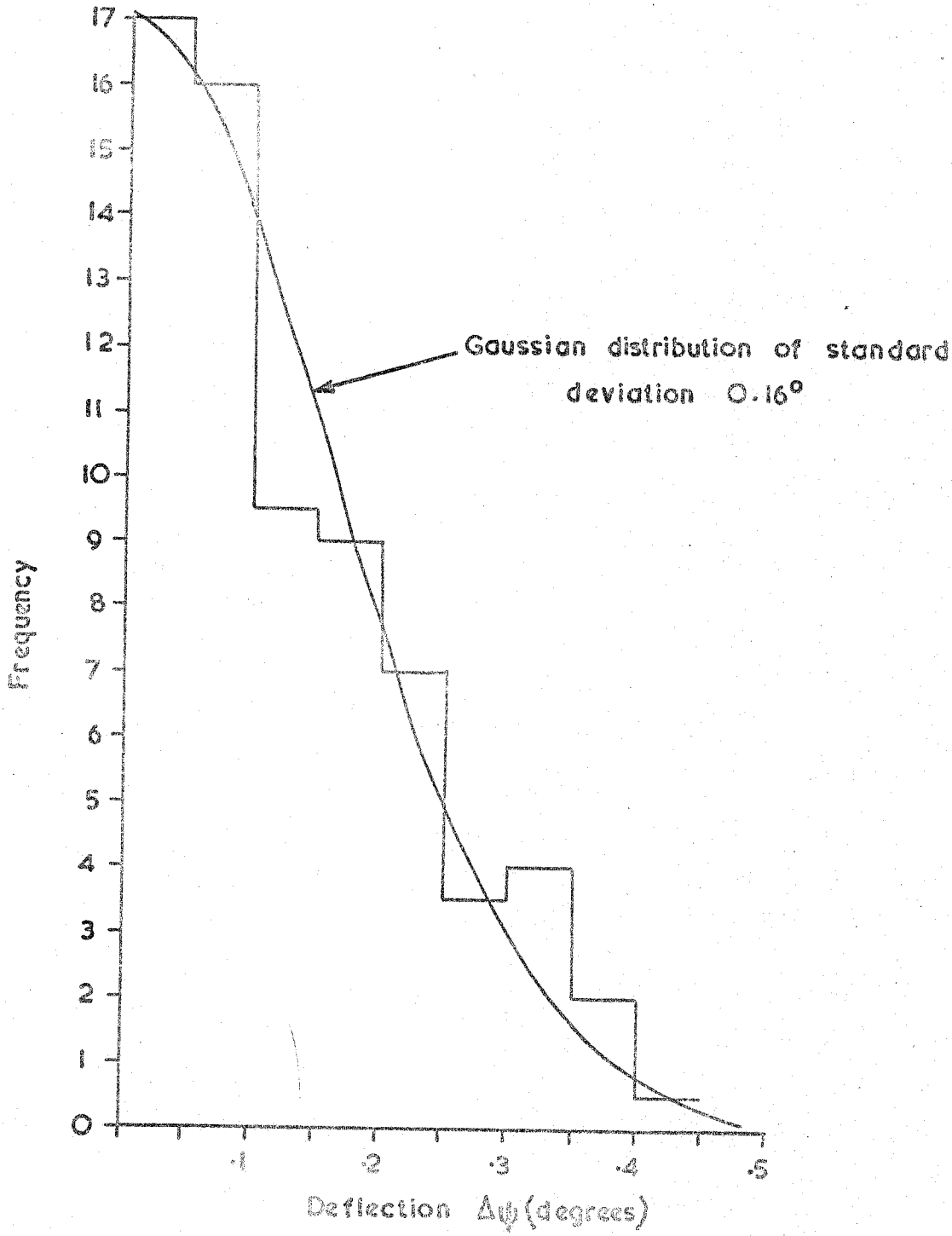
17
16
15
14
13
12
11
10
9
8
7
6
5
4
3
2
1
0
Frequency
Gaussian distribution of standard deviation 0.16°
·1
·2
·3
·4
·5
Deflection Δψ (degrees)

non-gaussian. The implications of this and of other possible non-gaussian effects are considered in Section 3.3.3.

3.4.2 The estimation of measurement noise

A proportion of all recorded events contain EAS muons which pass through the central rectangular "hole" in the magnet. This contains minimal scattering material so that coulomb scattering may be considered as taking place only in the material of the flash tubes and electrodes. The total amount of glass and aluminium in a single arm of the Mk2 spectrograph is 22.3 gm cm^{-2} and 5.8 gm cm^{-2} respectively. For a muon of momentum p, in GeV/c, the r.m.s. lateral deviation Δx, in cms, due to multiple coulomb scattering in one arm, using the formula given by Rossi (1952) is found to be:

$$\Delta x = \frac{0.103}{p}$$

The arm length of the Mk2 spectrograph is 85.9 cms so that the r.m.s. angular deviation, δ, in degrees, corresponding to the above lateral uncertainty is:

$$\delta = \frac{9.65 \times 10^{-2}}{p}$$

The observed contribution in angular deflection for EAS "hole" muons is shown in Figure 3.4. The standard deviation, σ_T, of this distribution is 0.16 $\pm$ 0.01 degrees. Denoting the standard deviation of the distribution in angular deflection due to measurement noise alone as σ_m we may write,

$$\sigma_T = \frac{\int_0^\infty S(p) \cdot (\sigma_m^2 + \delta^2)^{\frac{1}{2}} \, dp}{\int_0^\infty S(p) \, dp} \quad \ldots\ldots\ldots\ldots\ldots\ldots\ldots\ldots 3.2$$

where S(p)dp is the differential momentum spectrum of EAS muons. Using the spectrum derived from the Mk1 experiment, it is found that the value of σ_m obtained from Equation 3.2 is not significantly different from 0.16 $\pm$ 0.01 degrees.

FIGURE 3.5 The deflection spectrum of muons, measured using the Mk. 1 spectrograph, compared with that expected on the basis of an EAS model, (a) assuming a gaussian distribution in measurement noise characterised by a standard deviation of 0.3° and (b) assuming a compound distribution in measurement noise consisting of 90% with a standard deviation of 0.3° and 10% with a standard deviation of 0.6°.

Core distance interval : 250 m to 350 m.

Model : Orford and Turver (1969) ($A=1$, $n_s \propto E_p^{\frac{1}{4}}$)

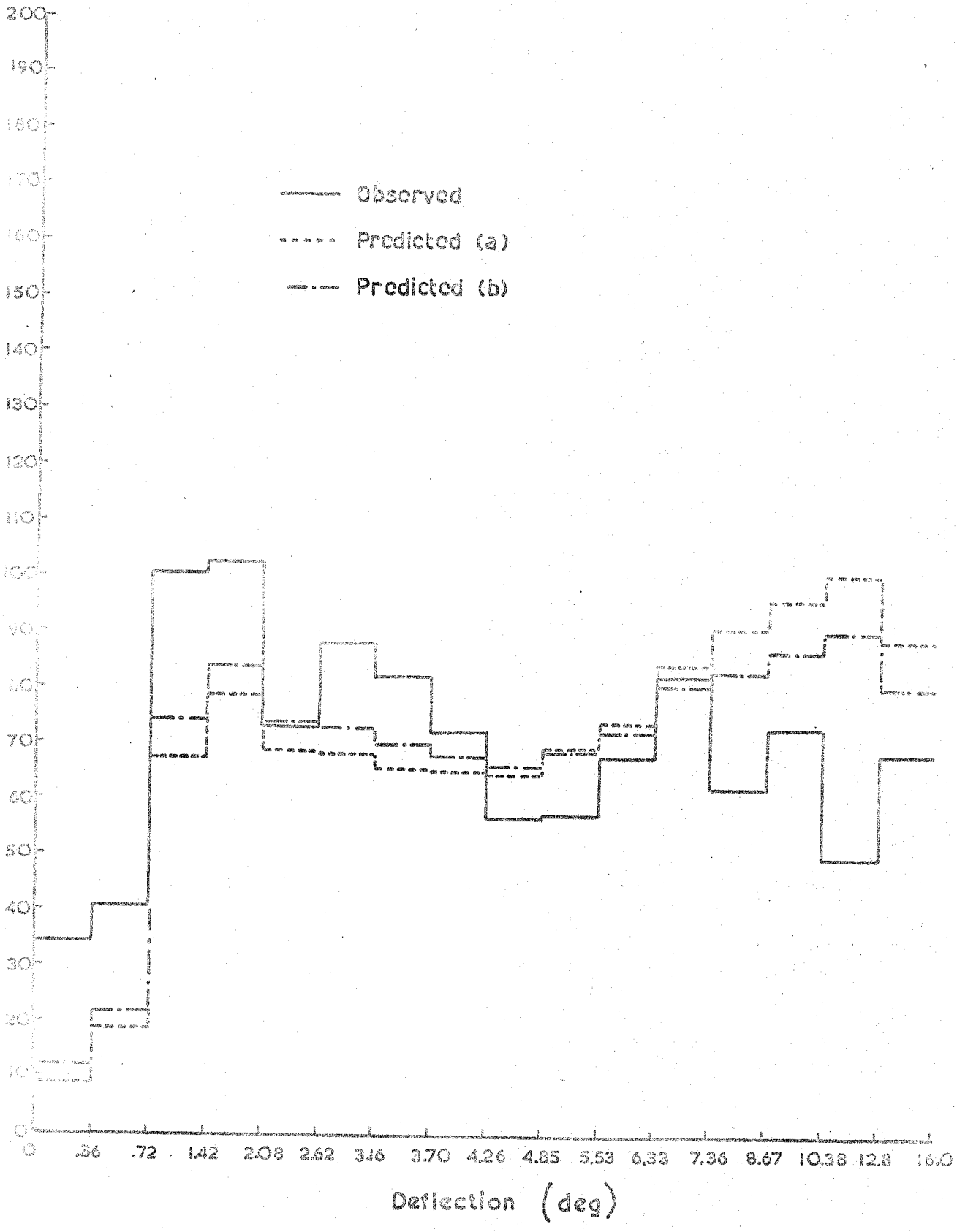
Observed
Predicted (a)
Predicted (b)
200
190
180
170
160
150
140
130
120
110
100
90
80
70
60
50
40
30
20
10
0
0
.36
.72
1.42
2.08
2.62
3.16
3.70
4.26
4.85
5.53
6.33
7.36
8.67
10.38
12.8
16.0
Deflection (deg)

3.4.3 The effect of non-gaussian measurement noise distribution

Although no direct evidence has been found indicating that the angular distribution due to measurement noise is other than gaussian, the distribution in angular deflection of EAS muons detected by the Mkl spectrograph and passing through the magnet hole was found to contain a small number ($<10\%$) forming an elongated tail to the distribution between 1.5 and 2.5 standard deviations from the mean. It is thought that these might have arisen from muons having "clipped" the front or back of the magnet. This is a very plausible explanation but one for which it has been difficult to obtain direct evidence owing to the absence of detectors to measure the front-back angle in the Mkl spectrograph. An alternative explanation is that such an extended tail is a characteristic of the angular distribution of estimated tracks about the "true" track when flash tubes are used as track delineators. Although unlikely in view of the recent work of Machin (1972) on this problem, this hypothesis, if correct would affect not only the measurement of those tracks passing through the magnet hole but also events in which muons passed through the magnet. To investigate the degree to which such a departure from the normal distribution might affect the interpretation of the data, a noise distribution consisting of two superimposed gaussians, the main one having a standard deviation of 0.3° and the other a standard deviation of 0.6° and containing, between 0.45° and 0.75°, 10% of the total area was used in the computation of the previously defined "weighting factors".

The effect of these modified weighting factors on the conversion of a momentum spectrum predicted by a model with $A = 1$ and $n_s \propto (k, E_p)^{\frac{1}{4}}$ to a deflection spectrum, is shown in Figure 3.5. It may be seen that in the $0 - 0.36^{\circ}$ deflection interval the predicted population is increased by 40%. In spite of this increase, however, the disparity between observed and predicted deflection spectra, is still large. It may be concluded, therefore, that even if there is a "real" non-gaussian noise distribution of the type described, the

disparity between these data and the predictions on the basis of a model in which A = 1 and $n_s \propto (k.E_p)^{\frac{1}{4}}$ is not significantly reduced.

3.5 Treatment of errors in the derivation of the momentum spectra

3.5.1 Introduction

Errors on spectral points arise from the following causes:

(i) the statistical uncertainty of the numbers in each deflection interval; this may be regarded as affecting the spectral shape.

(ii) the normalisation of the spectra; this affects the absolute intensities, but not the shape.

(iii) the angular resolution; again, this affects the spectral shape, but its consideration separately from (i) enables information on the spectral shape at momenta in the region of the m.d.m. to be obtained.

3.5.2 The effect of the sample size

Several methods exist for representing the uncertainty in a momentum spectrum resulting from statistical uncertainty in the deflection spectrum from which it is derived. The method used here has been developed and described by Orford (1968) and involves determining the flattest and steepest spectra which are produced by a single standard deviation fluctuation of the end cells of the deflection spectrum. The corresponding fluctuation in the non-extreme cells is found by percentile interpolation. This method has the advantage that the two spectra defined by the limits of the errors on the integral spectrum correspond directly to the two extreme cases of the differential spectra.

3.5.3 Normalisation of the spectrum

The integral spectra produced by the method described are normalised to the intensity, for the particular distance interval, at a momentum of 1 GeV/c obtained by Earnshaw (1968) from an absorption experiment. The error limits

FIGURE 3.6 The respective probabilities, for the Mk. 1 and Mk. 2 spectrographs of a muon, of observed deflection less than 0.36°, possessing a momentum greater than that corresponding to a pure magnetic deflection of 0.36°.

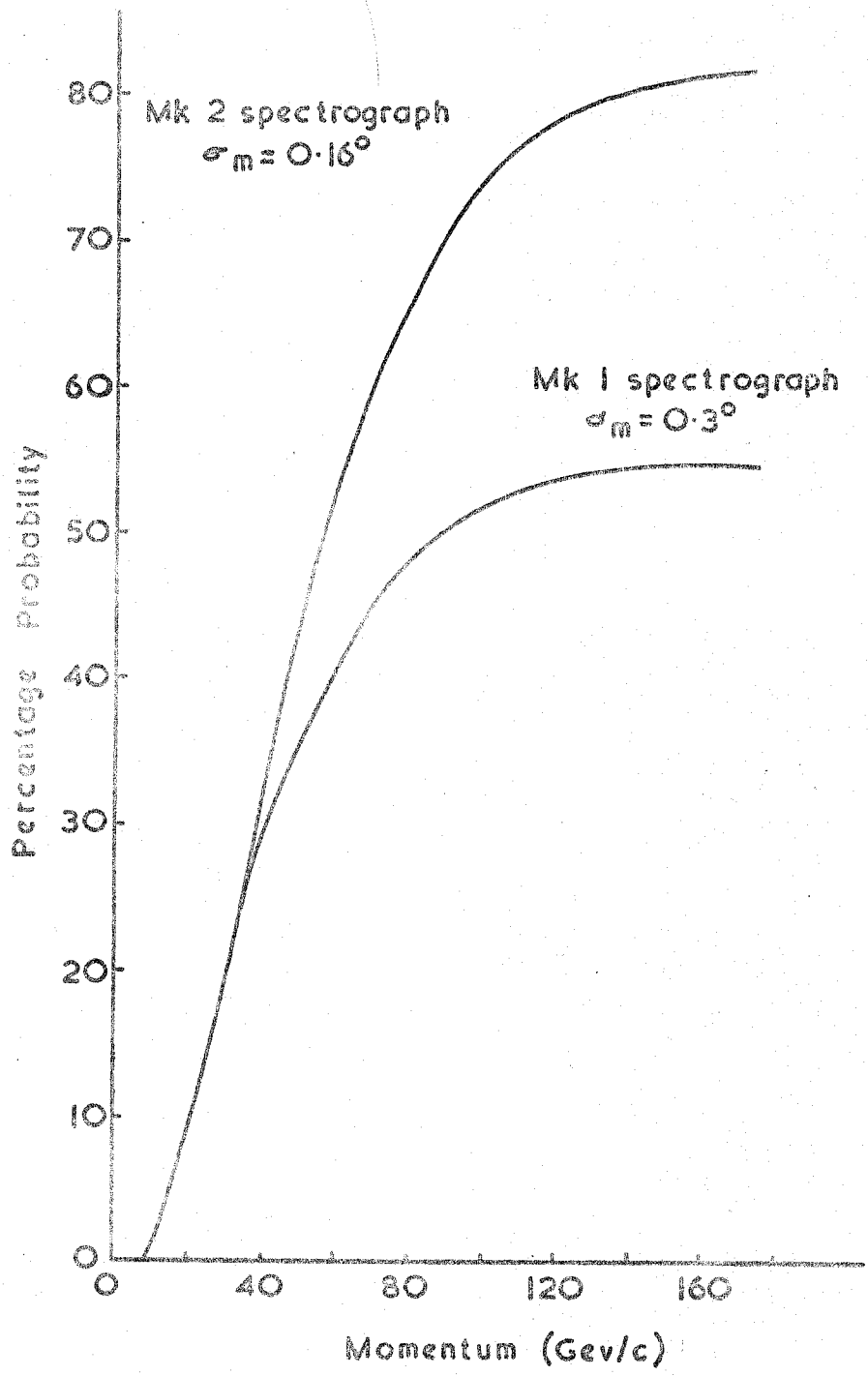
Mk 2 spectrograph
$\sigma_m = 0.16°$
Mk 1 spectrograph
$\sigma_m = 0.3°$
Percentage Probability
0
10
20
30
40
50
60
70
80
0
40
80
120
160
Momentum (Gev/c)

on the spectrum points are then modified by the quadratic addition of the percentage uncertainty in these absolute intensities.

3.5.4 Consideration of the effects of angular resolution

The effects of the finite angular resolution are allowed for in the "weighting factors" used in the derivation of the momentum spectra, as described in Section 3.3.1. It is possible, however, by separately considering the angular resolution, to obtain information on the distribution of "true" high momentum particles within that terminal cell of the deflection spectrum corresponding to the highest momentum.

If the quantity

$$\int_{\Delta\Psi=0}^{\Delta\Psi = 0.36^{\circ}} S(p)\, w(p,\Delta\Psi)\, dp\, d\Delta\Psi$$

in which $S(p)\, d\Delta\Psi$ is an arbitrary momentum spectrum and $w(p,\Delta\Psi)d\Delta\Psi$ is the weighting function described in Section 3.3.1, is plotted against momentum then the curve obtained represents the probability of observing a muon of momentum p in the deflection interval 0° to 0.36°. If the intensity of muons is assumed to be a δ-function in momentum then the respective resulting curves for the Mk1 and Mk2 spectrographs are as shown in Figure 3.6. As the momentum tends to infinity (with coulomb scattering and magnetic deflection tending to zero as a consequence) it may be seen that the curves approach a maximum value which is governed solely by the r.m.s. measurement noise. In contrast, if a falling momentum spectrum is considered then the above curves will show a peak followed by a tail the steepness of which will depend upon the rapidity with which the momentum spectrum falls. The area under such a curve between the limits of momentum 47 GeV/c and infinity then gives the probability, N, of observing a muon of momentum greater than that corresponding to a magnetic deflection of 0.36°, within the deflection interval 0° to 0.36°. Thus we may write

$$N(>47\ \text{GeV/c}) = \int_{\Delta\Psi=0^{\circ}}^{\Delta\Psi=0.36^{\circ}} \int_{p=47}^{p=\infty} S(p)\, w(p,\Delta\Psi)\, dp\, d\Delta\Psi$$

This integral when evaluated for the momentum spectrum corresponding to the core distance interval 250 m to 350 m obtained from the Mk1 experiment and for that produced by the model "E" of Hillas when two different values of measurement noise corresponding to the Mk1 and Mk2 spectrographs are taken into account gives values of N, expressed in a percentage, as shown in Table 3.2.

TABLE 3.2

Core distance interval (m)	Origin of differential momentum spectrum	Measurement noise σ_m	N(> 47 GeV/c)
250 - 350	Mk1 spectrograph	0.3°	30.5
	"	0.16°	44.0
	Hillas' model "E"	0.3°	2.4
	"	0.16°	4

3.6 The predictions of angular deflection spectra from momentum spectra

It has been found useful, to facilitate comparison between theory and observation, to be able to predict an angular deflection spectrum expected from a given spectrum of momentum of muons incident at the spectrograph. The method of computation is effectively the reverse of the method used for determining the momentum spectrum described in Section 3.3.1, and uses the same matrix of weighting factors w_{ij}. The population of an interval in the deflection spectrum is thus:

$$N(\Delta\Psi_j) = \sum_i S(p_i)\, \Delta p\, w_{ij}$$

where S(p) is the ordinate of the differential spectrum under consideration.

Deflection spectra predicted in this manner are compared by using the standard χ^2 test. This method has been found to be very suitable for the comparison of various models with theory (Orford and Turver (1969)).

Chapter 4

Results from the Mk1 and Mk2 Experiments

4.1 Introduction

At the Budapest Conference in 1969 data for the momentum spectra of EAS muons from the Mk1 experiment were presented (Machin et al., (1969)). Minor modification of these data has resulted from an improvement in the air shower analysis for the period of time covering the operation of the Mk1 spectrograph. These modified data are presented in Section 4.2 together with the previously unpublished results of an investigation into the dependence of the momentum spectra of zenith angle and shower primary energy.

To complement and reinforce checks made on the muon data during the running of the Mk1 instrument, two particular aspects of the data have been studied in the light of improved statistics, namely the effect of possible systematic core location errors and the distribution of high momentum events in small intervals of distance from the shower core. Details of the previously unpublished results of this study are given in Section 4.3.

The preliminary data from the Mk2 instrument are presented in Section 4.5, and the validity of a comparison between these and the corresponding data from the Mk1 experiment is discussed in Section 4.4.

4.2 Further consideration of the Mk1 data

4.2.1. Momentum spectra

The momentum spectra of muons in EAS due to primaries of mean energy approximately 2×10^{17} eV and having zenith angles less than 40° have been derived for the core distance intervals 150 m to 250 m, 250 m to 350 m, 350 m to 450 m and 450 m to 600 m, taking into consideration improved air shower data. Although chiefly concerned with an enhancement of the accuracy of the zenith and azimuth angles of the shower core, this improvement in air shower data also involved an increase in the accuracy of core location. Resulting from this last mentioned

FIGURE 4.1 The integral momentum spectra of muons in EAS of mean primary energy~2 x 10^{17} eV having core zenith angles of less than 40°, for four intervals of core distance. The key indicates the mean core distances for the 150 m to 250 m, 250 m to 350 m, 350 m to 450 m, and 450 m to 600 m intervals respectively.

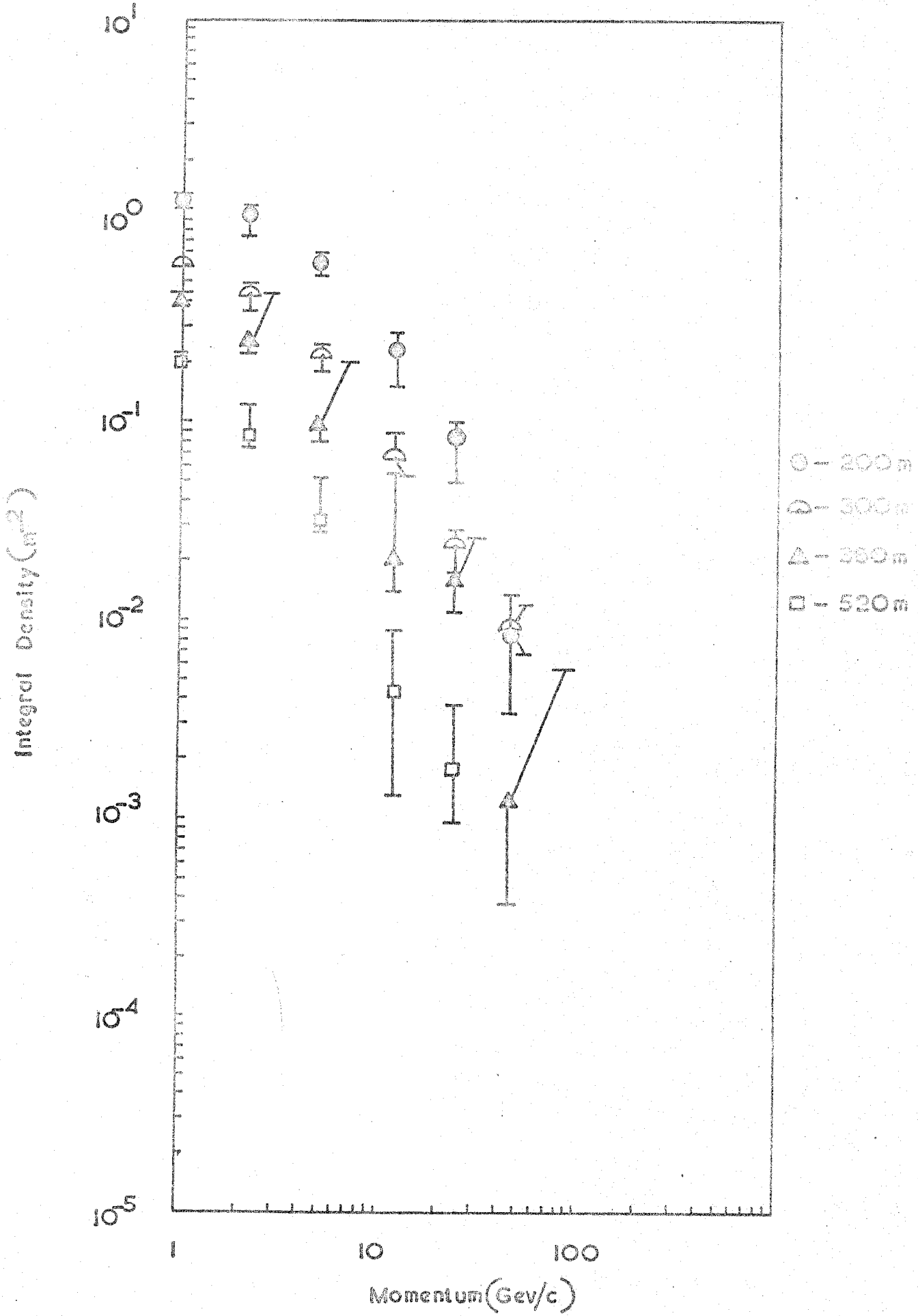
Integral Density (cm⁻²)
10¹
10⁰
10⁻¹
10⁻²
10⁻³
10⁻⁴
10⁻⁵
1
10
100
Momentum (Gev/c)
○ - 200 m
△ - 300 m
△ - 390 m
□ - 520 m

feature, a small proportion of showers originally analysed prior to revision of the analysis technique changed from one distance interval to an adjacent one.

The final integral spectra of muons detected by the spectrograph and falling in the stated core distance intervals are shown in Figure 4.1. The corresponding differential intensities are given in Table 4.1.

It is of interest to note that throughout the work reported here, in the derivation of the momentum spectra a more stringent iteration limit than has been applied than previously, namely that the predicted deflection spectrum should agree to within one per cent with the observed spectrum in the three extreme deflection cells corresponding to momenta greater than 8 GeV/c. The effect of this has been a slight reduction in the smoothness of the spectra for the 350 m to 450 m and 450 m to 600 m distance intervals in comparison with the spectra presented at Budapest.

Table 4.1

The differential intensities of muons in EAS of primary energies $\sim 2 \times 10^{17}$ eV, incident at zenith angles less than 40°, for various core distances. $((GeV/c)^{-1}m^{-2})$

Momentum (GeV/c) \ Distance (m)	200 m	300 m	380 m	520 m
1	$2.40\pm0.7 \times 10^{-1}$	$2.20^{+0.8}_{-0.7} \times 10^{-1}$	$1.50^{+0.6}_{-0.5} \times 10^{-1}$	$7.9^{+3.5}_{-2.8} \times 10^{-2}$
2	$1.90\pm0.6 \times 10^{-1}$	$1.35\pm0.2 \times 10^{-1}$	$8.80\pm1.5 \times 10^{-2}$	$4.9^{+1.8}_{-1.5} \times 10^{-2}$
5	$1.00\pm0.3 \times 10^{-1}$	$4.85\pm0.2 \times 10^{-2}$	$2.85\pm0.1 \times 10^{-2}$	$1.55\pm0.1 \times 10^{-2}$
10	$3.40\pm0.2 \times 10^{-2}$	$1.28\pm0.1 \times 10^{-2}$	$6.60\pm0.35 \times 10^{-3}$	$3.3\pm0.7 \times 10^{-3}$
20	$9.10\pm1.4 \times 10^{-3}$	$2.15\pm0.35 \times 10^{-3}$	$8.30\pm1.2 \times 10^{-4}$	$3.4^{+2.0}_{-1.7} \times 10^{-4}$
50	$6.70\pm1.7 \times 10^{-4}$	$2.00\pm0.4 \times 10^{-4}$	$1.10\pm0.35 \times 10^{-4}$	$2.1^{+3.1}_{-1.7} \times 10^{-5}$
100	$9.70\pm4 \times 10^{-6}$	$3.70^{+1.6}_{-1.3} \times 10^{-5}$	$2.40^{+1.5}_{-1.2} \times 10^{-5}$	$2.9^{+6.4}_{-2.8} \times 10^{-6}$

Table 4.2. The distribution of charge among muons recorded in prescribed intervals of lateral distance from the shower core and deflection in the spectrograph.

Table 4.2

r metres / Δψdeg.	200		300		380		520		Total	
	N^+	N^-	N^+	N^-	N^+	N^-	N^+	N^-	N^+	N^-
0 - 0.36	24.5	22	19.5	10	5	5	3	2	52	39
0.36 - 0.72	41	33	20	20.5	7	8	1	2	69	63.5
0.72 - 1.42	83	85	51	49.5	18	16.5	8	7	160	158
1.42 - 2.62	149.5	98	80.5	95	41	40.5	20	20	291	253.5
2.62 - 4.26	107.5	128.5	114	127	54	37	26	20	301.5	312.5
4.26 - 6.33	83	106.5	78	102	52	49	27	24	240	281.5
6.33 -16.0	168.5	157	165	159	109	98	51	50	493.5	464
	2 zero deflections		5 zero deflections		1 zero deflections					
Total	1289		1096		541		261		1607	1572
Charge Ratio	1.04±0.08		0.94±0.08		1.13±0.14		1.09±0.19		1.02±0.05	

FIGURE 4.2 The integral momentum spectra of muons falling between 250 m and 350 m from the cores of EAS of mean primary energy~2 x 10^{17} eV, for two intervals of core zenith angle, θ.

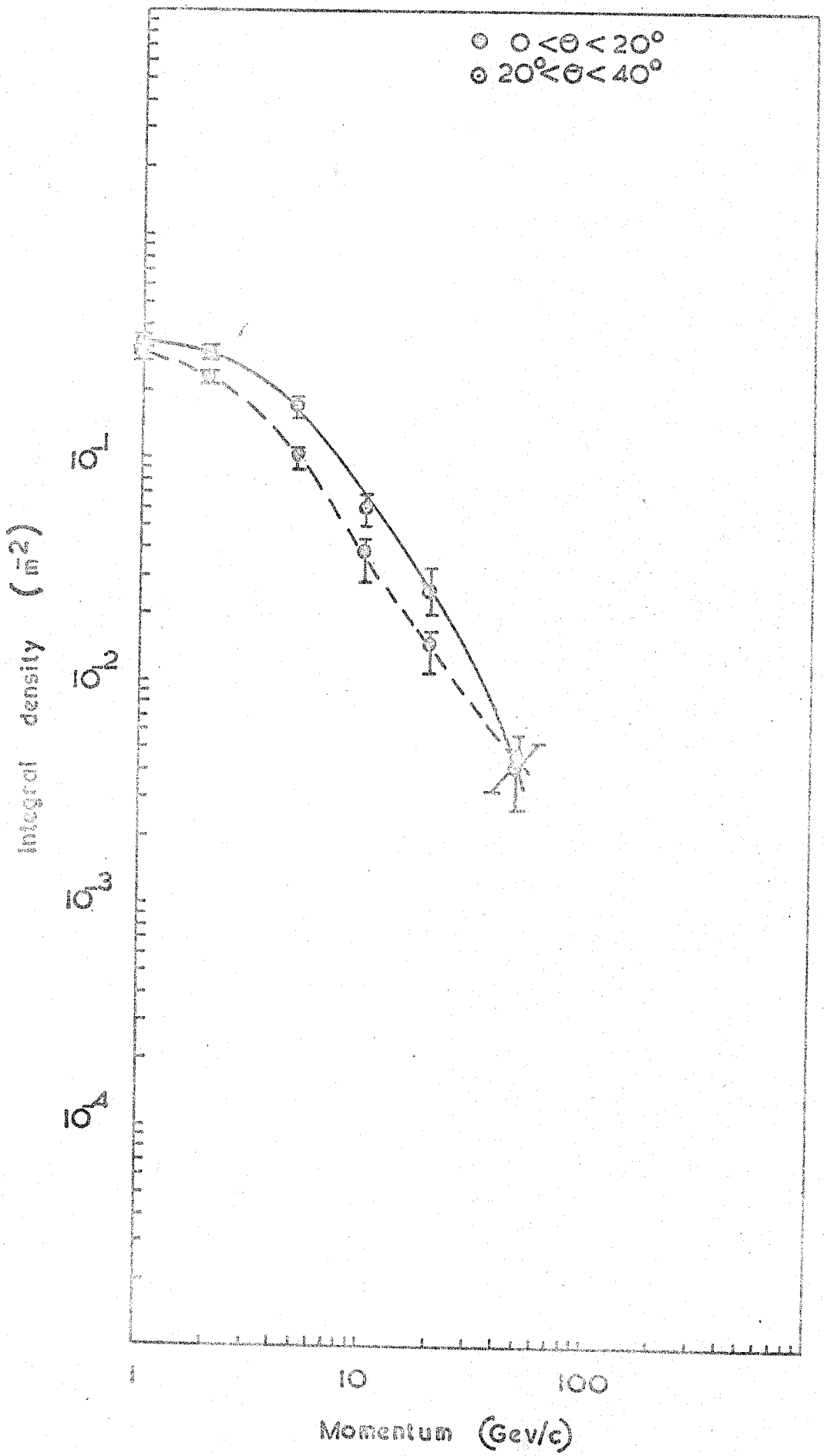
○ 0<θ<20°
⊙ 20°<θ<40°
Integral density (cm⁻²)
10⁻¹
10⁻²
10⁻³
10⁻⁴
1
10
100
Momentum (Gev/c)

4.2.2 The muon charge ratio

The charge ratio of those muons of momentum greater than 1 GeV/c falling in the core distance interval 150 m to 600 m and detected by the Mkl spectrograph has been found to be 1.02 ± 0.05. When the data is subdivided by angular deflection and core distance the resulting charge ratios obtained are those given in Table 4.2. The charge ratio of those muons which originate early in the development of the shower, say higher than 10 km, may be obtained using the simple relationship connecting muon momentum, p, height of origin, h, distance from the shower core at which the muon is observed, r, and the mean transverse momentum of the muon, p_t, namely $p/p_t = h/r$. If the maximum value of p_t is taken as 1 GeV/c then the value of p x r for all muons originating at a height greater than 10 km is given by:

$$p \times r > 10$$

For all data satisfying this condition the charge ratio has been found to be 1.17 ± 0.20.

4.2.3 The dependence of the momentum spectra on zenith angle

The final Mkl data has been analysed to investigate the variation of momentum spectra with zenith angle for the band of primary energies detected at Haverah Park, 10^{16} to 10^{18} eV, and for various distance intervals. To maintain statistically acceptable numbers, the showers have been sorted into two intervals of zenith angle only, namely 0° to 20° and 20° to 40°. The momentum spectrum for each interval has been derived using the method described in Section 3.3 involving the calculation of "weighting factors". In this context, however, it should be noted that the difference in the acceptance function for the two zenith angle bands necessitated the calculations of a separate set of "weighting factors" for each band.

The resulting momentum spectra for the two intervals of zenith angle are shown in Figure 4.2. It may be seen that the integral spectrum for large zenith angles is markedly flat between 1 GeV/c and 2 GeV/c whilst that for small zenith angles falls relatively steeply over the same region. The mean

FIGURE 4.3 The distribution of deflections in the Mk. 1 spectrograph for muons falling between 150 m and 250 m from the cores of EAS having $\theta < 40^{\circ}$ and primary energies within the ranges: 10^{16} eV to 10^{17} eV and 10^{17} eV to 10^{18} eV.

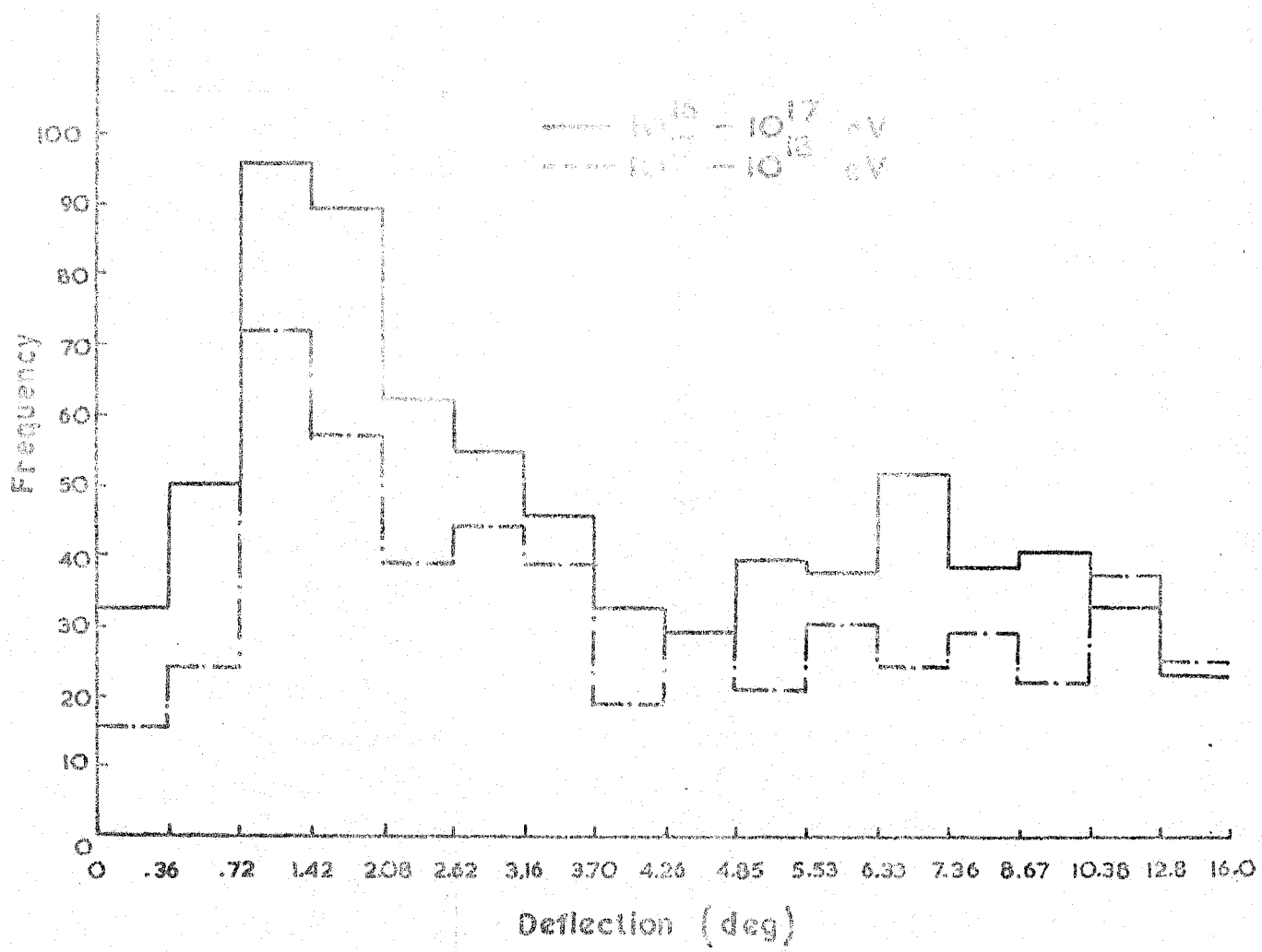
Frequency
100
90
80
70
60
50
40
30
20
10
0
0
.36
.72
1.42
2.08
2.62
3.16
3.70
4.26
4.85
5.53
6.33
7.36
8.67
10.38
12.8
16.0
Deflection (deg)

FIGURE 4.4. The distributions of deflections in the Mk. 1 spectrograph for muons falling between 250 m and 350 m from the cores of EAS having $\theta < 40^{\circ}$ and primary energies within the ranges: 10^{16} eV to 10^{17} eV and 10^{17} eV to 10^{18} eV.

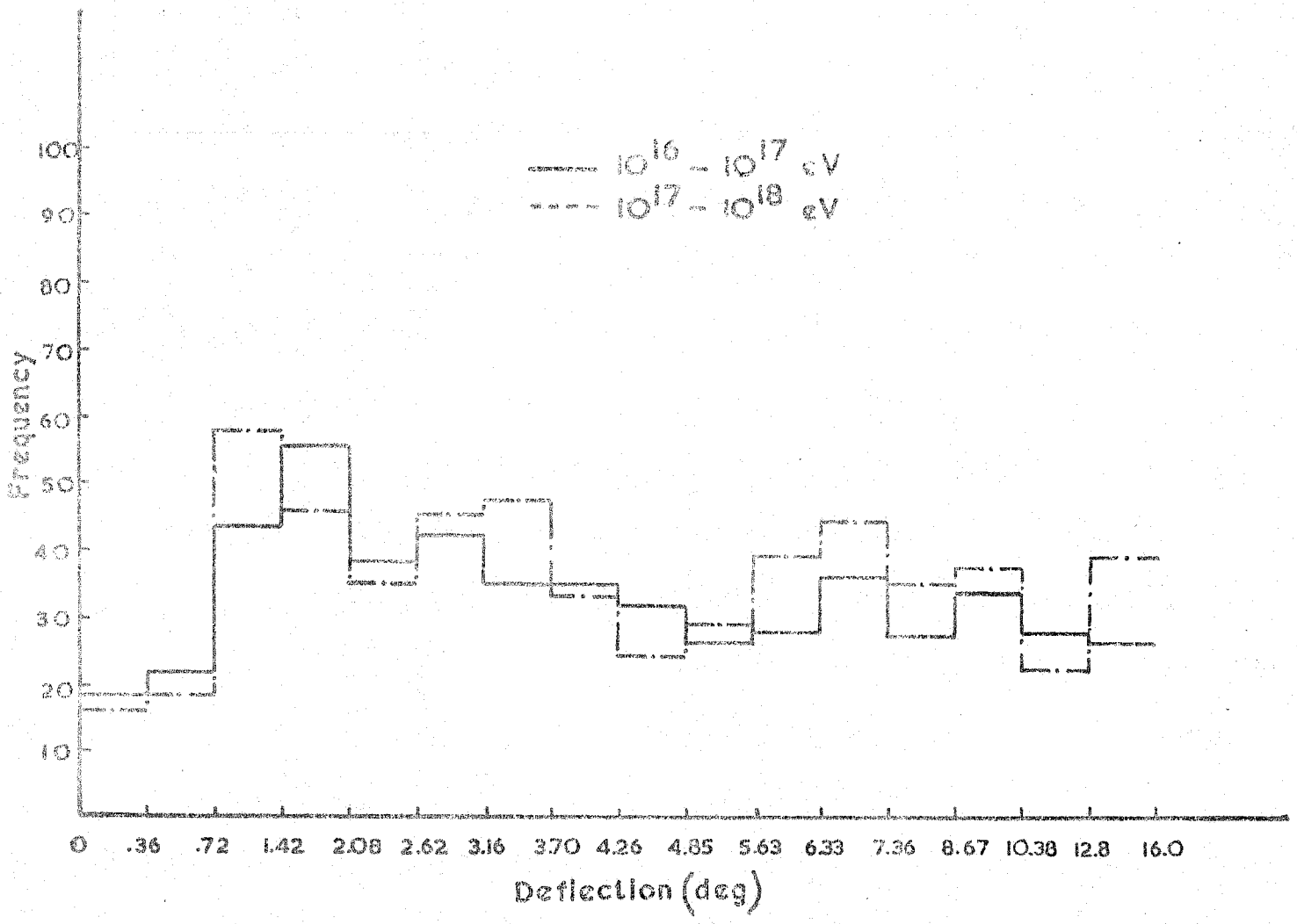
$10^{16} - 10^{17}$ eV
$10^{17} - 10^{18}$ eV
Frequency
100
90
80
70
60
50
40
30
20
10
0
.36
.72
1.42
2.08
2.62
3.16
3.70
4.26
4.85
5.63
6.33
7.36
8.67
10.38
12.8
16.0
Deflection (deg)

momenta for the 300 m distance interval typifying the spectra were:

Interval of zenith angle. (Degrees)	Mean momentum (GeV/c)
0 - 20	5.4 $\pm$ 0.5
20 - 40	9.5 $\pm$ 1.0

These values are in general agreement with those derived from models of EAS and reflect the progressive absorption of low energy muons in the atmosphere and iron magnet as the zenith angle increases.

4.2.4 The dependence of the momentum spectrum on primary energy

The dependence of momentum spectra on primary energy has been investigated within the range of primary energies detected at Haverah Park. For each of the core distance bands and for all zenith angles up to 40°, the data were sorted into two intervals of primary energy: 10^{16} eV to 10^{17} eV and 10^{17} eV to 10^{18} eV. The deflection spectra for the 150 m to 250 m and the 250 m to 350 m distance intervals are shown in Figures 4.3 and 4.4. For each distance interval a contingency test between the deflection spectra for each energy range indicated that there were no differences between the two spectra which had other than a high probability of occurring by chance.

4.3 Possible biasses in the Mkl spectrograph data

4.3.1 The effect of systematic core location errors

An estimation of the error involved in the measurement of the muon momentum spectra due to possible systematic errors in shower core location has been made. The data has been divided into 25 m distance intervals, and then re-grouped into larger intervals, namely 225 m to 325 m, 275 m to 375 m, 325 m to 425 m and 375 m to 475 m, thus simulating the effects of a systematic error in core location of 25 m. The deflection spectra for these bands have been

FIGURE 4.5 The integral momentum spectra of muons in EAS of mean primary energy 2×10^{17} eV and having $\theta < 40^{\circ}$, falling in three overlapping core distance intervals, the upper and lower extremes of which each differ by 25 m.

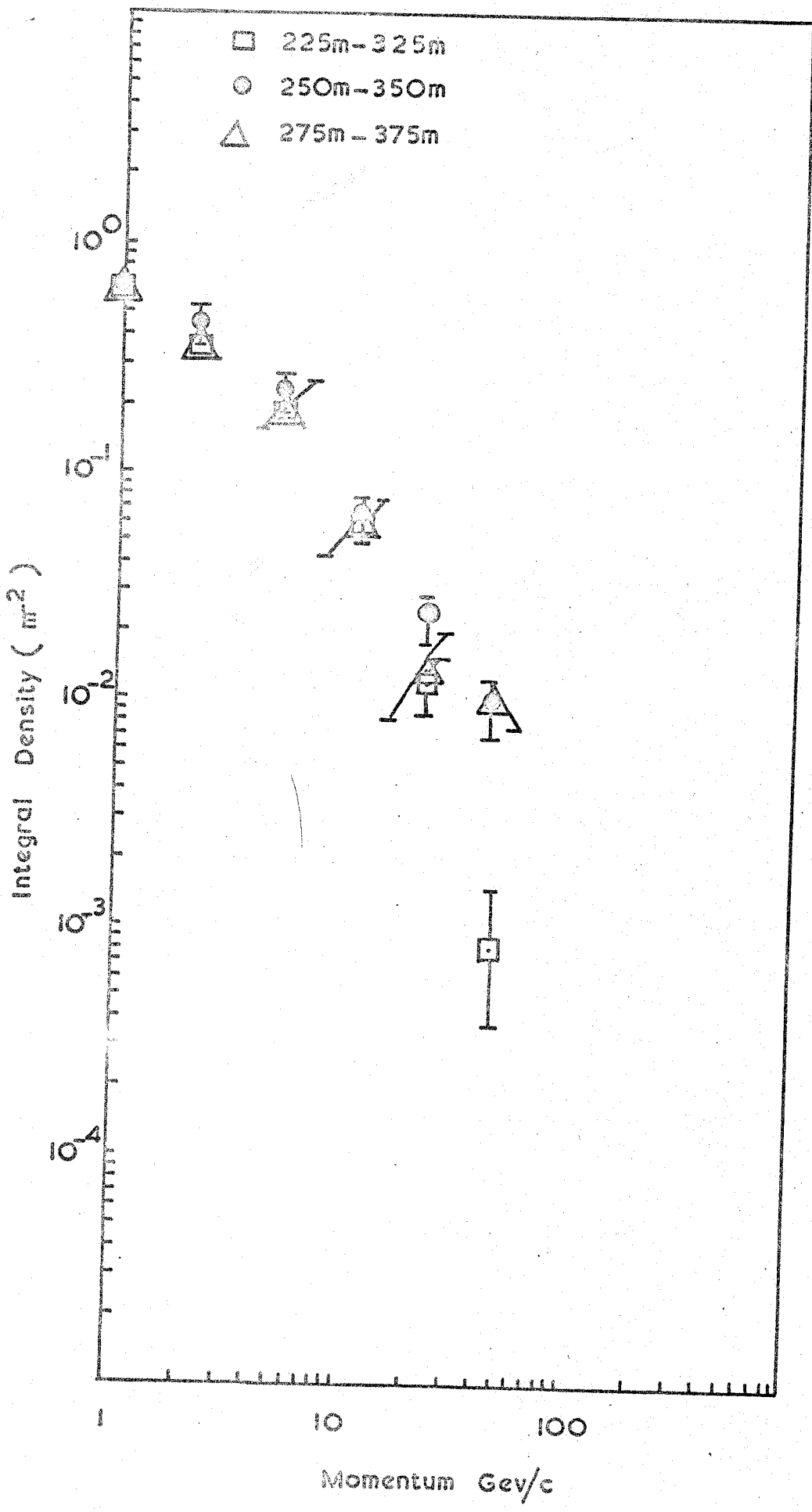
225m-325m
250m-350m
275m-375m
Integral Density (m⁻²)
10⁰
10⁻¹
10⁻²
10⁻³
10⁻⁴
1
10
100
Momentum Gev/c

FIGURE 4.6 The distributions in core distance for muons undergoing deflections less than 16° and 0.36°, respectively, in the Mk. 1 spectrograph. Also shown is that proportion of the observed distribution for $\Delta\Psi < 16^{\circ}$, expected to have $\Delta\Psi < 0.36^{\circ}$ on the basis of the 1971 model

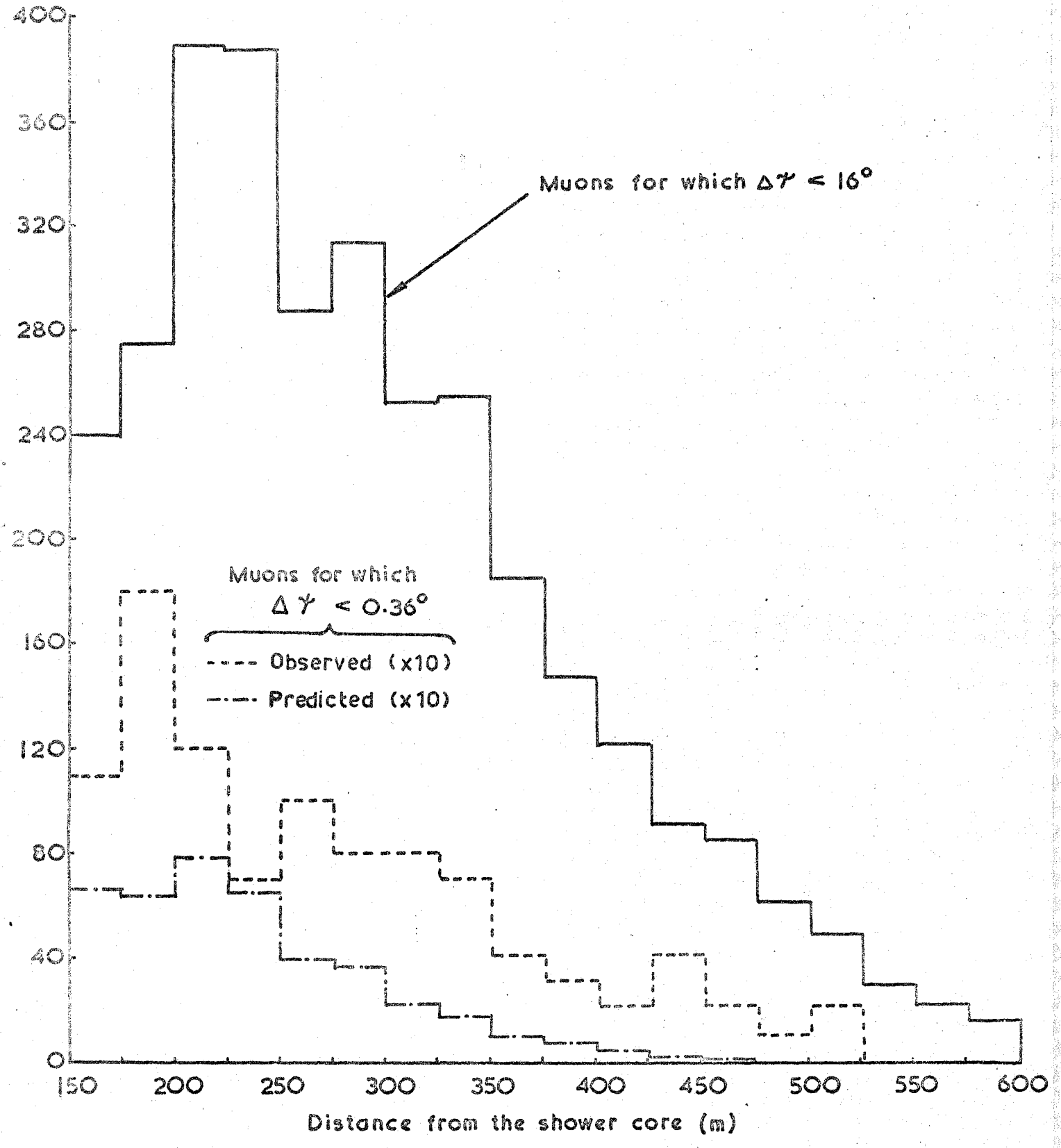
400
360
320
280
240
200
160
120
80
40
0
Muons for which Δγ < 16°
Muons for which
Δγ < 0.36°
---- Observed (x10)
-·-·- Predicted (x10)
150
200
250
300
350
400
450
500
550
600
Distance from the shower core (m)

converted to momentum spectra and compared with the corresponding momentum spectra for the normal 250 m to 350 m (see Figure 4.5) and 350 m to 450 m intervals. No fluctuations are apparent other than those of a statistical nature arising from sample size.

It is concluded that no appreciable distortions of the muon momentum spectra are caused by typical core location errors of the order of 25 m - even in the extreme cases of systematic over - or underestimation.

4.3.2 The distribution of high momentum events in core distance

Those muons detected by the Mk1 spectrograph and within it suffering a deflection of less than 0.36° have been sorted into 25 m intervals of distance from the shower core. The resulting distribution, together with the distribution for all muons undergoing a deflection of less than 16°, is shown in Figure 4.6. Also shown in this Figure is the distribution in core distance of the relative population of the 0° to 0.36° deflection interval predicted by the "1971" model as described in Chapter 6. Although agreement is not expected in terms of absolute numbers, resemblence in terms of general shape is expected. That this is in fact observed goes some way to providing evidence against any possible systematic bias towards selecting spurious high momentum muons from the relatively dense photographs obtained for events for which the shower core was comparatively close ($\lesssim$ 200 m) to the spectrograph.

4.4 Problems arising out of the data from the Mk1 spectrograph and their investigation using the Mk2 instrument

4.4.1 General

As the densities of muons possessing high momenta and falling at large core distances acquired greater statistical significance with enlargement of the sample size in the Mk1 experiment they also became increasingly difficult to reconcile with the lower values predicted by the majority of the then accepted models of EAS in which the primary was a proton. These models were typified by those of Hillas (1965), de Beer et al., (1966) and Orford and

FIGURE 4.7 The integral momentum spectrum, obtained from the Mk. I spectrograph data, for muons falling between 150 m and 250 m from the cores of EAS of mean primary energy 2×10^{17} eV and having $\theta < 40^{\circ}$, compared with various model predictions.

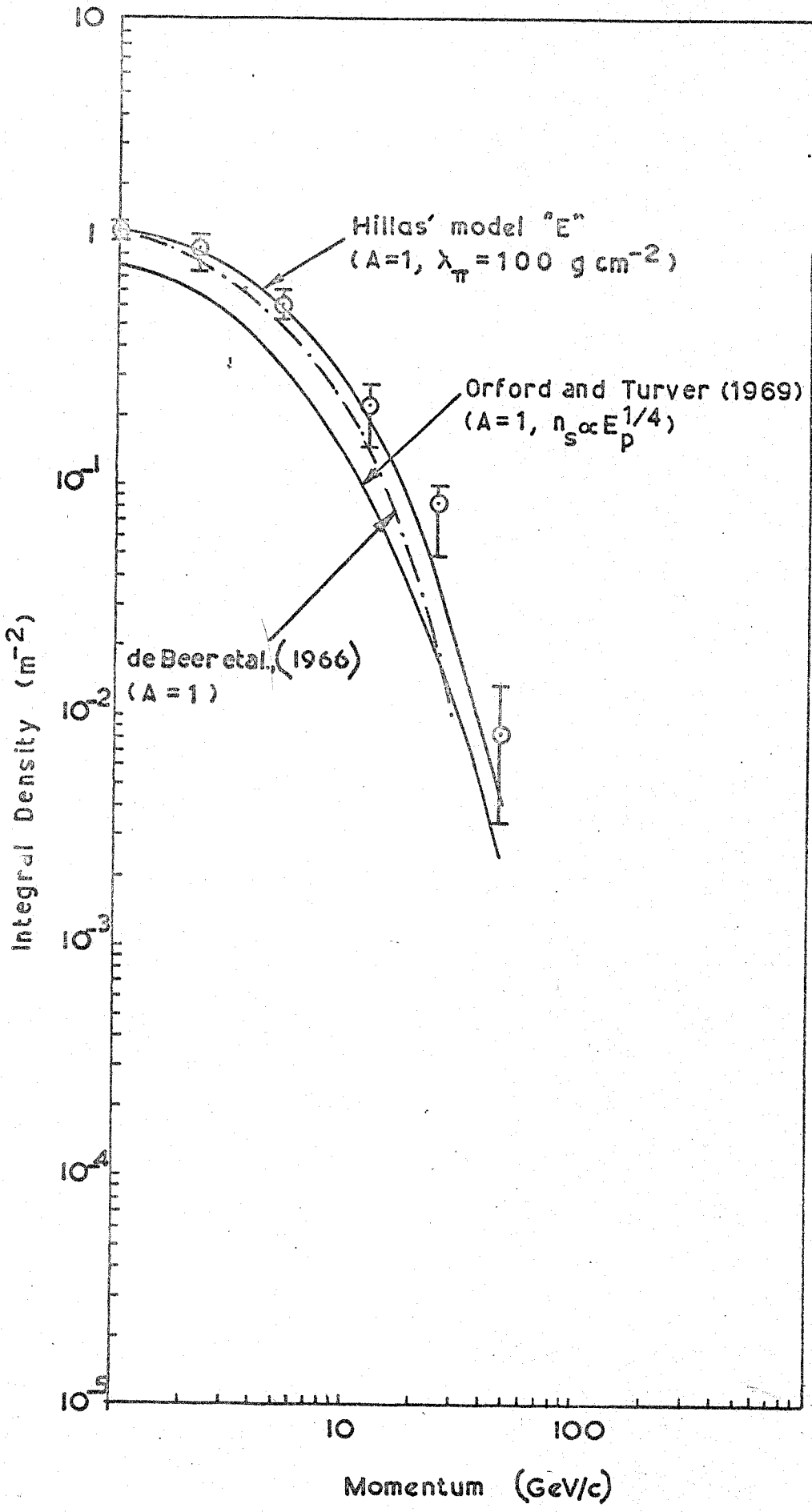
Hillas' model "E"
(A=1, λπ=100 g cm⁻²)
Orford and Turver (1969)
(A=1, ns∝Ep^1/4)
de Beer et al., (1966)
(A=1)
Integral Density (m⁻²)
Momentum (GeV/c)
10
1
10⁻¹
10⁻²
10⁻³
10⁻⁴
10⁻⁵
10
100

FIGURE 4.8 The integral momentum spectrum, obtained from the Mk. 1 spectrograph data, for muons falling between 250 m and 350 m from the cores of EAS of mean primary energy $\sim$ 2×10^{17} eV, and having $\theta < 40^{\circ}$ compared with various model predictions.

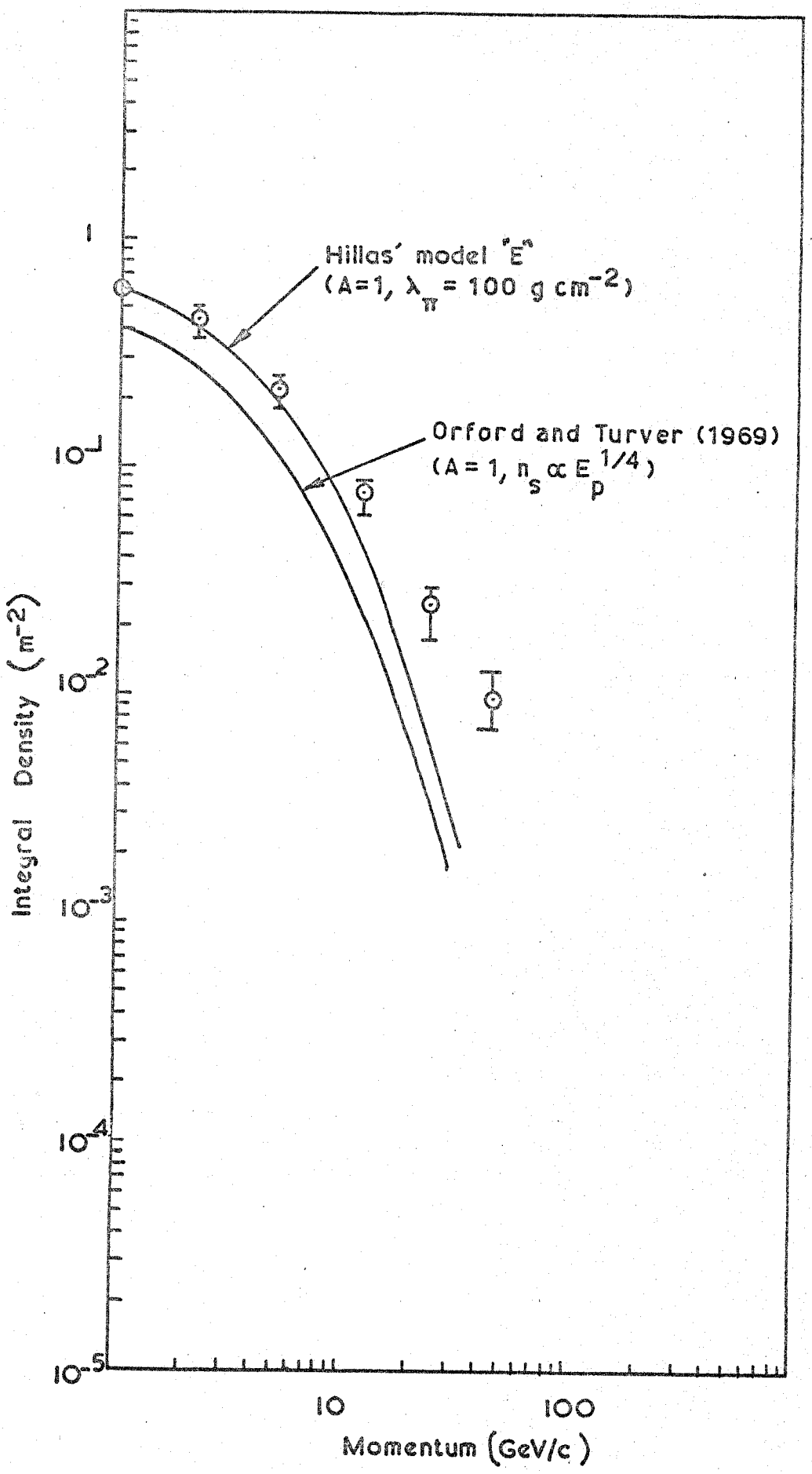
Hillas' model 'E^'
(A=1, λπ = 100 g cm⁻²)
Orford and Turver (1969)
(A = 1, ns ∝ Ep^1/4)
Integral Density (m⁻²)
1
10⁻¹
10⁻²
10⁻³
10⁻⁴
10⁻⁵
10
100
Momentum (GeV/c)

FIGURE 4.9 The integral momentum spectrum, obtained from the Mk.1 spectrograph data, for muons falling between 350 m and 450 m from the cores of EAS of mean primary energy 2×10^{17} eV and having $\theta < 40^{\circ}$, compared with various model predictions.

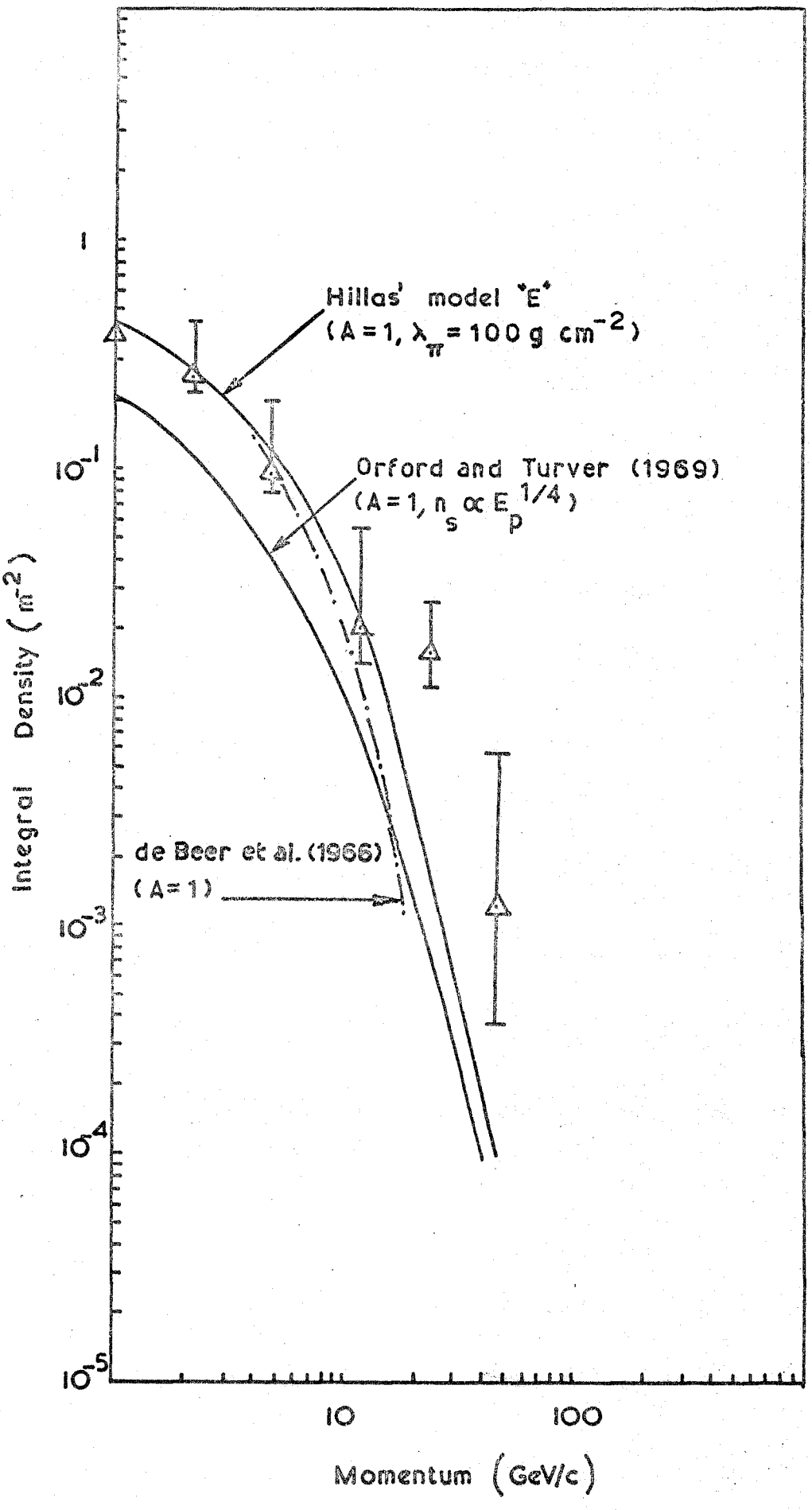
Hillas' model 'E'
(A = 1, λ_π = 100 g cm^{-2})
Orford and Turver (1969)
(A = 1, $n_s \propto E_p^{1/4}$)
de Beer et al. (1966)
(A = 1)
Integral Density (m^{-2})
1
10^{-1}
10^{-2}
10^{-3}
10^{-4}
10^{-5}
10
100
Momentum (GeV/c)

FIGURE 4.10 The integral momentum spectrum, obtained from the Mk.1 spectrograph data, for muons falling between 450 m and 600 m from the cores of EAS of mean primary energy 2×10^{17} eV and having $\theta < 40^{\circ}$ compared with various model predictions.

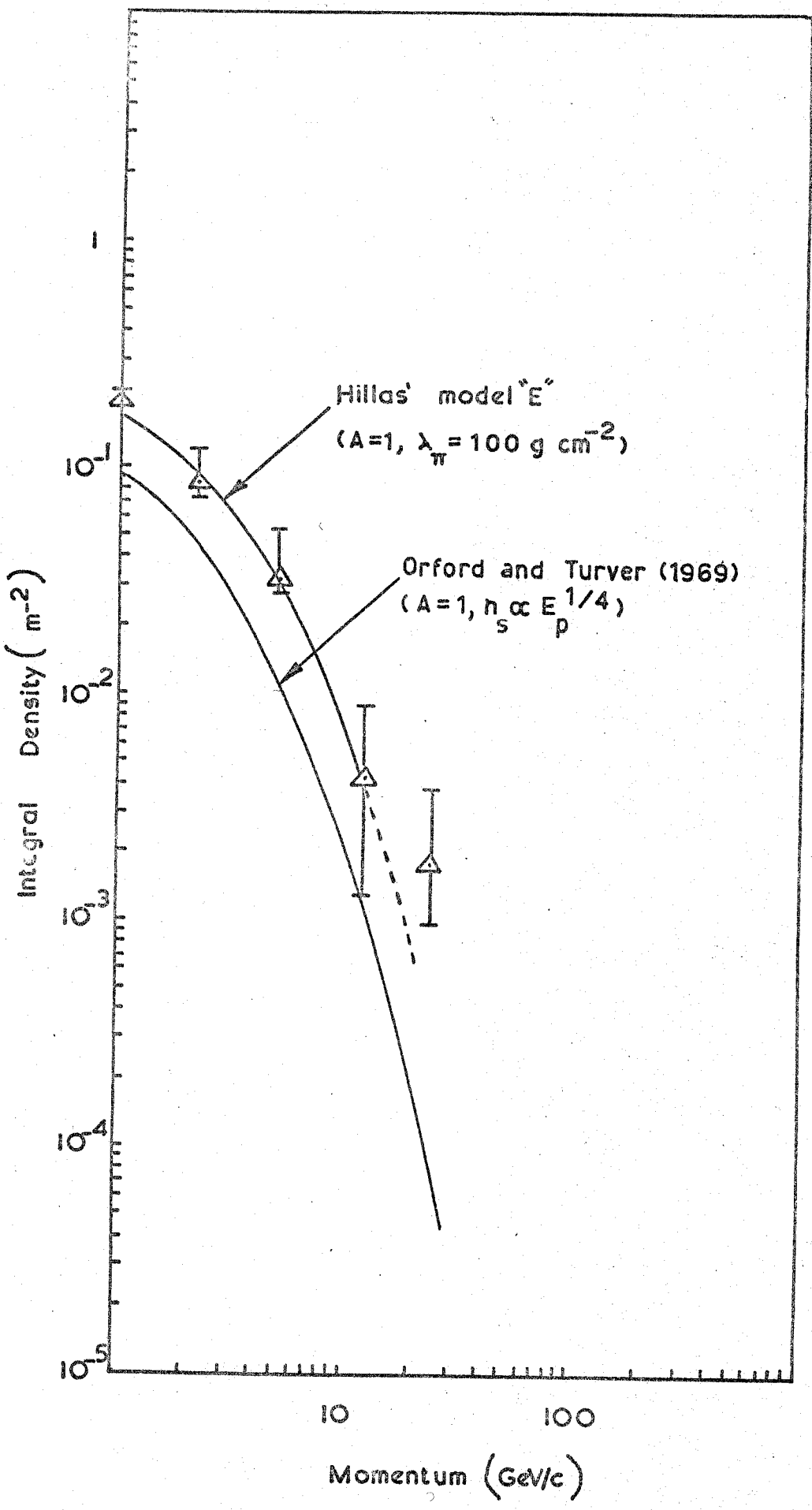
Hillas' model "E"
(A=1, λ_π = 100 g cm^{-2})
Orford and Turver (1969)
(A=1, $n_s \propto E_p^{1/4}$)
Integral Density (m^{-2})
1
10^{-1}
10^{-2}
10^{-3}
10^{-4}
10^{-5}
10
100
Momentum (GeV/c)

Turver (1969). The momentum spectra predicted by them are compared with the Mk1 data in Figures 4.7, 4.8, 4.9, and 4.10. Continued theoretical work by both Hillas (Private communication) and the Durham Haverah Park Group has reduced the size of the discrepancy but to a small extent only. With this in mind, the major function of the Mk2 spectrograph is seen as one of mounting a further experimental attack on the problem with the minimum aim of throwing the conflict between theory and experimental into sharper relief.

4.4.2 The method of testing agreement between model predictions and data

In order to give a numerical value to the level of agreement between the observed spectra of angular deflections in the magnet and those predicted by various models of EAS, the standard χ^2 test has been used. The test has been performed on the first ten intervals of deflection only, however, because of the possible difficulty in calculating the density of low momentum muons suffering larger deflections.

4.4.3 The statistical significance of the Mk2 data

To determine the point at which it would be justifiable to regard the Mk1 data as being supported or contradicted, a target figure has been calculated corresponding to the number of events required in the initial Mk2 spectrum to reduce to below one per cent the probability that fluctuations of a typical $A = 1, n_s = k E^{\frac{1}{4}}$ model spectrum could produce the observed deflection spectrum as a matter of chance. It was hypothetically supposed that the observed deflection spectrum would be similar to that obtained from the Mk1 spectrograph suitably modified to take into account the smaller measurement noise. This "observed" spectrum was compared with that predicted by the model of Orford and Turver (1969) in which $A = 1$ and $n_s = kE^{\frac{1}{4}}$ for each of the two distance intervals 150 m to 600 m and 250 m to 350 m.

The required number of events was determined as follows:

FIGURE 4.11 The variation, with the number of muons in a sample, of the probability that fluctuations in a deflection spectrum predicted using an EAS model could produce the deflection spectrum obtained from the Mk. 1 spectrograph data entirely as a matter of chance.
Model : Orford and Turner (1969) ($A = 1$, $n_s \propto E_p^{\frac{1}{4}}$)

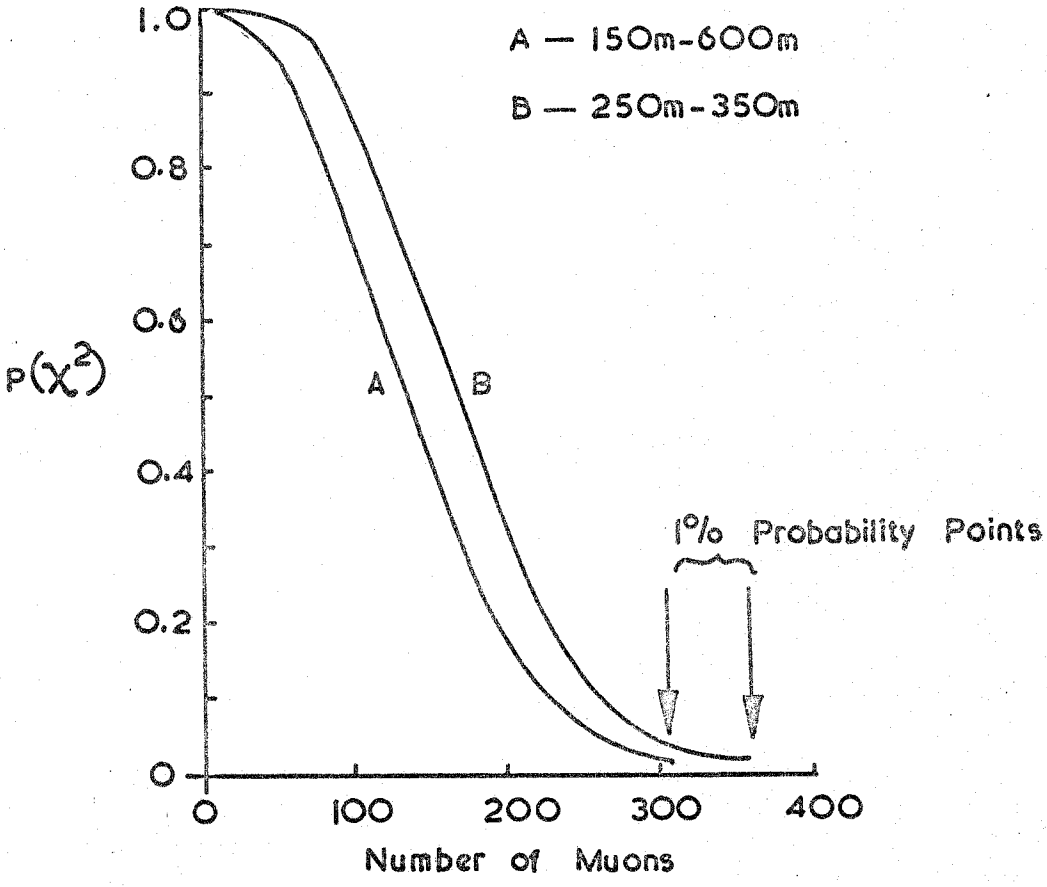
A — 150m-600m
B — 250m-350m
1.0
0.8
0.6
0.4
0.2
0
P(χ²)
A
B
1% Probability Points
0
100
200
300
400
Number of Muons

FIGURE 4.12 The distribution of deflections in the Mk. 2 spectrograph compared with the deflection spectrum obtained from the Mk. 1 spectrograph data assuming a measurement noise characterised by a standard deviation of 0.16^{o}.

Core distance interval : 150 m to 350 m

Mean primary energy : 2×10^{17} eV

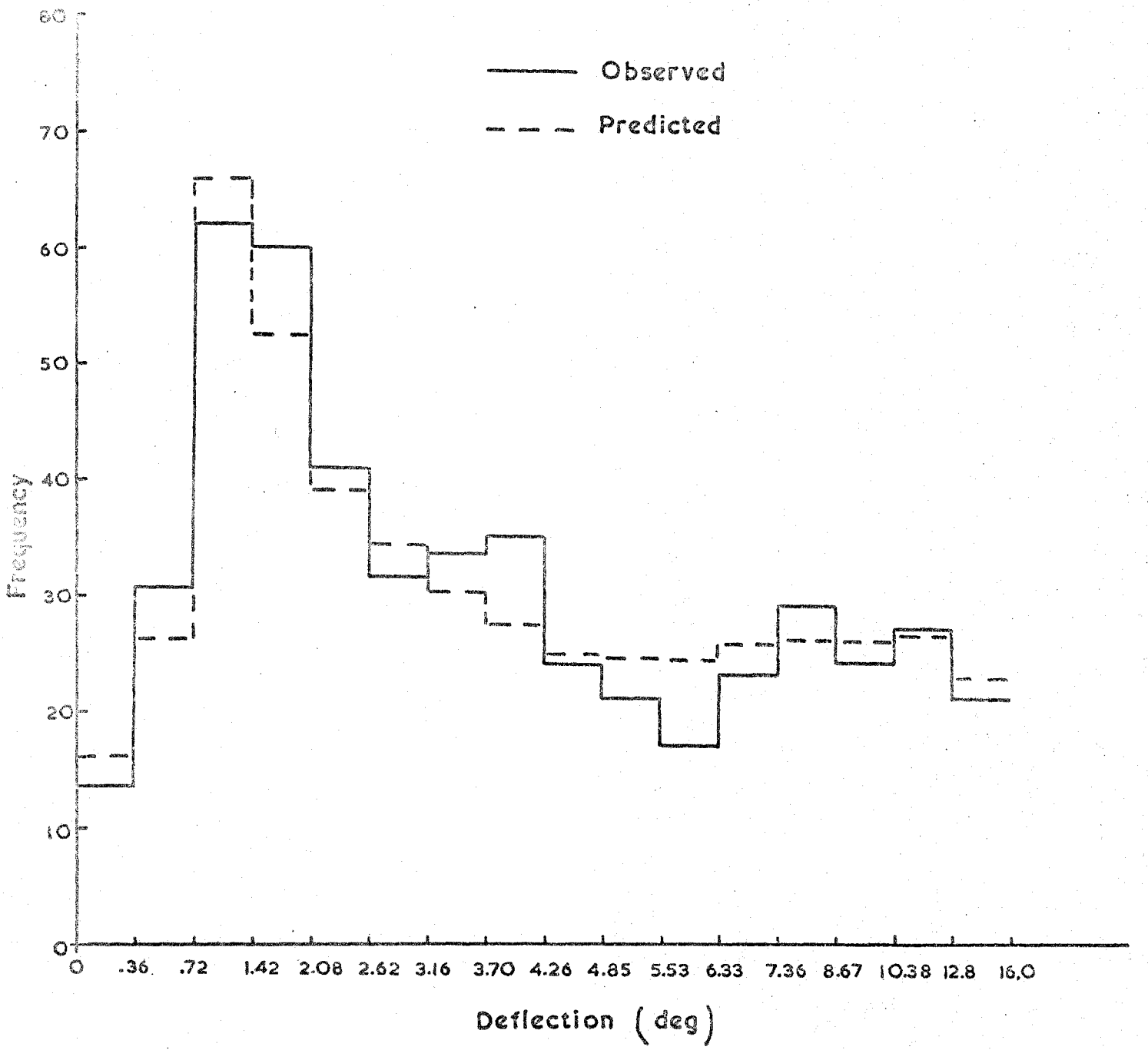
Observed
Predicted
Frequency
60
70
60
50
40
30
20
10
0
0
.36
.72
1.42
2.08
2.62
3.16
3.70
4.26
4.85
5.53
6.33
7.36
8.67
10.38
12.8
16.0
Deflection (deg)

(i) The "observed" spectrum was normalised to a given number of events.

(ii) This normalised spectrum was then allowed to fluctuate by plus and minus one standard deviation movement of the extreme cells. Intermediate spectrum points were then found by percentile interpolation.

(iii) The χ^2 values were calculated for the two spectra obtained by the method described in (ii) when each was compared with the model prediction.

(iv) The smaller χ^2 value was plotted against the number of events. (The smaller χ^2 value corresponds to the greater probability of the observed spectrum occurring by chance).

(v) The procedure was repeated for different numbers of events. On the resulting curve of χ^2 against the number of events, that number corresponding to a probability of one percent was taken as the target.

Curves of χ^2 against the number of events found in the above manner for the 150 m to 350 m and 250 m to 350 m core distance intervals are shown in Figure 4.11. It should be noted that these relate to the first ten intervals of the deflection spectrum only and that to compute the approximate number of events in the whole spectrum the value on the abscissa should be multiplied by 1.5. In this way, it may be estimated that to be able to differentiate between a Mk1 type spectrum and the spectrum obtained from the model for a proton initiated shower to a χ^2 probability of 1% the number of events must be greater than 460 for the 150 m to 350 m spectrum and greater than 540 for the 250 m to 350 m spectrum.

4.5 Preliminary results from the Mk2 spectrograph

Up to July 1971 a total of 493 muons had been analysed in the core distance band 150 m to 350 m, of which 165 were in the 250 m to 350 m band. The resulting deflection spectrum for the 150 m to 350 m core distance interval is shown in Figure 4.12 together with that obtained from the Mk1 spectrograph data

FIGURE 4.13 The distribution of deflections in the Mk. 2 spectrograph compared with the deflection spectra predicted by various models.

Core distance interval : 150 m to 350 m

Mean primary energy : 2×10^{17} eV

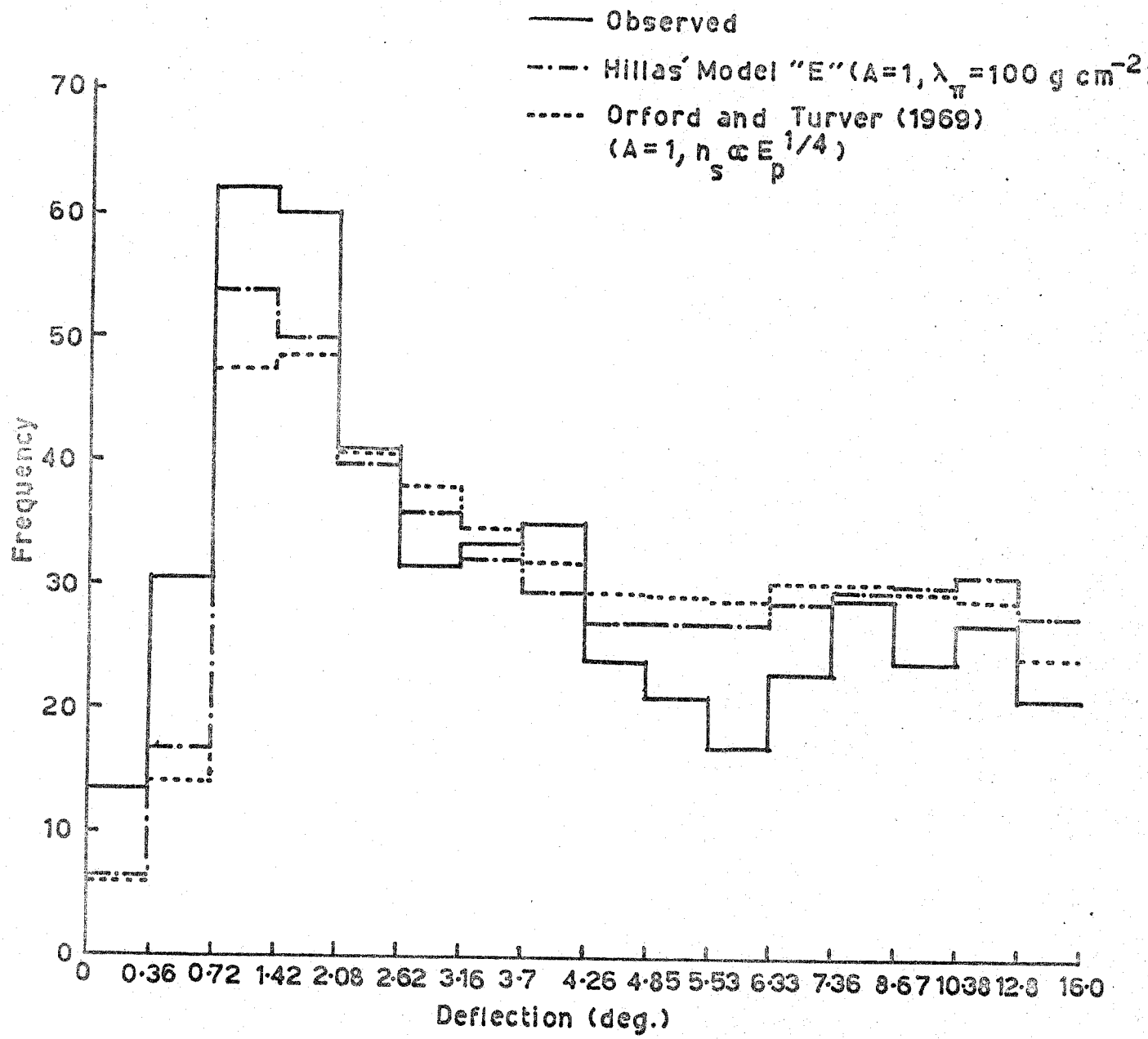
Observed
Hillas' Model "E" (A=1, λ_π=100 g cm^{-2})
Orford and Turver (1969)
(A=1, $n_s \propto E_p^{1/4}$)
Frequency
70
60
50
40
30
20
10
0
0
0·36
0·72
1·42
2·08
2·62
3·16
3·7
4·26
4·85
5·53
6·33
7·36
8·67
10·38
12·8
16·0
Deflection (deg.)

assuming an r.m.s. measurement noise of 0.16^{o}. From this limited comparison it appears that the Mk2 spectrograph data, so far, shows no indication of departure from that expected on the basis of the earlier experiment.

The deflection spectrum from the Mk2 spectrograph for the 150 m to 350 m interval is again shown in Figure 4.13, but here compared with the corresponding spectrum predicted by the model of Orford and Turver (1969) in which. $A = 1$ and $n_s = kE^{\frac{1}{4}}$ and with that predicted by Hillas' Model "E" for a proton primary. Because of the similarity between the deflection spectrum of the Mk2 experiment to date and that predicted from the Mk1 spectrograph data poor agreement is to be expected with the deflection spectrum predicted by the model of Orford and Turver. This is found to be so - the χ^2 probability of $6.2 \times 10^{-3}\%$ being very low. The Model "E" of Hillas, on the other hand, gives a slightly better fit - in this case the χ^2 probability is 8%. It is interesting to note that Hillas' model "E" gives similar results to the most recent model of the Durham Haverah Park Group for a proton primary (see Chapter 6).

4.6 The validity of the Mk1 data

Figure 4.11 gives some evidence in support of the general accuracy of the Mk1 data within statistical limitations. A χ^2 test has been performed on the two spectra and gives a value of 90% for the probability that the observed spectrum could occur as a matter of chance from the spectrum predicted on the basis of the earlier measurement. More statistically reliable evidence for or against the veracity of the Mk1 data will be available, at least for the 150 m to 350 m distance interval, only when the total population of the deflection spectrum for that interval is in excess of approximately 500.

Chapter 5

Determination of the height of origin of Muons in EAS from their deflections in the Earth's Magnetic Field

5.1 Introduction

The geomagnetic deflection of muons in EAS has been investigated in detail as a consequence of the suggestion made by Somogyi (1966) that the distortion of the charge ratio of muons by the geomagnetic field may yield information on their heights of origin. Experimental work on the basis of this proposal has been carried out by Orford et al.,(1967), and the present study is a detailed continuation of this work, reinforced by better statistics and more accurate calculations. Other workers (Kristiansen (1958), Clark et al., (1958), Oren (1959), Kamiya et al., (1962)) have made estimations of the deflection of muons in the geomagnetic field, but mainly in relation to the broadening effect on their lateral distribution function, rather than as a means of determining their heights of origin.

One potential advantage of using the geomagnetic effect to investigate the heights of origin of muons is that Coulomb scattering has very little effect on the geomagnetic deflection, provided the angular deflection is small. The geomagnetic deflection is superposed on all muons in the shower regardless of such scattering. Consequently, the deflection of muons in bulk, in the geomagnetic field, can be thought of as being directly related to their height of origin. Measurement of this bulk deflection is possible by consideration of the distortion produced in the charge ratio by the lateral shifts, in opposing directions, of positive and negative muons. The detailed consideration of the geomagnetic effect in this chapter is, in part, concerned with determining the degree to which the shape of the lateral distribution function influences the charge ratio distortion. It is shown that there is a sensitive dependence on the form of the lateral distribution function but

FIGURE 5.1 The orientation of the Haverah Park arrays with respect to the geomagnetic field. The broken lines pass through the centres of the "lobes". These "lobes" are designated $X^{+}Y^{+}$, $X^{+}Y^{-}$, $X^{-}Y^{\pm}$ on the basis of a Cartesian coordinate system having the X and Y axes along the geographic east and north respectively.

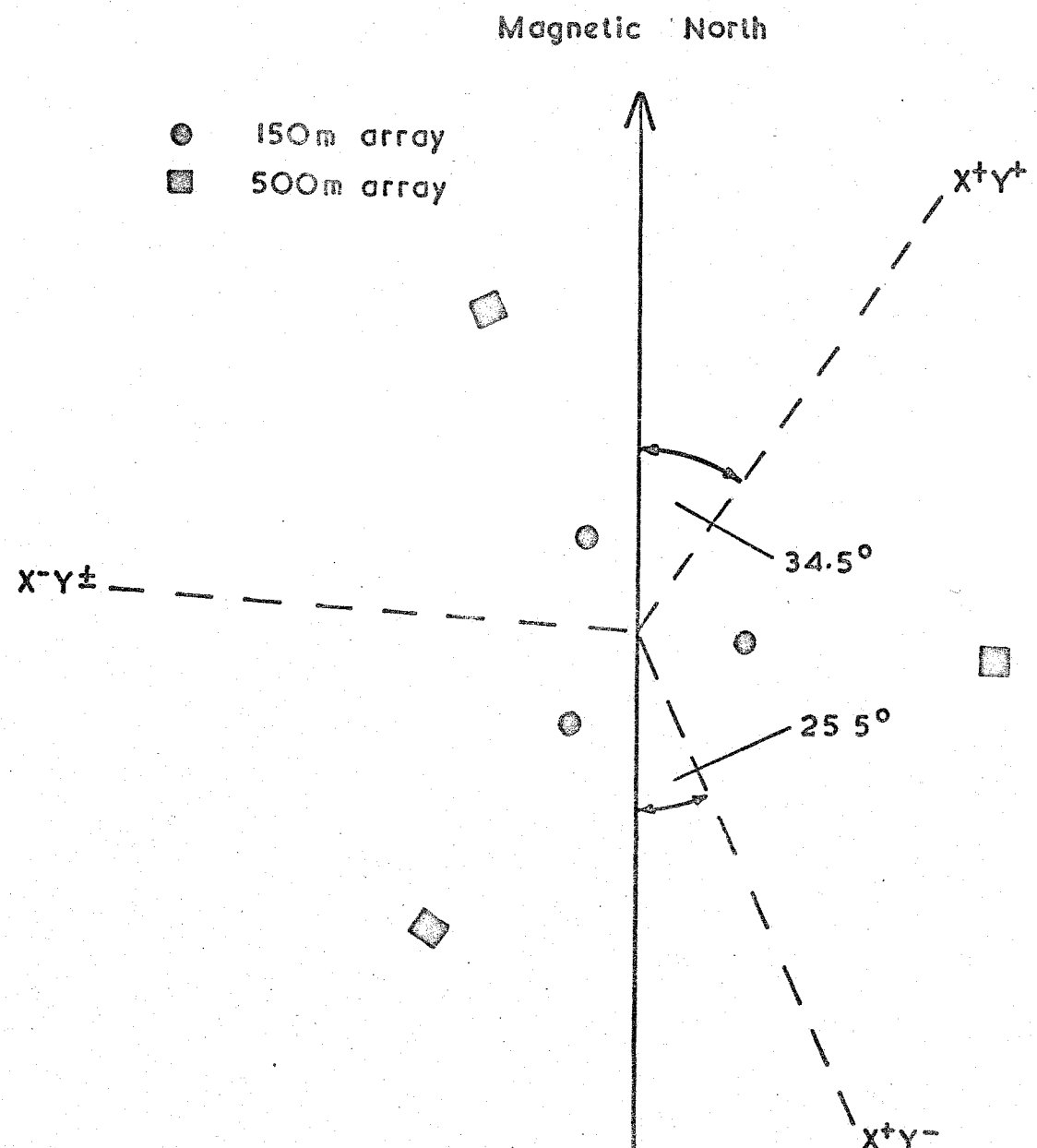
Magnetic North
150m array
500m array
X+Y+
34.5°
X-Y±
25 5°
X+Y-

that, because of the way in which the longitudinal development of the shower is linked with the lateral distribution, geomagnetic charge distortion is not sensitive to the height of origin of muons in EAS.

5.2 Calculation of the deflection of muons in the geomagnetic field and the resulting distortion of the charge ratio

5.2.1 Calculation of the deflection of a muon due to the geomagnetic field

A detailed mathematical treatment of the deflection of a charged particle in the earth's magnetic field is given in Appendix A. For given values of momentum and production height, the geomagnetic deflection of a positively charged muon which has an initial direction specified by zenith angle θ, and azimuth angle ϕ, is calculated for equal intervals of θ from 0° to 40° and of ϕ from 0° to 360°. The actual value of momentum used in the calculations is a mean value of the initial and final momenta, after energy loss due to ionisation has been taken into account. (See Appendix B). The mean of the deflection, weighted by the observed zenith angle distribution of showers for the whole array, is obtained for each value of ϕ. The projected component of this mean deflection along the direction of each of the three "lobe" lines, is then found (see Figure 5.1).There are three "lobe" lines, each of which passes through the centre of area of one of the three distinct regions in which, due to the geometry and triggering criteria of the array, the majority of the showers studied here, are detected.

5.2.2 Calculation of the distortion of the charge ratio of muons in EAS by the geomagnetic field

The charge ratio of muons in EAS having cores which fall in each of the three lobes is obtained by assuming (i) that in the absence of a geomagnetic field the lateral distribution of positive muons is the same as that for negative muons; (ii) that when the effect is considered to be present, the "two" lateral distributions, appropriate to μ^{+} and μ^{-}, are separated by twice the

mean geomagnetic deflection for that lobe; and (iii) that at a given distance the ratio of the ordinates of the "positive" and "negative" lateral distributions gives a value of the charge ratio. For the purposes of determining a mean height of origin a lateral distribution derived from the Mk 1 data and appropriate to the mean momenta considered, was used. Where the predictions of models have been compared with observation, the lateral distribution used has been that predicted by the model.

Estimation of the charge ratio for several distance-intervals was not possible because the number of events was statistically insufficient and therefore a single distance-interval of 150 m to 600 m was considered. The distance at which the charge ratio was determined theoretically, was the distance which divided the data in this interval into approximately equal halves, and this was found to be 300 ± 10 m.

Models of the development of the muon component of EAS have been compared with observation by using the predicted distribution in height of origin for muons of a particular momentum to derive the charge distortion expected due to the earth's magnetic field. In this technique the following weighting procedure was adopted:

If w_i is the predicted fraction of muons of momentum p originating from the ith height interval, and r_i the predicted geomagnetic charge ratio of these muons at the point of observation, then the fraction of positive muons, P_i, arriving at the point of observation from the ith height interval is:-

$$P_i = \frac{r_i \cdot w_i}{(1 + r_i)}$$

The total predicted charge ratio, R, defined as the ratio of the total number of positive to the total number of negative muons arriving at the point of observation and originating from all height intervals (i) up to the highest,

TABLE 5.1 (a) and (b) The geomagnetic deflection in the horizontal geographic north and east directions, of a positively charged muon in a shower having a core direction defined by zenith angle "THETA" and azimuth angle "PHI", and possessing a given sea-level momentum.

S.L. MOM.(GEV/C)= 2.0

HEIGHT(KMS)= 2.5

THETA(DEG)= 0.

PHI(DEG)	EAST(M)	NORTH(M)
0.	5.7	0.0

THETA(DEG)= 10.

PHI(DEG)	EAST(M)	NORTH(M)
0.	9.8	0.0
45.	9.0	-2.0
90.	7.0	-3.0
135.	4.7	-2.2
180.	3.7	0.0
225.	4.7	2.4
270.	6.9	3.3
315.	8.9	2.3

THETA(DEG)= 20.

PHI(DEG)	EAST(M)	NORTH(M)
0.	13.6	0.1
45.	12.1	-4.1
90.	8.0	-6.5
135.	2.9	-5.0
180.	0.5	0.0
225.	2.7	5.2
270.	7.8	6.7
315.	12.0	4.5

THETA(DEG)= 30.

PHI(DEG)	EAST(M)	NORTH(M)
0.	18.6	0.1
45.	16.6	-6.5
90.	10.1	-11.0
135.	1.0	-9.1
180.	-3.5	-0.0
225.	0.7	9.1
270.	9.8	11.3
315.	16.5	7.0

THETA(DEG)= 40.

PHI(DEG)	EAST(M)	NORTH(M)
0.	26.2	0.1
45.	23.9	-9.5
90.	14.3	-17.7
135.	-1.2	-15.5
180.	-9.5	-0.1
225.	-1.7	15.5
270.	13.9	18.1
315.	23.8	10.1

S.L. MOM.(GEV/C)= 2.0

HEIGHT(KMS)= 15.0

THETA(DEG)= 0.

PHI(DEG)	EAST(M)	NORTH(M)
0.	187.8	0.0

THETA(DEG)= 10.

PHI(DEG)	EAST(M)	NORTH(M)
0.	274.6	5.5
45.	253.1	-51.9
90.	196.5	-80.5
135.	133.5	-59.9
180.	104.8	2.4
225.	131.6	66.3
270.	194.5	89.6
315.	252.2	62.7

THETA(DEG)= 20.

PHI(DEG)	EAST(M)	NORTH(M)
0.	376.6	7.1
45.	336.9	-107.8
90.	223.5	-174.9
135.	83.4	-138.2
180.	14.9	0.4
225.	78.0	143.5
270.	219.5	187.2
315.	336.1	122.6

THETA(DEG)= 30.

PHI(DEG)	EAST(M)	NORTH(M)
0.	509.1	9.2
45.	453.9	-169.5
90.	277.8	-293.1
135.	32.3	-245.7
180.	-96.0	-2.8
225.	21.9	250.8
270.	272.0	312.5
315.	455.5	190.4

THETA(DEG)= 40.

PHI(DEG)	EAST(M)	NORTH(M)
0.	698.3	11.8
45.	632.8	-242.5
90.	382.2	-457.9
135.	-23.6	-410.3
180.	-251.7	-8.5
225.	-46.1	417.7
270.	376.7	493.0
315.	641.9	273.5

S.L. MOM.(GEV/C)= 5.0

HEIGHT(KMS)= 5.0

THETA(DEG)= 0.

PHI(DEG)	EAST(M)	NORTH(M)
0.	11.2	0.0

THETA(DEG)= 10.

PHI(DEG)	EAST(M)	NORTH(M)
0.	16.4	0.1
45.	15.1	-3.3
90.	11.7	-5.0
135.	7.9	-3.7
180.	6.3	0.0
225.	7.7	4.1
270.	11.4	5.6
315.	14.9	4.1

THETA(DEG)= 20.

PHI(DEG)	EAST(M)	NORTH(M)
0.	22.7	0.1
45.	20.3	-6.9
90.	13.4	-10.8
135.	4.9	-8.5
180.	0.9	0.0
225.	4.5	8.7
270.	12.9	11.4
315.	20.0	7.7

THETA(DEG)= 30.

PHI(DEG)	EAST(M)	NORTH(M)
0.	31.3	0.1
45.	28.0	-10.9
90.	17.0	-18.5
135.	1.7	-15.2
180.	-5.9	-0.0
225.	1.1	15.3
270.	16.3	19.1
315.	27.6	11.9

THETA(DEG)= 40.

PHI(DEG)	EAST(M)	NORTH(M)
0.	44.3	0.1
45.	40.4	-16.1
90.	24.1	-29.9
135.	-2.0	-26.2
180.	-16.0	-0.1
225.	-3.0	26.1
270.	23.2	30.7
315.	40.0	17.2

S.L. MOM.(GEV/C)= 5.0

HEIGHT(KMS)= 10.0

THETA(DEG)= 0.

PHI(DEG)	EAST(M)	NORTH(M)
0.	42.5	0.0

THETA(DEG)= 10.

PHI(DEG)	EAST(M)	NORTH(M)
0.	62.3	0.4
45.	57.4	-12.6
90.	44.5	-18.9
135.	30.2	-14.1
180.	23.8	0.2
225.	29.9	14.9
270.	44.1	20.1
315.	57.2	14.0

THETA(DEG)= 20.

PHI(DEG)	EAST(M)	NORTH(M)
0.	86.2	0.6
45.	77.1	-25.8
90.	50.9	-40.9
135.	18.7	-32.0
180.	3.4	0.0
225.	18.0	32.6
270.	50.1	42.4
315.	76.7	27.6

THETA(DEG)= 30.

PHI(DEG)	EAST(M)	NORTH(M)
0.	118.4	0.7
45.	105.7	-40.9
90.	64.3	-69.6
135.	6.7	-57.6
180.	-22.4	-0.2
225.	5.3	57.9
270.	63.1	71.6
315.	105.5	43.4

THETA(DEG)= 40.

PHI(DEG)	EAST(M)	NORTH(M)
0.	166.5	1.0
45.	151.6	-60.1
90.	90.8	-111.8
135.	-7.3	-98.5
180.	-60.1	-0.7
225.	-9.9	98.9
270.	89.5	115.2
315.	151.9	63.5

S.L. MOM.(GEV/C)= 15.0

HEIGHT(KMS)= 5.0

THETA(DEG)= 0.

PHI(DEG)	EAST(M)	NORTH(M)
0.	4.0	0.0

THETA(DEG)= 10.

PHI(DEG)	EAST(M)	NORTH(M)
0.	5.8	0.0
45.	5.4	-1.2
90.	4.2	-1.8
135.	2.8	-1.3
180.	2.2	0.0
225.	2.4	2.3
270.	3.6	3.2
315.	5.0	2.9

THETA(DEG)= 20.

PHI(DEG)	EAST(M)	NORTH(M)
0.	8.1	0.0
45.	7.3	-2.5
90.	4.8	-3.9
135.	1.7	-3.0
180.	0.3	0.0
225.	0.8	3.5
270.	3.6	5.2
315.	6.5	4.4

THETA(DEG)= 30.

PHI(DEG)	EAST(M)	NORTH(M)
0.	11.3	0.0
45.	10.1	-4.0
90.	6.1	-6.7
135.	0.6	-5.5
180.	-2.1	-0.0
225.	-0.8	5.4
270.	4.3	7.9
315.	9.0	6.0

THETA(DEG)= 40.

PHI(DEG)	EAST(M)	NORTH(M)
0.	16.1	0.0
45.	14.7	-5.9
90.	8.8	-10.9
135.	-0.8	-9.5
180.	-5.8	-0.0
225.	-2.8	8.9
270.	6.5	12.0
315.	13.5	8.0

S.L. MOM.(GEV/C)= 15.0

HEIGHT(KMS)= 7.5

THETA(DEG)= 0.

PHI(DEG)	EAST(M)	NORTH(M)
0.	8.9	0.0

THETA(DEG)= 10.

PHI(DEG)	EAST(M)	NORTH(M)
0.	13.0	0.0
45.	12.0	-2.7
90.	9.3	-4.0
135.	6.3	-3.0
180.	5.0	0.0
225.	5.8	4.0
270.	8.6	5.4
315.	11.6	4.4

THETA(DEG)= 20.

PHI(DEG)	EAST(M)	NORTH(M)
0.	18.1	0.0
45.	16.2	-5.5
90.	10.7	-8.7
135.	3.9	-6.8
180.	0.7	0.0
225.	2.9	7.3
270.	9.4	10.0
315.	15.4	7.5

THETA(DEG)= 30.

PHI(DEG)	EAST(M)	NORTH(M)
0.	25.1	0.0
45.	22.4	-8.8
90.	13.6	-14.8
135.	1.4	-12.2
180.	-4.7	-0.0
225.	-0.2	12.2
270.	11.8	16.1
315.	21.3	10.9

THETA(DEG)= 40.

PHI(DEG)	EAST(M)	NORTH(M)
0.	35.7	0.1
45.	32.6	-13.1
90.	19.5	-24.2
135.	-1.7	-21.2
180.	-12.9	-0.0
225.	-3.8	20.5
270.	17.1	25.5
315.	31.4	15.3

S.L. MOM.(GEV/C)= 50.0

HEIGHT(KMS)= 7.5

THETA(DEG)= 0.

PHI(DEG)	EAST(M)	NORTH(M)
0.	2.7	0.0

THETA(DEG)= 10.

PHI(DEG)	EAST(M)	NORTH(M)
0.	4.0	0.0
45.	3.7	-0.8
90.	2.9	-1.2
135.	1.9	-0.9
180.	1.5	0.0
225.	0.5	4.1
270.	0.9	5.6
315.	2.4	6.3

THETA(DEG)= 20.

PHI(DEG)	EAST(M)	NORTH(M)
0.	5.6	0.0
45.	5.0	-1.7
90.	3.3	-2.7
135.	1.2	-2.1
180.	0.2	0.0
225.	-1.8	3.7
270.	-0.6	6.9
315.	2.5	8.0

THETA(DEG)= 30.

PHI(DEG)	EAST(M)	NORTH(M)
0.	7.8	0.0
45.	7.0	-2.7
90.	4.2	-4.6
135.	0.4	-3.8
180.	-1.5	-0.0
225.	-4.3	3.6
270.	-1.5	8.5
315.	3.6	9.4

THETA(DEG)= 40.

PHI(DEG)	EAST(M)	NORTH(M)
0.	11.2	0.0
45.	10.2	-4.1
90.	6.1	-7.6
135.	-0.5	-6.6
180.	-4.0	-0.0
225.	-6.9	4.5
270.	-1.3	11.0
315.	6.2	10.7

S.L. MOM.(GEV/C)= 50.0

HEIGHT(KMS)= 15.0

THETA(DEG)= 0.

PHI(DEG)	EAST(M)	NORTH(M)
0.	10.9	0.0

THETA(DEG)= 10.

PHI(DEG)	EAST(M)	NORTH(M)
0.	16.1	0.0
45.	14.8	-3.3
90.	11.4	-4.9
135.	7.8	-3.7
180.	6.1	0.0
225.	6.3	6.9
270.	9.4	9.4
315.	13.4	8.9

THETA(DEG)= 20.

PHI(DEG)	EAST(M)	NORTH(M)
0.	22.3	0.0
45.	20.0	-6.8
90.	13.2	-10.7
135.	4.8	-8.3
180.	0.9	0.0
225.	1.7	10.0
270.	9.2	15.0
315.	17.5	13.1

THETA(DEG)= 30.

PHI(DEG)	EAST(M)	NORTH(M)
0.	31.0	0.0
45.	27.7	-10.9
90.	16.8	-18.4
135.	1.7	-15.1
180.	-5.9	-0.0
225.	-3.1	14.9
270.	11.0	22.3
315.	24.3	17.6

THETA(DEG)= 40.

PHI(DEG)	EAST(M)	NORTH(M)
0.	44.4	0.0
45.	40.5	-16.3
90.	24.2	-30.1
135.	-2.1	-26.3
180.	-16.0	-0.0
225.	-8.7	24.2
270.	15.7	33.7
315.	36.5	23.1

(i_{max}), is then given by:

$$R = \sum_{i=0}^{i=i_{max}} \frac{P_i}{(w_i - P_i)}$$

5.2.3 Typical predictions

Calculated values for the deflections of muons in the geomagnetic field, originating at a vertical height h above sea level and having a direction specified by zenith angle θ and azimuth angle ϕ, for two values of momentum and two values of height, are given in Tables 5.1(a) and 5.1(b). Values for any other momentum/height/θ/ϕ combination may be obtained with sufficient accuracy by extrapolation or interpolation of these data.

5.3 Possible sources of inaccuracy in the method

5.3.1 General

It is shown in Section 5.4 that the gross effect of the geomagnetic field on EAS muons at Haverah Park is not sufficiently masked by any competitive process to make it undetectable. Nevertheless, it is possible for the relationship between the charge ratio distortion and the height of origin of muons, on the one hand, and the extent to which the relationship is sensitive to the shape of the lateral distribution function, on the other, to be obscured by several sources of inaccuracy, both in the experimental method and in the theoretical calculations. These sources are considered in this chapter, and are shown to have a negligible effect, in the context of charge distortion, for the showers providing the data used in this study.

5.3.2 The muon charge ratio of the undistorted shower

The recent evidence of Machin et al., (1969) suggests that the overall charge ratio of muons in EAS is not significantly different from unity

in all momentum bands considered up to 60 GeV/c. This is in agreement with the work of Bennett and Greisen (1961), and, at the energies considered here, it is also to be expected from theory if kaon production, perhaps charge asymmetric, is dominated by charge symmetric pion production.

5.3.3. The effect of variations of the earth's magnetic field

Measurements made by Appleton (1934) indicated that the earth's dipole magnetic field varied as the inverse of the cube of the distance from the geocentre. Excluding the effect of local anomalies, current theory predicts just such a variation, (Runcorn (1956)), and measurements by Bowen et al., (1950), have confirmed this. On this basis the reduction in the magnetic field, at a height of 40 Km, is approximately 2% and is thus negligible for the purposes of the present calculations.

Temporal changes in the magnetic declination and inclination, typically of the order of 2% to 3%, over several years, have very little effect on the charge ratio predictions, and no attempt has been made to obtain very accurate values of these quantities. Thus the values used were those given by Kaye and Laby (1960), suitably corrected using the mean values of annual change. The corrected value of declination was 9°W and that of inclination $68{\cdot}5^{\circ}$.

5.3.4 The effect of the earth's electric field

Up to a height of 1 Km the earth's electric field is approximately 150V m^{-1}. Above 1 Km it decreases very rapidly until, at a height in the region of 5 Km, it reaches a value of about 20 V m^{-1} beyond which its decrease is less rapid. At 15 Kms it has a value of approximately 5 V m^{-1}, thereafter decreasing smoothly to 1 V m^{-1} at approximately 30 Km (Handbook of Geophysics, 1960).

Considering a non relativistic muon originating at a height h(Km) in a

FIGURE 5.2 The effect of projecting the geomagnetic deflection of a muon onto the plane of the shower front.

Lobe : X^{-} Y^{+}

Muon momentum : 14.9 GeV/c

Height of origin : 15 km

Shower zenith angle : 40°

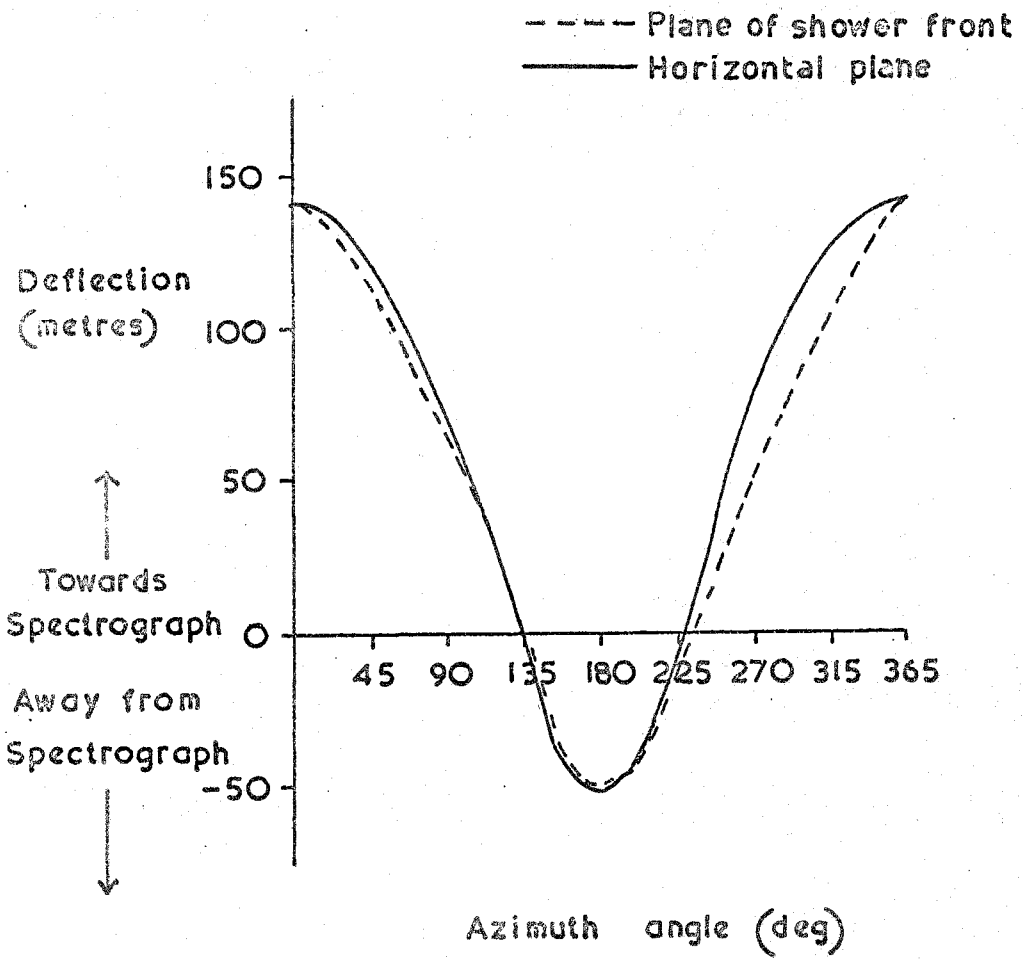
Plane of shower front
Horizontal plane
150
100
50
0
-50
Deflection (metres)
Towards Spectrograph
Away from Spectrograph
45
90
135
180
225
270
315
365
Azimuth angle (deg)

shower, the core of which makes an angle θ with the vertical, the electrostatic force, F, on the muon, of charge q, is

$$F = q \cdot E$$

Inserting the appropriate value for q and assuming, as a worst case estimate, that up to 5 km E has an average value of 80 V m^{-1} and above 5 km a value of 15 V m^{-1} then for a muon originating at a height of 10 km the consequent acceleration down to 5 km will be 1.3×10^{10} m s^{-2} and from 5 km onwards: 7×10^{10} m s^{-2}. The resulting vertical deflection at sea level will be approximately 12 m which at a zenith angle of 20° corresponds to a horizontal deflection of approximately 4 m and approximately 10 m at a zenith angle of 40°.

It may be concluded that in the context of the present study, the earth's electric field has relatively little influence on the motion of a muon in an extensive air shower. For zenith angles larger than 40° however the effect becomes considerable although relatively simple to make allowance for since there is no azimuthal dependence.

5.3.5 Deflections in the horizontal plane and in the plane of the shower front

The geomagnetic deflections were calculated in the horizontal plane passing through the centre of the array. The transformation of the deflections onto the plane of the shower front was found to take an excessive amount of computing time, and the error involved in taking the horizontal plane deflections proves trivial for the range of zenith angles considered. Figure 5.2 shows the variation for an extreme case, of the geomagnetic deflection with the azimuth angle of the shower core, in the horizontal plane and in the plane of the shower front. No deflections greater than the ones shown in this example were used in the results presented here.

5.3.6 The effect of errors in core location

The accuracy of core location obtained with the Haverah Park 500 m array has been discussed in Chapter 2. There is no reason to suppose that the inaccuracies involved are other than statistically random with a maximum

error of less than 30 m. It is interesting, nevertheless, to consider the effect of a systematic error in core location. Over-estimation of the true core distance, r, by an amount δ for all showers results in the predicted charge ratio being obtained from the lateral distribution function at a distance $r + \delta$. Due to the general shape of the lateral distribution function the predicted charge ratio will be smaller. Under-estimation, on the other hand, results in the exact opposite. The effect of a systematic error of $\pm$ 30 m, in the determination of core distance on the predicted charge ratio has been considered and ranges from 2% for a charge ratio of 1·0 to 10% for a charge ratio of 2·0.

5.3.7 The acceptance by the spectrograph of EAS muons deflected by the geomagnetic field

For the Haverah Park spectrograph the acceptance function, $A(\theta,\phi,p)$, defined as the probability of a particle of momentum p incident at a zenith angle θ and azimuth angle ϕ entering the spectrograph and being detected, is not a rapidly varying function of either θ or ϕ, (Orford (1968)). Because of this, and since the maximum geomagnetic angular deflection, $\partial\alpha$, is less than $1{\cdot}5^{\circ}$ we may assume:

$$A\left\{\left(\theta + \frac{\partial\theta}{\partial\alpha}\,.\,\delta\alpha\right),\left(\phi + \frac{\partial\phi}{\partial\alpha}\,.\,\delta\alpha\right),p\right\} \simeq A\left\{\left(\theta - \frac{\partial\theta}{\partial\alpha}\,.\,\delta\alpha\right),\left(\phi - \frac{\partial\phi}{\partial\alpha}\,.\,\delta\alpha\right),p\right\}$$

5.3.8 Errors in the determination of the mean values of the momentum bands

The deflection intervals into which the data were sorted for the purpose of investigating the variation of charge ratio with momentum, were those used by Earnshaw (1968). The method used by this author for determining the mean momentum of these intervals involves the derivation of the differential spectrum, $S(p)\,dp$, for the interval, and this, in turn, requires assuming a trial momentum spectrum.

TABLE 5.2

The Mean Momentum of the Deflection Intervals used for studying the Variation of Charge Ratios with Momentum

DEFLECTION INTERVAL DEGREES	MEAN MOMENTUM GeV/c
5·0 - 16·0	$1{\cdot}61 \begin{smallmatrix} +\ 0{\cdot}28 \\ -\ 0{\cdot}26 \end{smallmatrix}$
2·1 - 5·0	$3{\cdot}25 \begin{smallmatrix} +\ 0{\cdot}80 \\ -\ 0{\cdot}85 \end{smallmatrix}$
1·1 - 2·1	$6{\cdot}61 \begin{smallmatrix} +\ 2{\cdot}3 \\ -\ 2{\cdot}2 \end{smallmatrix}$
0·57 - 1·1	$14{\cdot}93 \begin{smallmatrix} +\ 4{\cdot}6 \\ -\ 3{\cdot}0 \end{smallmatrix}$
0 - 0·57	$45{\cdot}0 \begin{smallmatrix} +\ 22{\cdot}8 \\ -\ 19{\cdot}3 \end{smallmatrix}$

The limits shown on the mean momenta are such that they include 40% of the area above and below the mean.

FIGURE 5.3 The variation of the observed muon charge ratio with azimuth angle in the X^+Y^+ and X^+Y^- (zenith angle reversed) lobes, for all momenta greater than 1 GeV/c. Also shown is the predicted variation assuming a mean height of origin of 5 km and a lateral distribution as given by Earnshaw (1968).

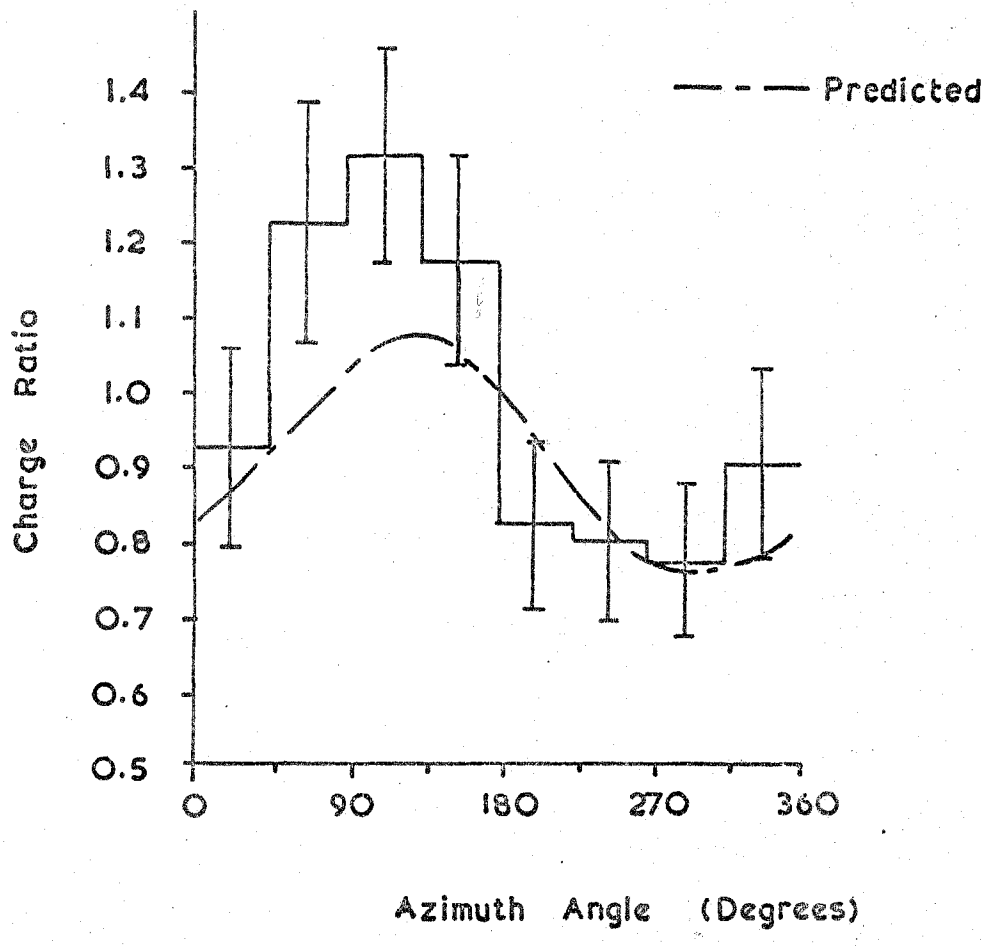
Predicted
Charge Ratio
1.4
1.3
1.2
1.1
1.0
0.9
0.8
0.7
0.6
0.5
0
90
180
270
360
Azimuth Angle (Degrees)

The mean momentum is defined as $\bar{p}$ where

$$\bar{p} = \frac{\int_1^{1000} S(p).\ p\ dp}{\int_1^{1000} S(p)\ dp}$$

The resulting mean momenta are given in Table 5.2.

A recent modification to the method has been to "feed back" the output spectrum as the trial spectrum for the next cycle, and to continue this process until the output spectrum for one cycle to the next is sensibly constant. Preliminary results indicate that the uncertainty in the value of mean momentum is of the order of 10%. Nevertheless, because of the uncertainty in the observed charge ratios, caused by the statistically small samples, even larger uncertainties in the mean momenta, say 20%, would have little effect on the conclusions arrived at in this chapter.

5.4 Comparison of data and predictions

5.4.1 General

As an overall check on the validity of the calculations the variation of the charge ratio in each lobe with azimuth angle was predicted for all momenta greater than 1 GeV/c and for a mean height of origin of 5 Km, using the appropriate lateral distribution function given by Earnshaw et al., (1967). The predicted variation of charge ratio for the X^+Y^+ lobe was found to be sensibly the same as for the X^+Y^- lobe with reversed azimuth angle, so that to improve the statistical accuracy the events in the two lobes were added together. Thus the events in the $0^\circ - 45^\circ$ bin of the X^+Y^+ lobe were added to those in the $315^\circ - 360^\circ$ bin of the X^+Y^- lobe and so on. The resulting charge ratio variation is shown in Figure 5.3,and it will be seen that there is good agreement with observation. In a similar way, since the predicted variation of

FIGURE 5.4 The variation of the observed muon charge ratio with azimuth angle in the $X^{-}Y^{\pm}$ lobe, for all momenta greater than 1 GeV/c. Also shown is the predicted variation assuming a mean height of origin of 5 km and a lateral distribution as given by Earnshaw (1968).

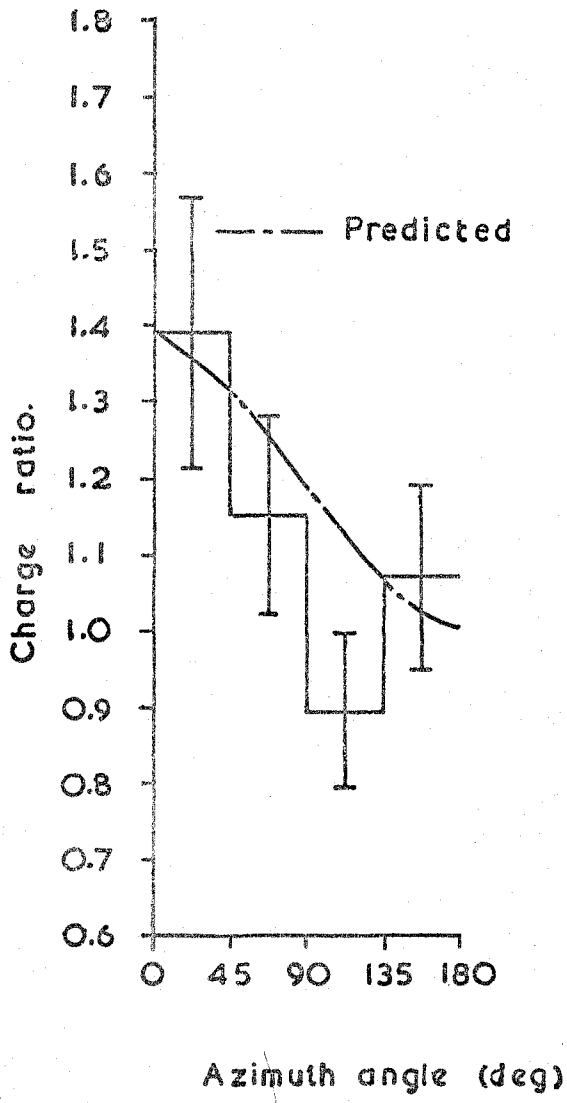
1.8
1.7
1.6
1.5
1.4
1.3
1.2
1.1
1.0
0.9
0.8
0.7
0.6
Charge ratio.
Predicted
0
45
90
135
180
Azimuth angle (deg)

FIGURE 5.5 The variation with momentum of the observed muon charge ratio in : (a) the combined X^+Y^+/X^+Y^- lobes, and (b) the X^-Y^+ lobe. Also shown is the charge ratio predicte on the basis of the model of Orford and Turver (1969) i which the primary mass and multiplicity are chosen to give opposite extremes in height of origin.

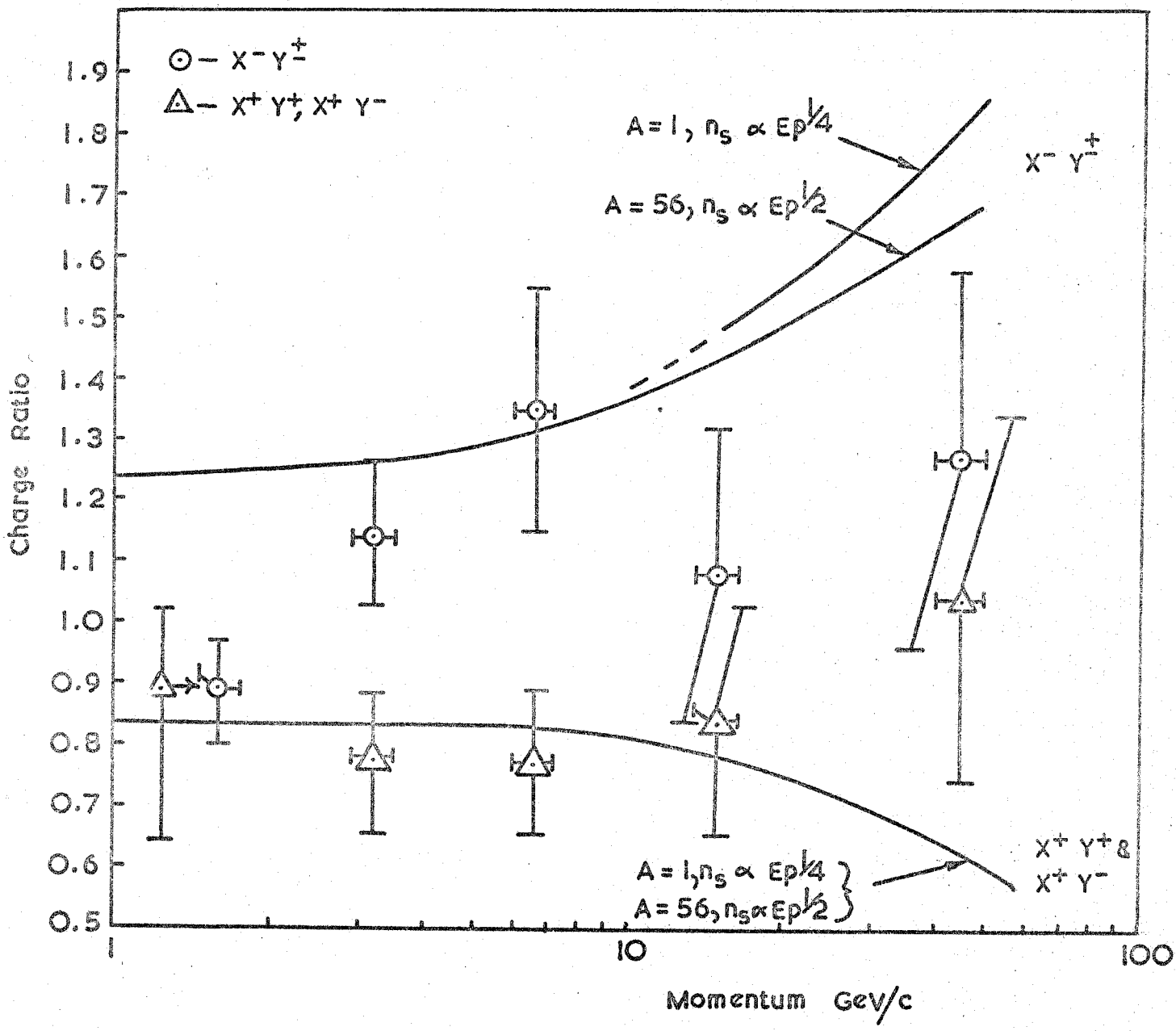
⊙ – X⁻ Y±
△ – X⁺ Y±; X⁺ Y⁻
A = 1, $n_s \propto Ep^{1/4}$
A = 56, $n_s \propto Ep^{1/2}$
X⁻ Y±
X⁺ Y⁺ &
X⁺ Y⁻
A = 1, $n_s \propto Ep^{1/4}$
A = 56, $n_s \propto Ep^{1/2}$
Charge Ratio
1.9
1.8
1.7
1.6
1.5
1.4
1.3
1.2
1.1
1.0
0.9
0.8
0.7
0.6
0.5
1
10
100
Momentum Gev/c

FIGURE 5.6 The heights of origin of muons estimated on the basis of the observed charge ratios in : (a) the combined $X^{+}Y^{+}$, $X^{+}Y^{-}$ lobes, and (b) the $X^{-}Y^{\pm}$ lobe. The broken lines represent the heights of origin predicted by the model of Orford and Turver (1969) in which the primary mass and multiplicity are varied.

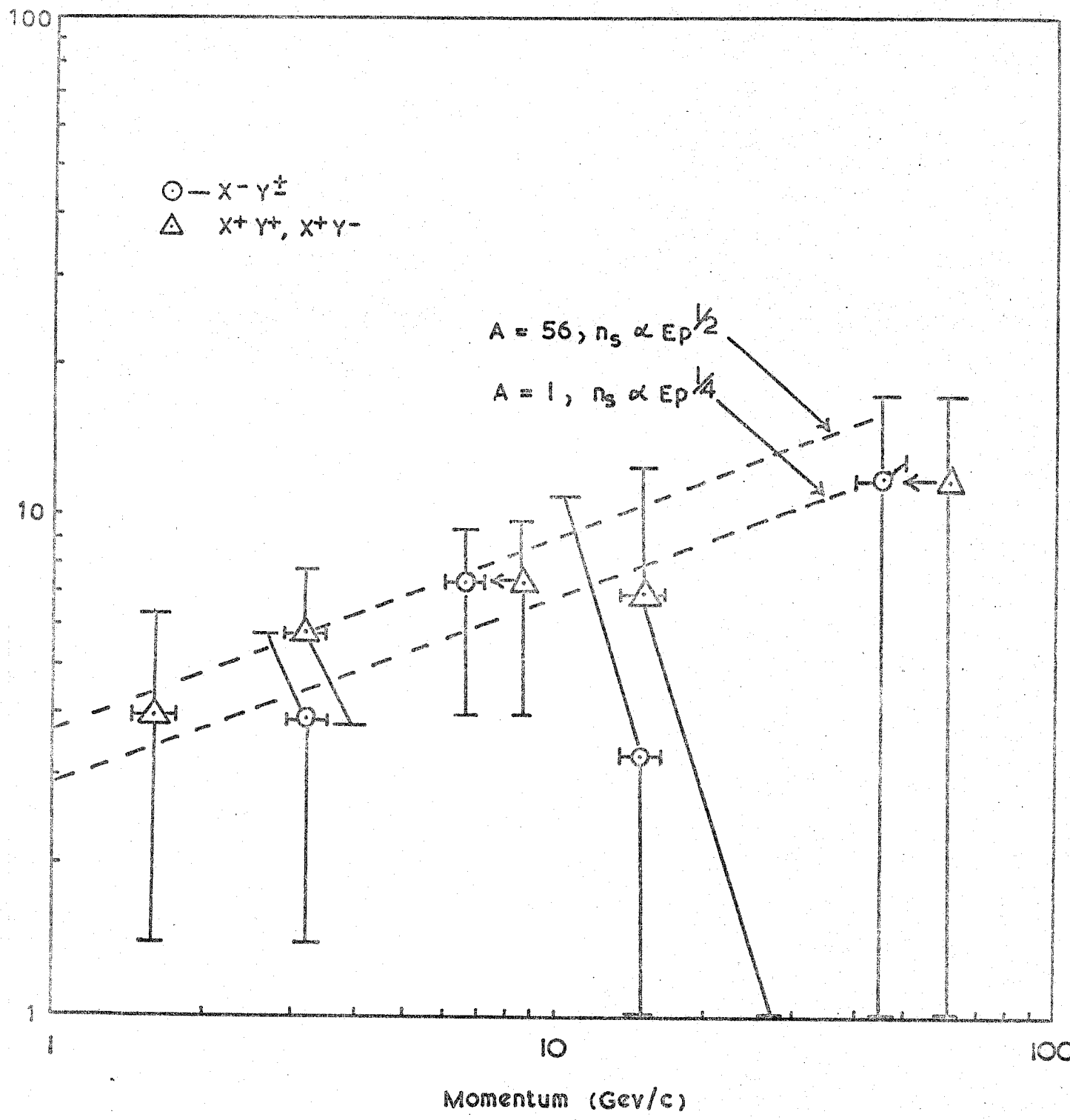
100
10
1
1
10
100
⊙— X⁻ Y±
△ X⁺ Y⁺, X⁺ Y⁻
A = 56, $n_s \propto Ep^{1/2}$
A = 1, $n_s \propto Ep^{1/4}$
Momentum (Gev/c)

charge ratio for the X^-Y^+ lobe us symmetrical about 180° azimuth, the data for the 0 - 45° azimuth bin were added to those for the 315° - 360° azimuth bin and so on, and this is shown in Figure 5.4.

5.4.2 Mean heights of origin of muons in EAS

Comparison between the predicted variation of charge ratio with height of origin and the observed charge ratio, for a given momentum, has provided an estimation of the heights of origin of muons.

To improve statistics the data were combined as described in the preceding Section, and the mean charge ratio found. Where appropriate the range of azimuth angle over which the mean was taken was limited to include either positive or negative charge ratios, but not both. In the case of the X^-Y^+ lobe no limitation was imposed, as the predicted charge ratio was greater than unity throughout the range, 0° - 360°. For the X^+Y^+/X^+Y^- combined lobes, the range taken was 180° through 360° to 45°. In this range the predicted ratio was always less than unity.

Thus for all the values of mean momentum bands there are two estimates of the height of origin: one for the X^-Y^+ lobe in which the predicted charge excess is positive, and one for the combined X^+Y^+/X^+Y^- lobe over the azimuth range giving a negative charge excess. Figure 5.5 shows the variation of the two observed charge ratios with momentum.

Estimated heights of origin are shown in Figure 5.6. The vertical error bars indicate the one standard deviation point due to Poissonian errors on the number of events combined with the error due to the uncertainty in the lateral distribution function. The horizontal error bars indicate a 10% uncertainty in momentum. Also shown are the predicted mean heights of origin according to two shower models. It will be seen that although the uncertainty is very large, in general there is agreement between theory and experiment.

5.4.3 The charge ratio distortion predicted by different models of EAS

A proton initiated shower with a multiplicity law varying as the quarter power of the primary energy, and a shower initiated by an iron nucleus and having a multiplicity following a half power law, represent two extremes insofar as the muon height of origin distributions are concerned. For this reason they have been used to test the sensitivity of the charge ratio to the height of origin of muons. The method of calculating the muon charge ratio expected for a given momentum and distribution of heights of origin appropriate to a particular model is described in Section 5.2.2. The actual models used were those of Orford and Turver (1969), and the charge ratios were predicted for the mean momenta given in Table 5.2. It is interesting to note that the lateral distribution for the A = 56, $n_s \alpha E_p^{\frac{1}{2}}$ model is flatter than that for the A = 1, $n_s \alpha E_p^{\frac{1}{4}}$ model, so that even though the former develops earlier and is more influenced by the geomagnetic field, the effect of this increased deflection on the charge ratio is not so great as it would have been had the lateral distribution been steeper. The predicted charge ratios are shown in Figure 5.5., and it is apparent that the ratios for all momenta except the highest are the same for the two models.

It may be concluded that the geomagnetic charge ratio is not very sensitive to the particular model used due to the general feature of all models that early development, although providing muons with a longer path length in the geomagnetic field, implies a flatter lateral distribution. This compensates for the effect of the large predicted deflections when the expected charge ratio is calculated.

5.5 Comparison with heights of origin obtained from a study of the lateral and angular separation of muons from the shower core

The estimation of the heights of origin of muons using the distribution in the angular separation of muons from the shower core, has been attempted

FIGURE 5.7 The distribution in the separation between Ψ_p the angle of the shower core projected onto the spectrograph measurement plane and Ψ_o, the angle of incidence of the muon on the spectrograph, similarly projected, for muon of momentum 1 - 3 GeV/c falling in the core distance interval 250 m to 350 m. Also shown is the distributio predicted using the model of Orford and Turver (1969) in which A = 1 and $n_s \propto E_p^{\frac{1}{4}}$.

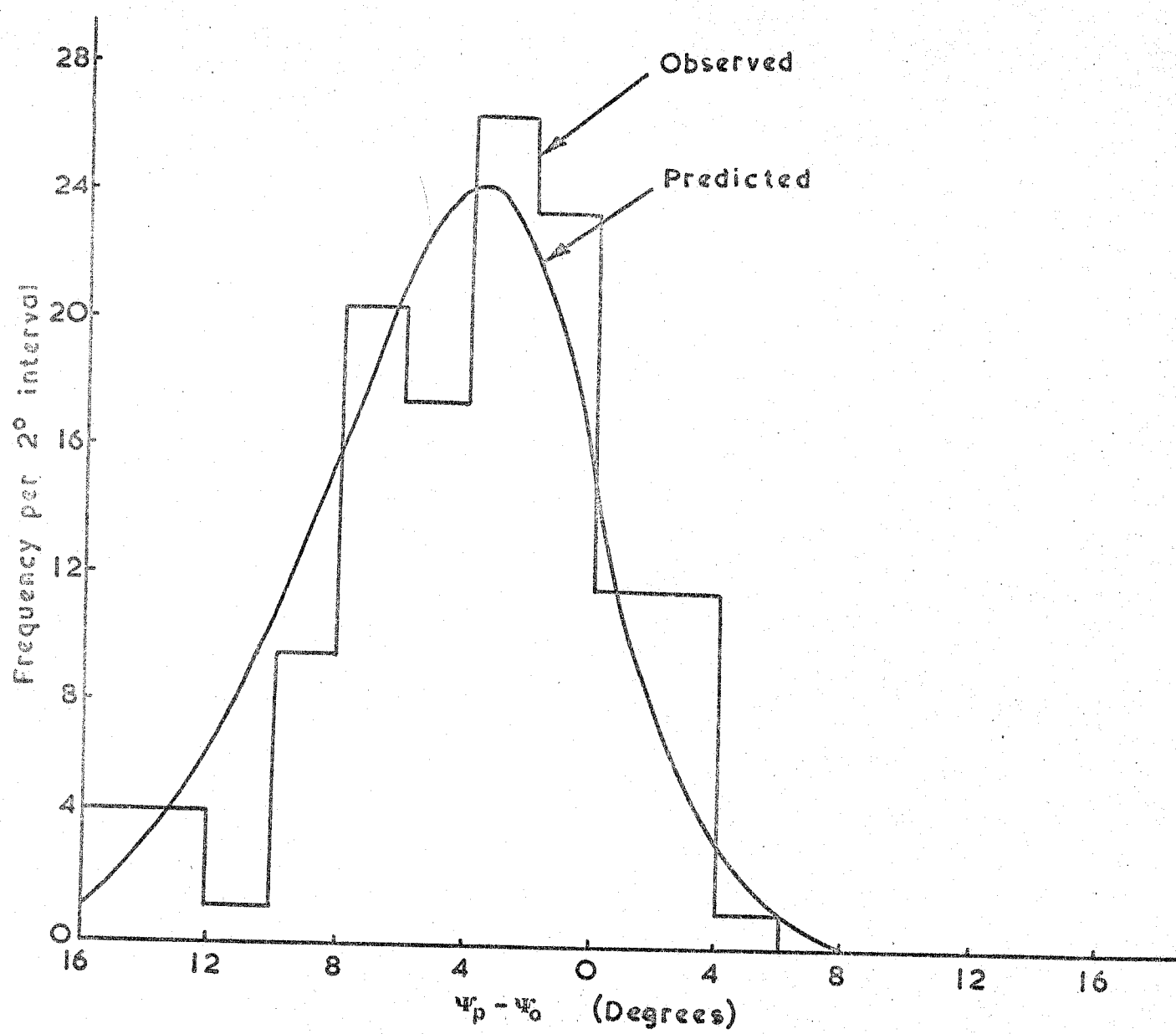
Observed
Predicted
Frequency per 2° interval
28
24
20
16
12
8
4
0
16
12
8
4
0
4
8
12
16
$\Psi_p - \Psi_o$ (Degrees)

FIGURE 5.8 The heights of origin of muons, of given momentum, predicted on the basis of the observed angular deviation from the shower core. The broken lines represent the heights of origin of muons predicted by the model of Orford and Turver (1969) in which the primary mass and multiplicity are varied.

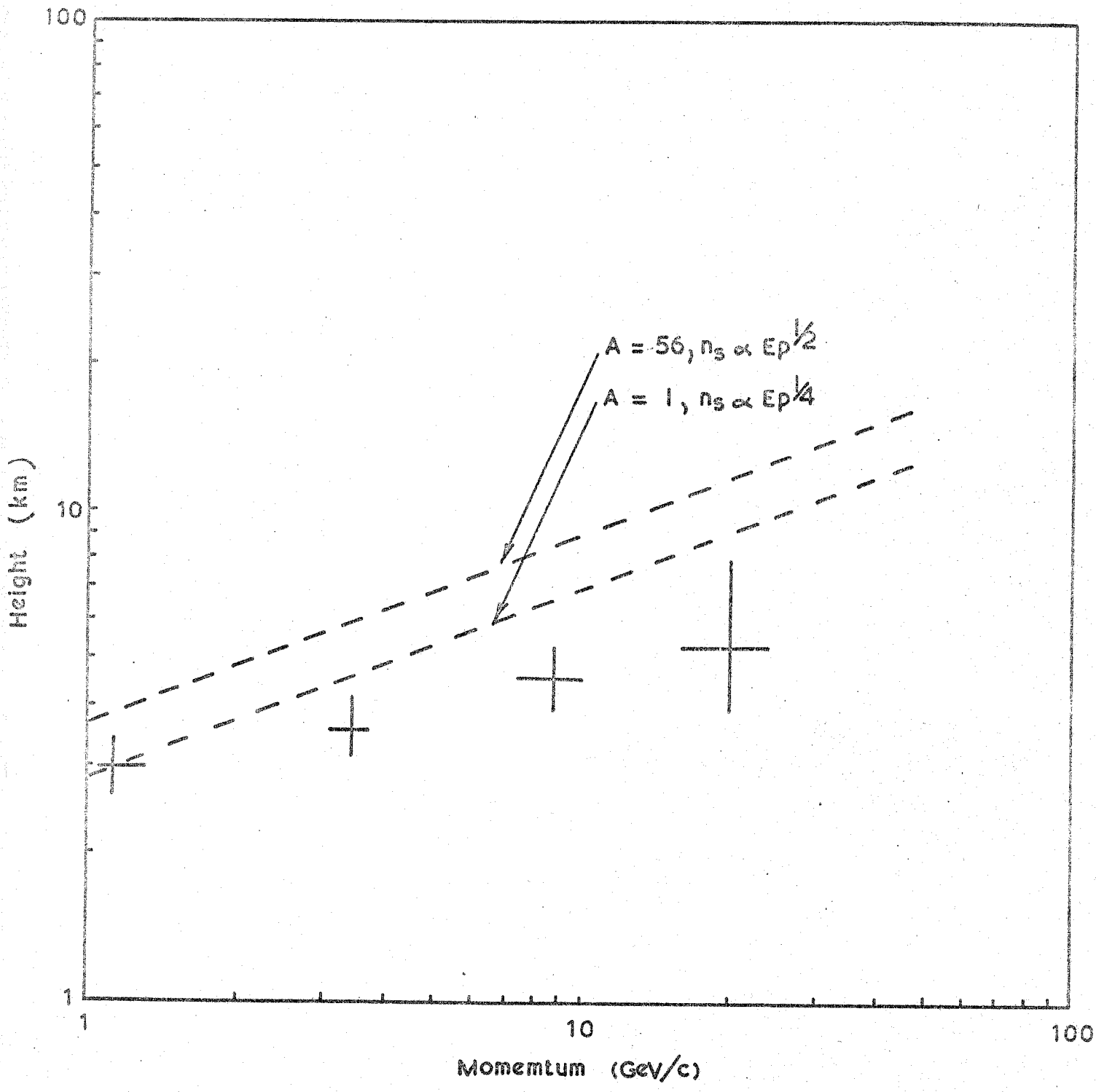
100
10
1
1
10
100
Height (km)
Momemtum (GeV/c)
A = 56, $n_s \propto Ep^{1/2}$
A = 1, $n_s \propto Ep^{1/4}$

by Earnshaw (1968), de Beer et al., (1969) and recently, in greater detail, by Machin (1972).

The distribution in angular separation between the shower core direction and the direction of muons of a given momentum, and falling at a particular point in an EAS detecting array, is affected by the height of origin of the parent pions together with their distribution in transverse momentum, the angle of the $\pi - \mu$ decay and the Coulomb and geomagnetic scattering. For the highest momentum muons the significance of these effects will be small, and the distribution in angular separation will arise from the uncertainty in the determination of the muon's trajectory and the core direction; in particular the uncertainty is dominated by the inaccuracy in the direction of the shower core. For the Haverah Park 500 m array Machin estimates the value of this latter uncertainty to be $2{\cdot}6 \pm 0{\cdot}2^{\circ}$.

The mean height of origin, h, is related to the mean angular deviation from the core, Ω, by the following formula:

$$h = \frac{r}{\tan \Omega}$$

In this, r is the distance to the spectrograph in the plane in which Ω is measured.

Typical results obtained by Machin (private communication) are shown in Figures 5.7 and 5.8.Figure 5.7 shows the distribution in angular deviation predicted for muons having momentum within the range 1 - 3 GeV/c, and falling at a distance of 300 m to one side of the spectrograph. The predicted distribution was derived using the muon heights of origin derived from the model of Orford and Turver (1969) for a proton primary, and a thermodynamic interaction model.Figure 5.8 shows the predicted mean heights of origin of muons of different momenta, at a distance of 300 m, in showers of primary energy of approximately 10^{17} eV. By comparing this figure with Figure 5.6 it

FIGURE 5.9 The expected distortion of the muon lateral distributio function, produced by a given lateral deflection, for muons of momentum greater than 47 GeV/c.

Model : Orford and Turver (1969) ($A = 1$, $n_s \propto E_p^{\frac{1}{4}}$)

Primary energy : 2×10^{17} eV.

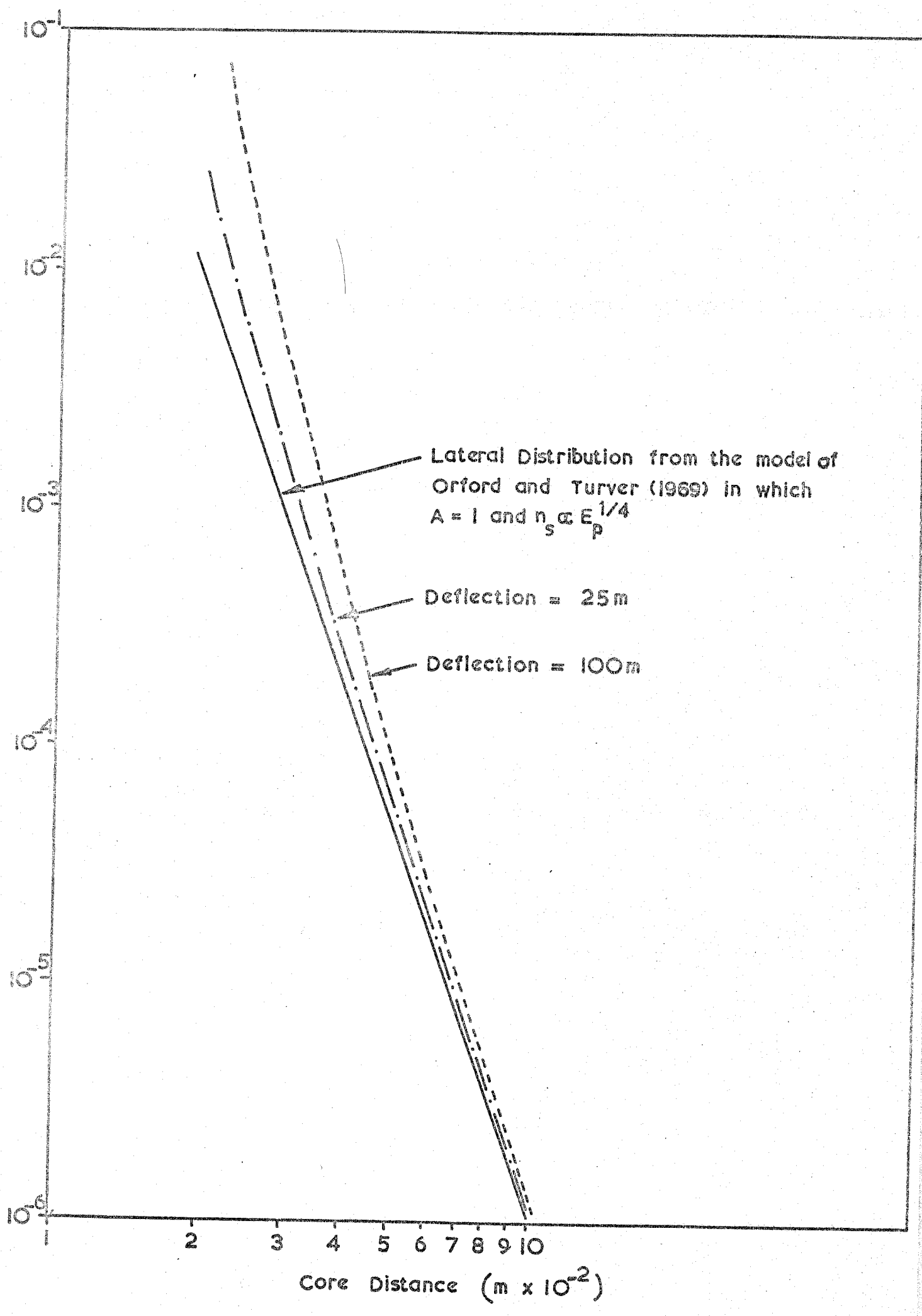
Lateral Distribution from the model of Orford and Turver (1969) in which A = 1 and $n_s \propto E_p^{1/4}$
Deflection = 25m
Deflection = 100m
Core Distance (m x 10^{-2})

may be seen that this method gives a more accurate estimation of the heights of origin than that using the geomagnetic charge distortion of muons. The reasons for the large errors involved in the latter have already been discussed in Section 5.4.3.

5.6 Effects of geomagnetic deflection on the lateral distribution of muons

Figure 5.9 shows the effects of different deflections of positive and negative muons of momentum 45 GeV/c on the lateral distribution for this momentum obtained from the model of Orford and Turver (1969) in which A = 1 and $n_s \propto E_p^{\frac{1}{4}}$. It will be seen that for a deflection of 25 m, which is the mean deflection predicted for a muon of this momentum originating from 18 Km, there is little effect on the function. Similarly, for the lateral distribution function corresponding to other momenta, it can be shown that for the expected deflections there is little or no distortion. In general, the earlier experiments of Clark et al.,(1958) confirm this. This group found that for particles of all momenta greater than 1 GeV/c there was no detectable difference between the lateral distribution when measured along an East-West baseline, and that measured along a North-South baseline.

Chapter 6

EAS Model Simulations

6.1 Introduction

The processes involved in the development of an extensive air shower are complex. Studies of the observable phenomena at various depths in the atmosphere can be of significance in helping to understand these processes only if an accurate model representation is available so that measurements may be compared with predictions. Such a model, indeed, is important in indicating which measurements should be made since these should be of quantities which are particularly sensitive to changes in either the mass compositions of the primary particles or the various fundamental interaction processes.

Comparison of the results of the Mkl experiment have shown that there is agreement with many accepted models at low momenta, but that at high momenta and large core distances the observed intensity exceeds that predicted by a significant amount. Because of these discrepancies and the fact that different authors, using the same broad model parameters, apparently obtain differing results (for example, Hillas (1965), and de Beer et al., (1966), - see Figures 4.6 to 4.9) a model was formulated specifically for the Haverah Park muon experiment (Orford and Turver (1969)). A step-by-step approach was adopted in this model, for although the Monte-Carlo method, as used by Bradt and Rappaport (1967), McCusker et al., (1969) and Grieder (1971(a)), directly takes account of the important aspect of fluctuations, it involves a prohibitive amount of computing time for primary energies greater than 10^{16} eV. A step-by-step method can be made much less demanding in this respect whilst the effect of fluctuations may be investigated in a limited way by selectively fluctuating those parameters to which the model is most sensitive.

6.2 A model employing the method of successive collisions to sea level

6.2.1 General

The model of Orford and Turver (1969), hereafter called the "1969" model,

was devised with the intention of treating the longitudinal and lateral development of the muon component as carefully as possible using conventional values of the high energy interaction parameters. Because of the extra precision which is obtained in this particular approach, a method of successive collisions, similar to that used by Bhabha and Heitler (1937), was adopted for the treatment of the nucleon and meson cascades. Preliminary investigations indicated, however, that since nearly all the muons of momentum greater than 100 GeV/c originated from heights above 10 kilometers, a saving in computing time could be effected, without attendent loss of precision, if the development below 10 kilometers was treated in a manner similar to that of Holyoak (1967) using fixed heights of interaction.

The predictions of the complete model were presented at the Budapest Conference in 1969 and it was pointed out that, where comparable, the results were in essential agreement with those of de Beer et al., (1966), and Murthy et al., (1967). In terms of shape of muon momentum spectra there was good agreement with the model of Hillas (1965) for a proton primary, although the number of muons was less than that predicted by this author. To investigate this discrepancy and to test the simplification adopted in the 1969 model, a new model - the "1971" model - has been established which continues the use of the method of successive collisions to sea level, as originally suggested by Orford, K.J., and Turver, K.E., (private communication). As an adjunct to this a review of those parameters characterising the nuclear physics and other aspects of the model has also been undertaken in the light of recent experimental work.

6.2.2 The new model

The basic step-by-step method is described in detail in Appendix C and involves the numerical evaluation of the pion generation function for a matrix of pion energy intervals and intervals of atmospheric depth. The intervals of energy used are $\frac{1}{4}$ decades and those of atmospheric depth 25.8 g cm^2.

Initially 1/6th decade energy intervals were used but $\frac{1}{4}$ decades give similar results and a useful saving in computation time. Again for reasons of economy of computing time, only vertical showers are considered in the present work.

The pion generation function gives the probability that a pion of a particular energy will be produced in an interaction at a certain depth. The probability that a pion is emitted from the interaction in a particular direction is found by using the C.K.P. distribution described in Section 6.2.3.6. Any pion so produced is then assumed to continue in this direction and the probability that a charged pion assumed to have a probability of production two thirds that for all pions - will decay into a muon is found by taking into account its lifetime dilation factor, $E/m_{\pi}c^2$, and its potential path length. Any change of direction occurring during $\pi - \mu$ decay is ignored. The probability that a muon possesses a particular energy is then found by approximating the pion energy spectrum, over a small energy range, to a power law and allowing the decay muon to have an equal probability of having an energy between 0.56 E_{π} and E_{π} . Finally a small correction is made to take into account energy loss due to ionisation and the probability of muon decay.

6.2.3 Theoretical considerations and experimental evidence governing the choice of nuclear physics in the model.

6.2.3.1 Introduction

Some of the features of more recent models of high energy interactions have their origins in earlier theories. The models of Fermi (1950), Heisenberg (1952) and Landau (1953) are similar insofar as they consider the energy from the interaction to be released in a small volume and to be dissipated in the form of created particles. Unlike Heisenberg's model, however, Fermi's statistical model supposes that the energy of the incident particle is shared among all the secondaries, and that a high proportion of

these secondaries consist of nucleons and antinucleons together with K mesons, rather than mesons alone. Furthermore, as a result of assuming an energy density proportional to the fourth power of the energy per created particle, it predicts a multiplicity varying as the quarter power of the radiated energy. In the Landau model, although a multiplicity law similar to this is predicted, a more pronounced anisotropic distribution of secondaries results. In contrast to these three models those of Kraushaar and Marks (1954), Cocconi (1958) and Ciok et al.,(1958) consider that the collision leaves the nucleons or their meson clouds in a highly excited state, and that after the collision there may be up to four distinct regions moving with different velocities and capable of emitting mesons.

Turning now to consider some of the main features of current models, this last mentioned concept of meson clouds, or fireballs, moving slowly in the C.M.S., is frequently used although some authors, Gurwitz et al.,(1971), for example, consider that the evidence for such systems is weak. In addition to the production of pions and kaons in these fireballs Peters (1964, 1966) and Grieder (1969, 1971(a)), for instance, include the production of nucleon-antinucleon pairs, which may be important in view of the recent data on nucleon-antinucleon pair production fromthe CERN Intersecting Storage Rings experiment.

The inclusion of isobars in interaction models is a relatively recent feature of such models. In general the decay of the isobar provides two or three fast pions or kaons which penetrate deeply with the leading nucleon, as, for example, in the model of Peters (1962). This production of pions and kaons in comparable numbers may be contrasted with the pionization process in which the number of kaons produced is only of the order of 10% of the number of pions.

6.2.3.2 Multiplicity

The largest possible multiplicity, n_s, for a particular nucleon energy

E_p corresponds to the creation of particles having some standard energy which is independent of the total energy of the collision and is given by $n_s \propto (K.E_p)^{\frac{1}{2}}$, where K is the fraction of the primary energy radiated in the form of created particles. Such a multiplicity dependence is used in the isobar-pionization model of Pal and Peters (1964). A less strong dependence on the radiated energy is produced by the Fermi statistical and Landau hydrodynamical models. Both these give $n_s \propto (K.E_p)^{\frac{1}{4}}$, although it is interesting to note that if viscosity is introduced into the hydrodynamical theory, the exponent is increased to one third. A multiplicity law varying as $\ln(K.E_p)$ is a consequence of 'scaling' (Feynmann (1969)), but also derives from the multiperipheral model first proposed by Amati et al., (1962).

Up to an energy of 70 GeV the majority of hydrogen bubble chamber data indicate a relationship of the form $n_s \propto (K.E_p)^{\frac{1}{4}}$ although the recent work of Jones et al., (1971) using a liquid hydrogen target, spark chambers and an ionization calorimeter seems to favour a logarithmic dependence on the radiated energy.

In the context of EAS however, a knowledge of the multiplicity of proton-air nucleus rather than proton-proton collisions is the more relevant, and because of possible intranuclear cascading it is to be expected that the multiplicity will be greater in the former. For the collision of two nuclei of atomic mass number A the hydrodynamical theory of Belenky and Landau (1954) indicates that the dependence on A is of the form $n_s \propto A^{0.19}$. It would seem reasonable, therefore, to suppose that for a nucleon-nucleus collision the dependence on A is certainly no stronger than this. A recent analysis by Hough, J.H., (private communication), of multiplicities obtained from emulsion data and hydrogen targets, for energies up to 1 GeV, indicates such an $A^{0.19}$ dependence. Beyond 1 GeV no proton-proton data were available for the survey, but it is suggested that, because of the high energies, collimation of the secondaries will dampen the intranuclear cascading in the struck

nucleus so that if anything the dependence of multiplicity on A should be less strong than at lower energies. As a conclusion to this survey a charged particle multiplicity for proton-proton collisions of the form $n_s = 1{\cdot}9(K.E_p)^{\frac{1}{4}}$ is suggested and it is this form which is used in the model described here.

Turning now to consideration of pion-nucleus interactions, the experimental data is more sparse than that for nucleon-nucleus interactions, but accelerator data indicate that, for a given energy of the primary, the number of pions produced is greater than for the latter. The difference in number is found to be approximately 20%, which is consistent with a multiplicity law of the form $n_s = 1{\cdot}9\ (K.E_p)^{\frac{1}{4}}$ in which K has a value very close to unity.

6.2.3.3 Inelasticity

Up to energies of approximately 20 GeV, accelerator data indicate that the inelasticity - the fraction of the incident energy radiated in the form of created particles - is 0·4 for proton-proton collisions. Taking into account the possibility of further interactions within the nucleus, the inelasticity of proton-air nucleus collisions, K_p, at these energies should certainly be no lower than this. Confirmation that this is a lower limit comes from measurements of the ratio of the interaction length to the absorption length of the nuclear cascade. Further evidence, suggesting that K_p is independent of energy is given by Azimov et al.,(1964). This author suggests that the mean inelasticity of proton-air nucleus collisions has a value of 0·5 ± 0·07 up to an energy of 10 TeV. Such an energy independence is in accord with the result of "scaling" as suggested by Feynmann and is also supported by cosmic ray emulsion work: Abraham et al., (1967), Gierula and Krzywdzinski (1968), and Yameda and Koshiba (1967).

It is concluded that there exists little evidence to suggest a mean value for K_p of other than approximately 0·5 for proton-air nucleus interactions. Throughout the work reported here a value of 0·5 has been used except

where comparison is made with the models of Hillas et al., (1971) who uses a value of 0·44.

Accelerator data at lower energies and cosmic ray calorimeter and hadron attenuation length measurements at higher energies, indicate that the pion-air nucleus inelasticity, K_π , lies between 0·8 and 1·0. Furthermore, a value approaching unity is consistent with the experimental evidence for the lack of leading pions in pion-nucleus collisions. Although the evidence is sparse for higher energies, there are indications that the value of K_π remains constant and has a value which is very nearly 1·0. Such a value is assumed here.

6.2.3.4 Interaction mean free paths

Accelerator data for energies up to 30 GeV indicate that λ_p, the interaction mean free path for protons in air, has a value of 80 ± 5 g cm^{-2}. At higher energies there are some indications from cosmic ray experiments that the total inelastic cross section for proton-nucleus interactions increases, and thus that λ_p decreases, with energy. Yodh and Pal (1971), from an analysis of hadron spectra at different depths in the atmosphere find the value of this cross section to be 250 mb at an energy of 100 GeV and 350 mb at 30 TeV. Furthermore, an increase in the cross section over the energy range 1 GeV to 100 GeV is one explanation given by Kaneko et al., (1971) of a burst spectrum, thought to be produced by surviving protons, at Chacaltaya. Evidence for a steady increase in the cross section above a few hundred GeV has been presented by Bolotov et al., (1965), Grigorov et al., (1965) and by Akimov (1969). Against this evidence however, Jones et al., (1971), using a liquid hydrogen target, spark chambers and an ionization calorimeter find nothing to suggest that the proton-proton cross section is other than constant over the energy range 100 GeV to 1 TeV. Within this energy range a constant cross section is also suggested by the work of Alakov et al., (1967) Andronikashvili et al., (1967) and

Bozoki et al. (1967).

Above 1 GeV there is a paucity of data, but it is interesting to consider the implications of a cross section increasing with energy. Grieder (1971(c)) points out that if such an increase takes place it implies an increased overlapping of the colliding nuclei so that more nucleons should take part in the interaction. Although this would explain an apparent rapid increase in multiplicity at very high energies, a stronger dependence on the nuclear mass than that observed would be expected.

It is concluded that there is little reliable evidence, for energies above 1 GeV, to suggest that the value of λ_p is different from that found at accelerator energies, and a value of 80 g cm^{-2} has therefore been used in this model.

Even less data exists concerning the pion interaction mean free path at high energies, but the indications are that no rapid change occurs above 1 GeV. Where comparison has been made to the work of Hillas et al., (1971) a value of 100 g cm^{-2} has been used in this model. Elsewhere, however, a value of 120 g cm^{-2} has been taken.

6.2.3.5 The energy spectra of secondaries

For protons of energy 20 - 30 GeV, incident on light element targets, measurements of the C.M.S. energy distribution of the produced pions have shown this to be approximately exponential. In the laboratory system the differential energy spectrum giving the best fit to these experimental results is of the form given by Cocconi, Koester and Perkins (1961):

$$f(E)dE = C\left(\frac{1}{U}e^{-E/U} + \frac{1}{T}e^{-E/T}\right) dE \quad \ldots\ldots\ldots\ldots 6.1$$

in which U and T are the mean laboratory system energies of the secondaries in the forward and backward cones respectively. At cosmic ray energies of the order of 10^6 GeV there is some indirect confirmation of this from emulsion measurements of the energy of γ rays from the decay of π^o mesons

produced by collisions of cosmic ray primaries (Fowler and Perkins (1964)).

The manner in which the values of U,T and the constant C are calculated so as to conserve energy once the multiplicity and inelasticity of the collision have been decided upon,is similar to the method used by Hillas et al. (1971), and is as follows: In the laboratory system the radiated energy, E_r, can be written:

$$E_r = n_s . V . \gamma_s \quad \ldots\ldots\ldots\ldots\ldots\ldots\ldots\ldots 6.2$$

where V is the mean energy of the secondaries in the centre of symmetry system. This system has a Lorentz factor, γ_s, which is given by: $\gamma_s = \sqrt{\frac{1}{2}\left(1 + \frac{E'}{M_p c^2}\right)}$

where M_p is the mass of the primary, and in the case of a colliding nucleon, E' is equal to the primary energy. For the collision of a pion, of energy E_p, with a nucleus, the system is assumed, following Salzman and Salzman (1960), to behave kinematically as though the incident particle is a "ghost" nucleon of energy $E' = E_p/K$ and that E_p is radiated in the form of pionization. Having calculated V from 6.2, U and T may be obtained from the relationships

$$U = (V + \beta_s . c . \pi)\gamma_s \qquad \text{and } T = (V - \beta_s . c . \pi)\gamma_s$$

$$\text{where } \beta_s = \sqrt{1 - \frac{1}{\gamma_s^2}} \qquad \text{and } \pi^2 = V^2 - m_\pi^2 . c^4$$

in which m_π is the pion rest mass. Integration of 6.1 gives an expression for the total energy radiated in the laboratory system, namely $E_r = C(U + T)$, in which $C = n_s/2$.

6.2.3.6 Transverse momentum

The mean transverse momentum, $\bar{p}_t$, of the secondaries from a high energy interaction, although invariant under a Lorentz transformation, is difficult to study directly, and the data, particularly at high energies, are not abundant. At accelerator energies most experimental data suggest a value

for $\bar{p}_t$ of 0·3 GeV/c for both proton-nucleus and pion-nucleus collisions, whilst direct cosmic ray experiments indicate a possible gradual increase of $\bar{p}_t$ to approximately 0·5 GeV/c at an energy of 10^5 GeV (Kazuno (1967)). Nevertheless, these data do not exclude the possibility of a constant value of $\bar{p}_t$ over this energy range. Similarly, a value of $\bar{p}_t$ tending asymptotically to 0·38 GeV/c at higher energies, and arising as a consequence of "scaling" as suggested by Feynmann, cannot be ruled out, although it seems unlikely in view of the indirect evidence from EAS studies mentioned in Chapter 1.

The theoretical work of Wang (1969), based on a statistical interaction model and cell structured nucleons, predicts a value of $\bar{p}_t$ which is energy independent over the energy range from a few GeV to 250 GeV, although there is some doubt about the validity of statistical theories at higher energies (Gurwitz et al.,(1971)). If other interaction models are considered then it is interesting to note that Feinberg and Ivanenko (1969) consider that it is unlikely that $\bar{p}_t$ remains independent of energy. In the case of the two fireball model, for example, these authors point out that if the multiplicity is fixed at $n_s \propto E^{\frac{1}{4}}$, say, where E is the energy radiated in the laboratory system, then unless the energy per pion increases, the fireballs will have a Lorentz factor, and thus a value of the mean transverse momentum per created particle, proportional to $E^{\frac{1}{4}}$. For the hydrodynamical model, these authors suggest that $\bar{p}_t$ should vary with energy as ln E, and for the multifireball theory that the mean transverse momentum per fireball should vary as $\sqrt{\ln E}$.

In the absence of more conclusive evidence to the contrary, a constant value of $\bar{p}_t$ of 0·4 GeV/c has been assumed in the work reported here.

With regard to the distribution of transverse momentum, the so-called C.K.P. distribution, due to Cocconi, Koester and Perkins (1961), is used in the present model. This distribution is of the form:

$$f(p_t)dp_t = \frac{p_t}{p_o} \exp\left(-\frac{p_t}{p_o}\right)\frac{dp_t}{p_o}, \quad \text{with } p_o = \frac{\bar{p}_t}{2} \qquad \ldots\ldots\ldots\ldots\ 6.3$$

and is derived from accelerator data prior to 1961 although cosmic ray data up to an energy of 300 GeV are in good agreement (Fowler and Perkins (1964). Recent accelerator work on $\pi^- p$ multiple pion production at 27 GeV by Elbert et al., (1968), indicates a distribution of the form:

$$f(p_t)dp_t = \left(\frac{p_t}{p_o}\right)^{1.5} \exp\left(-\frac{p_t}{p_o}\right)\frac{dp_t}{p_o}, \quad \text{with } p_o = \frac{2}{5}\bar{p}_t \quad \ldots\ldots\ldots\ldots 6.4$$

Hillas (1971) (Haverah Park Internal Note) finds that the use of 6.3 rather than 6.4 makes only a neglible difference in the calculation of muon densities at all momenta.

6.2.3.7 Isobars

If, as suggested by Peters (1962), nucleon isobars carry away almost the whole of the available C.M.S. energy, then the subsequent decay pion carries energy which rises linearly with primary energy. This is in contrast to the less steep rise of the energy of pions from the pionization process. As a consequence the differential unassociated γ-ray spectrum and the integral muon spectrum should follow the differential primary spectrum, whereas they are steeper (Fowler and Perkins (1964)). Even if this is considered to be an extreme case and if, in fact, only a relatively small amount of the available energy goes into a baryon resonance, a group of fast decay pions should exist. Jones et al., (1971) find no evidence for such a separate group of mesons in the energy range 200-600 GeV, although a study of the energy spectrum of mesons in the Tien Shan magnet cloud chamber (Azimov et al., (1964)) shows 4% of the mesons having energies well separated from the main spectrum.

The study of other phenomena which might indicate isobar production yields a similarly conflicting picture. At Haverah Park, the variation of muon densities with shower size and core distance predicted by three models of Hillas et al., (1971) are in agreement with the observation of Blake et al., (1971) and two of these, namely models "K" and "I", are isobar models. To

give a muon number agreeing with experiment, however, model "K" requires a primary mass greater than one, and model "I", although giving a satisfactory muon number for a proton primary, predicts a Cerenkov response structure function which is too steep. Elsewhere, Tonwar and Sreekantan (1971) find that "isobar" models, as opposed to "fireball" models, predict EAS hadron time spectra in better agreement with experimental observations at Ootacamund. The K/π ratio measurements of Koshiba (1967) at a primary energy of 10 GeV also support an increased isobar production cross section.

Emulsion data in the energy range 100 GeV to 10 TeV show a slower increase in anisotropy than would be expected if isobar production of pions were important. If this is taken together with the other evidence the inference seems to be against any significant contribution from isobars in the context of muons in EAS, and none has been considered here.

6.3 Model Results

6.3.1 Comparison of the 1969 and 1971 models

The mean primary energy of the showers on which measurements were made in the Mkl experiment has been assessed by Andrews et al.,(1969(a)) as $1{\cdot}7 \times 10^{17}$eV on the basis of total energy loss measurements. Comparison of the observed muon densities at 300 m, obtained by Earnshaw (1968), with those predicted by the 1969 model, as described at the Budapest Conference, for a primary proton and $n_s \propto K E_p^{\frac{1}{4}}$, suggests a primary energy of $7{\cdot}8 \times 10^{17}$eV. When the dynamics of the interaction are modified as described in section 6.2.3.2 and the pion mean free path and inelasticity of the proton-air nucleus collisions taken as 100 g cm^{-2} and 0·44 respectively, this discrepancy is reduced. The primary energy then required is $6{\cdot}3 \times 10^{17}$eV. For similar values of λ_p and K_p the 1971 model predicts a primary energy slightly lower than this, namely $5{\cdot}3 \times 10^{17}$eV. It is of interest to note that the sensitivity

FIGURE 6.1 The integral momentum spectra of muons falling at 300 m from the core of a shower of primary energy 2×10^{17} eV predicted by the 1969 and 1971 models.

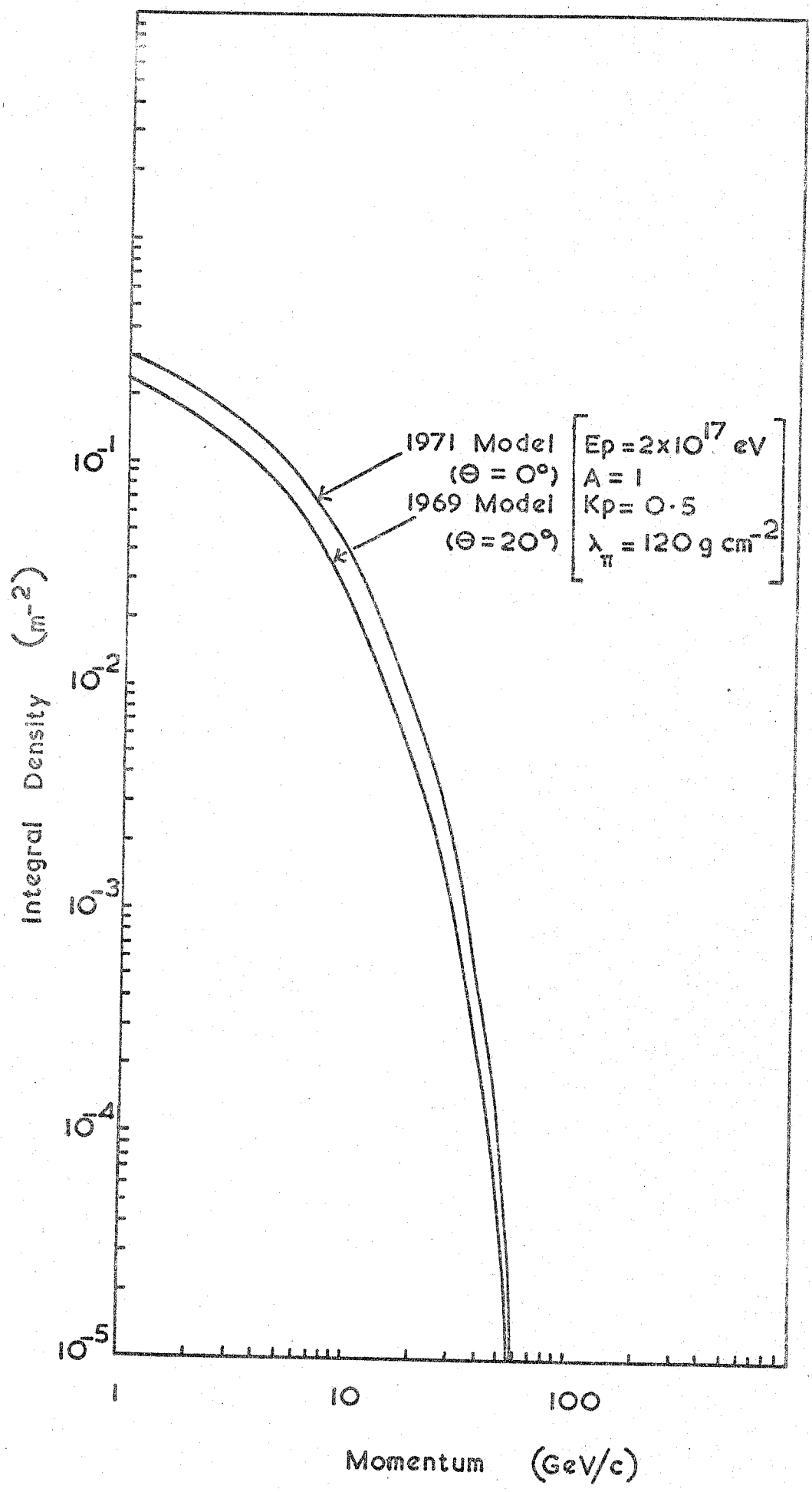
1971 Model
(Θ = 0°)
1969 Model
(Θ = 20°)
Ep = 2x10^17 eV
A = 1
Kp = 0·5
λπ = 120 g cm^-2
Integral Density (m^-2)
10^-1
10^-2
10^-3
10^-4
10^-5
1
10
100
Momentum (GeV/c)

to changes in the values of λ_p and K_p is such that a similar value for primary energy is obtained if the preferred values of 120 g cm^{-2} and 0·5 respectively are used.

Table 6.1 shows the densities of muons having energies greater than 1 GeV for different values of pion mean free path and proton-air nucleus inelasticity for the 1969 and 1971 models.

Figure 6.1 shows the integral spectra predicted by the two models at a core distance of 300 m. When allowance is made for the small effect due to the difference in zenith angles for the two models it may be seen that there is good agreement at all momenta.

TABLE 6.1

The predicted density of muons, $\Delta\mu$, of energy greater than 1 GeV falling at a core distance of 300 m for a primary energy of 2×10^{17} eV

Model	λ_π (gm cm^{-2})	K_p	$\Delta\mu$ (m^{-2})
1969	100	0·44	0·27
	120	0·44	0·25
	120	0·5	0·23
1971	100	0·44	0·3
	120	0·44	0·27
	120	0·5	0·3

6.3.2 Comparison with other models of EAS

Partly on the basis of a recent study by the Nottingham University group of the variation of muon densities with shower size and core distance (Blake et al.,(1971)) and partly on the basis of a comparison of the

FIGURE 6.2 The integral momentum spectra of muons falling at 300 m from the core of a shower of primary energy 2×10^{17} eV predicted by the 1971 model and by the model "E" of Hillas.

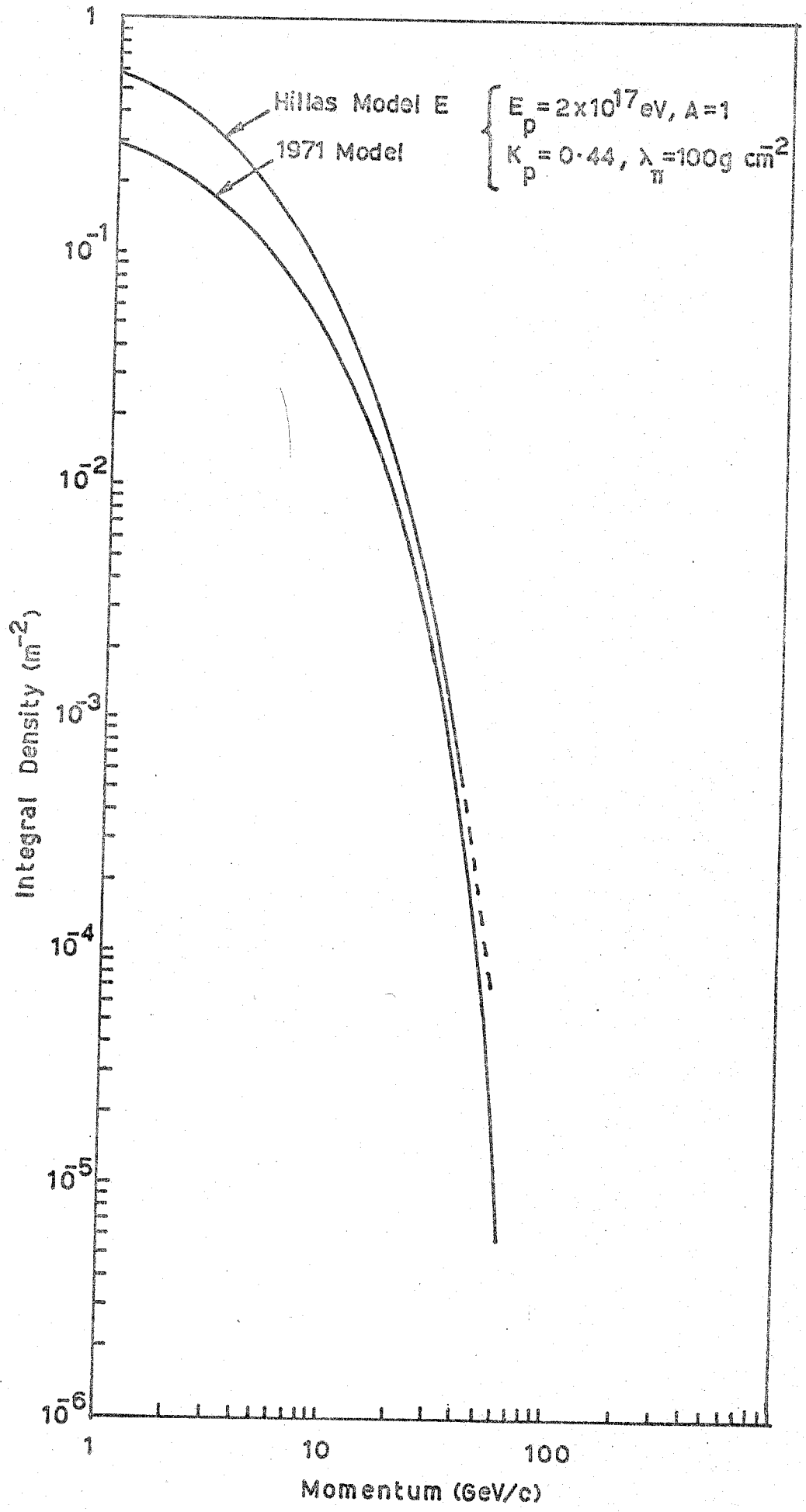
Hillas Model E
1971 Model
$E_p = 2 \times 10^{17}$ eV, A = 1
$K_p = 0.44$, $\lambda_\pi = 100$ g cm^{-2}
Integral Density (m^{-2})
1
10^{-1}
10^{-2}
10^{-3}
10^{-4}
10^{-5}
10^{-6}
1
10
100
Momentum (GeV/c)

FIGURE 6.3 The observed lateral distribution of muons of energy greater than 1 GeV compared with the predictions of the 1971 model and the model "E" of Hillas.

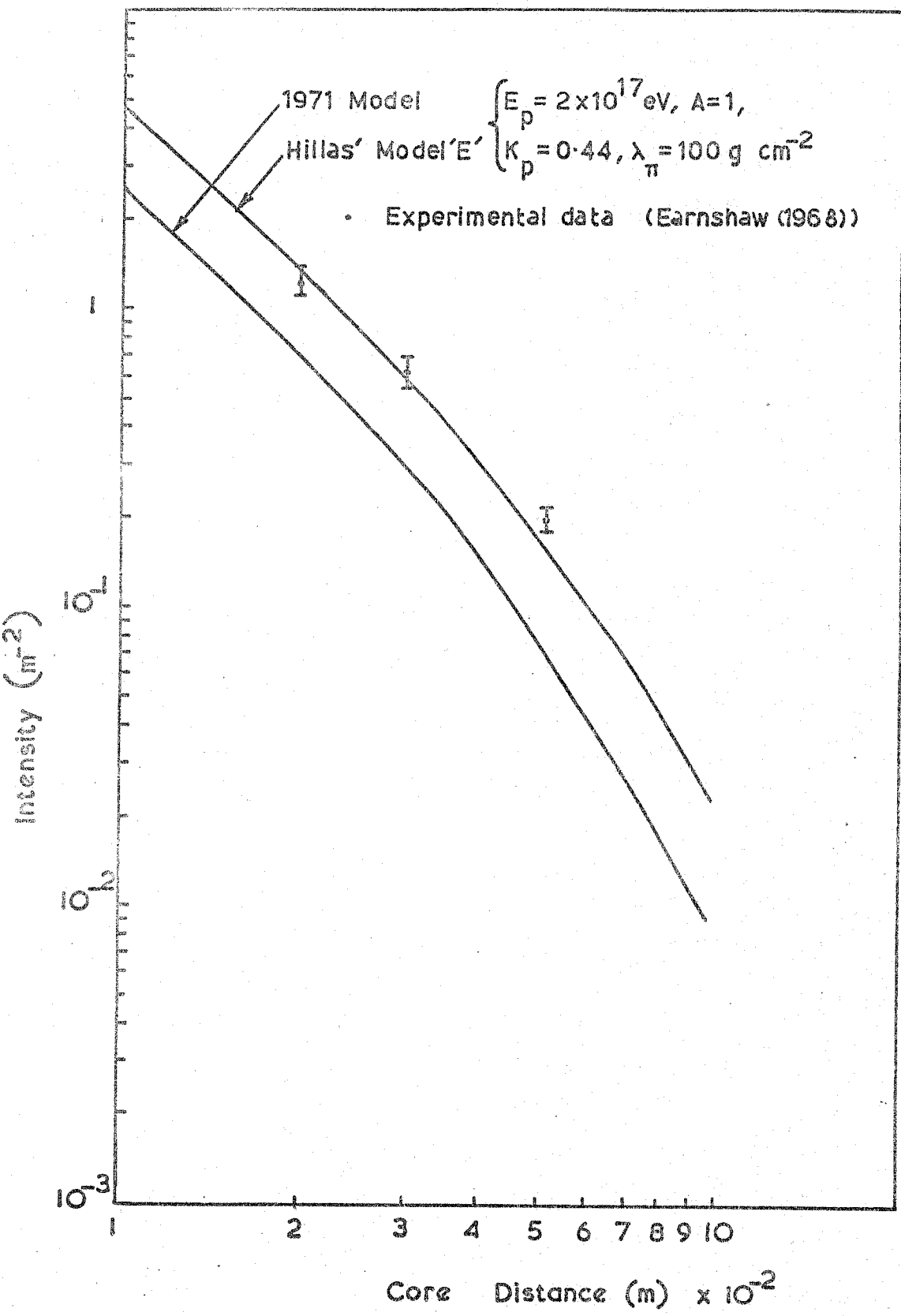
1971 Model
Hillas' Model 'E'
$E_p = 2 \times 10^{17}$ eV, A=1,
$K_p = 0{\cdot}44$, $\lambda_\pi = 100$ g cm^{-2}
Experimental data (Earnshaw (1968))
Intensity (m^{-2})
1
10^{-1}
10^{-2}
10^{-3}
1
2
3
4
5
6
7
8
9
10
Core Distance (m) x 10^{-2}

FIGURE 6.4 The variation of muon number with atmospheric depth predicted by the 1971 model and by Hillas' model "E".

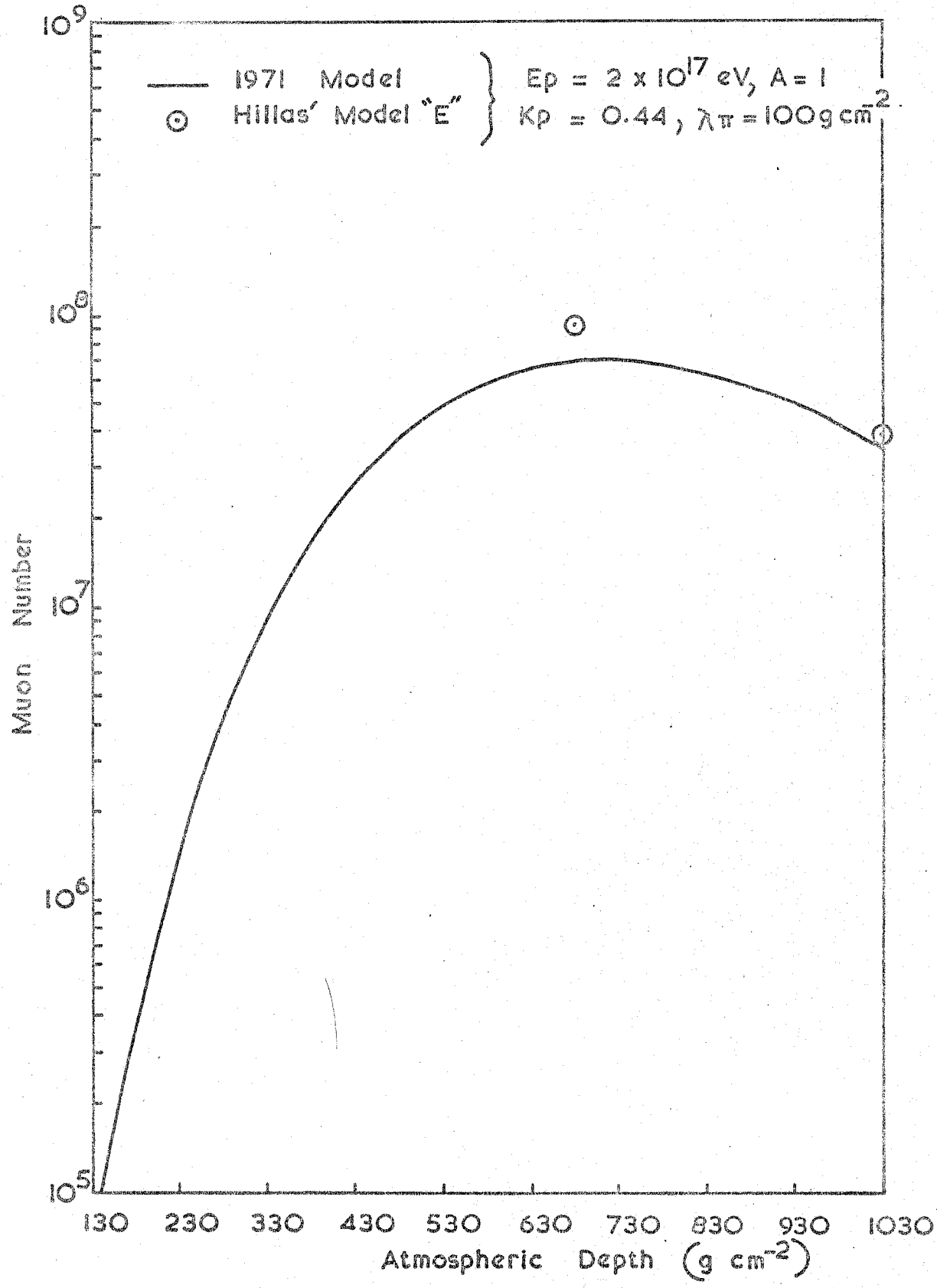
1971 Model
Hillas' Model "E"
Ep = 2 x 10^17 eV, A = 1
Kp = 0.44, λπ = 100 g cm^-2
Muon Number
10^9
10^8
10^7
10^6
10^5
130 230 330 430 530 630 730 830 930 1030
Atmospheric Depth (g cm^-2)

FIGURE 6.5 The mean number of muons in EAS, having energy above a particular threshold value, predicted by various workers

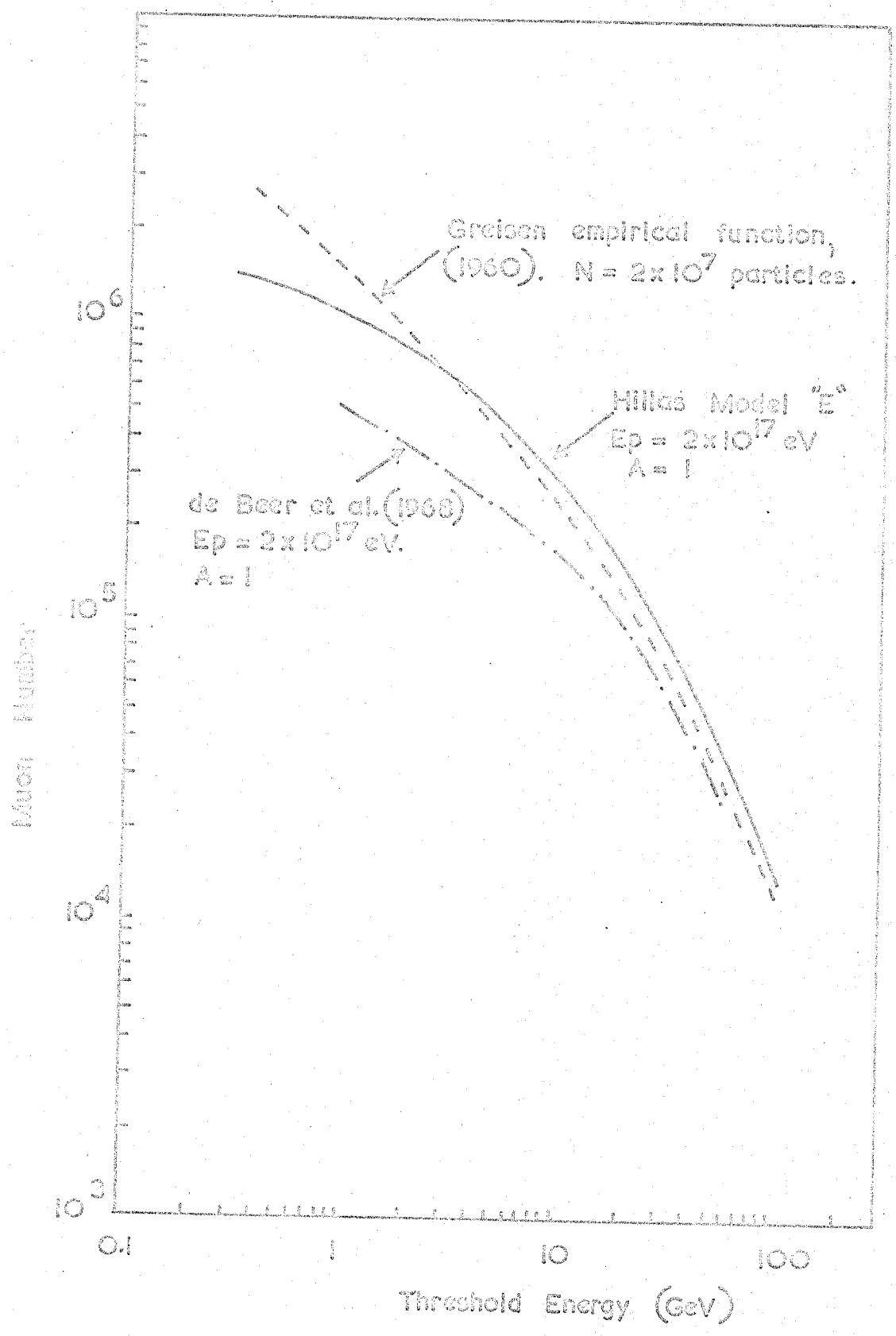
Greisen empirical function, (1960). N = 2x10^7 particles.
Hillas Model "E"
Ep = 2x10^17 eV
A = 1
de Beer et al.(1968)
Ep = 2x10^17 eV.
A = 1
Muon Number
10^6
10^5
10^4
10^3
0.1
1
10
100
Threshold Energy (GeV)

predicted and observed lateral Cerenkov response function, Hillas et al., 1971, suggest that their model "E" with a proton primary gives the best agreement with observation at Haverah Park. This model is similar to the 1971 model in that both involve step-by-step procedures, have a charged particle multiplicity which follows a $(K.E_p)^{\frac{1}{4}}$ form, have "normal" C.K.P. distributions of secondary energies and transverse momentum, and neither include an isobar.

The integral momentum spectra predicted by model "E" and the 1971 model for a core distance of 300 m and for a proton primary of energy 2×10^{17} eV are shown in Figure 6.2 . It can be seen that insofar as the shapes are concerned there is good agreement, but that there is a discrepancy between the muon densities at 1 GeV/c. Figure 6.3 shows the lateral distribution of muons having energy greater than 1 GeV predicted by the two models. It is apparent that the factor by which the 1971 model densities differ from those of model "E" is sensibly constant for all core distances. The discrepancy in muon densities is also reflected in the variation of muon number with atmospheric depth predicted by the two models shown in Figure 6.4. It may be seen that the number of muons at maximum is greater in the case of model"E" than for the 1971 model.*

The mean muon number per shower, $N_\mu(>E)$, having energy above a particular threshold energy, predicted by model "E" and the 1971 model, is shown in Figure 6.5 together with (i) the relationship due to Greisen (1960) obtained by equating the frequency of showers as a function of mean muon number to the frequency of EAS at sea level with N charged particles, namely

$$N_\mu(>E,N) = 1{\cdot}7 \times 10^5 \left(\frac{2}{E+2}\right)^{1{\cdot}37} \left(\frac{N}{10^6}\right)^{0{\cdot}75}$$

---

* Recent work (Dixon, H.E., and Turver, K.E., Private Communication) using a hybrid model in which important processes in the shower development are allowed to fluctuate has substantially removed this discrepancy.

FIGURE 6.6 The integral momentum spectrum of muons falling within the core distance interval 150 m to 250 m obtained from the Mk. 1 spectrograph data. Also shown is that predicted by the 1971 model for muons falling at a core distance of 200 m, normalised to the observed density at 1 GeV/c.

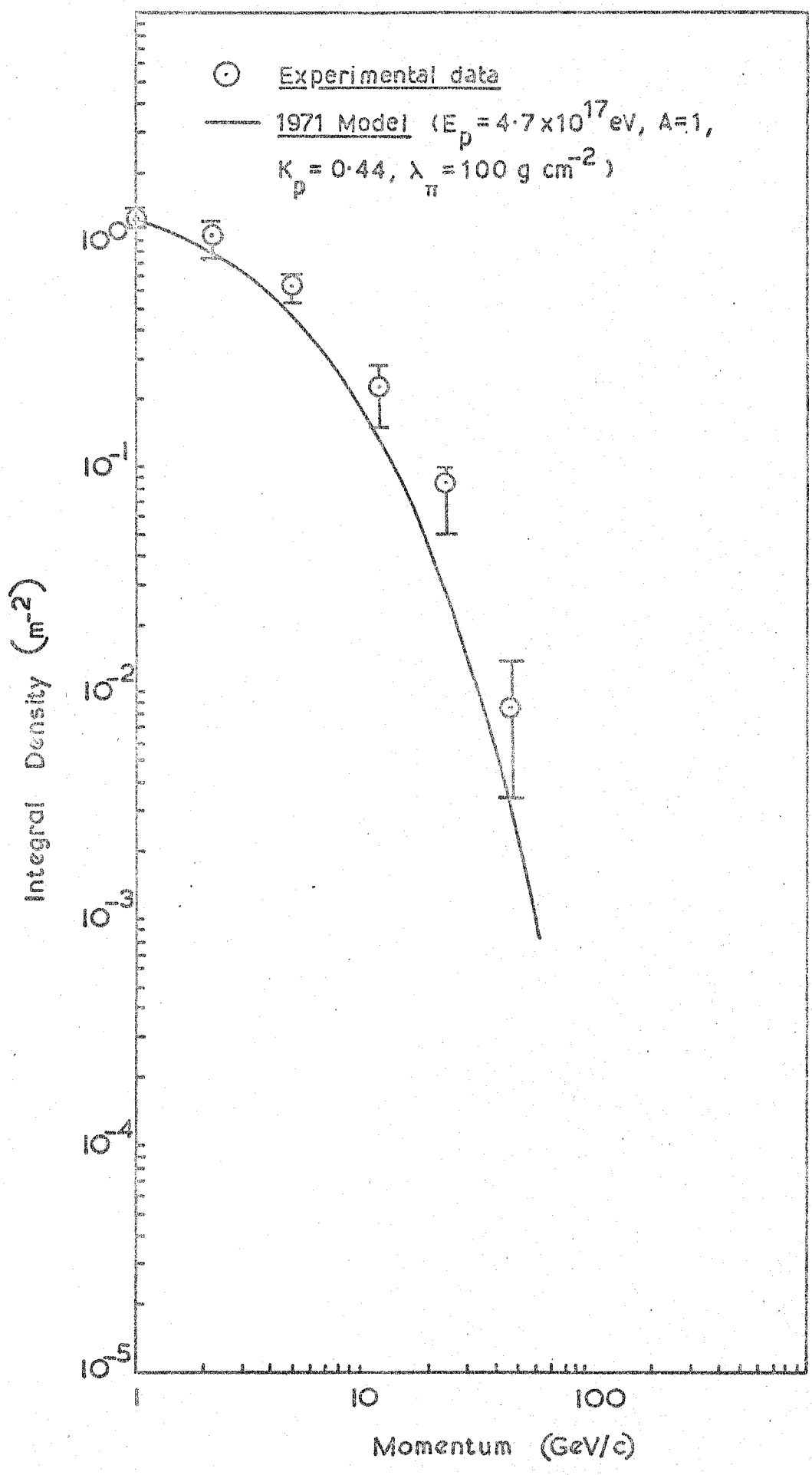
Experimental data
1971 Model ($E_p = 4{\cdot}7 \times 10^{17}$ eV, A=1,
$K_p = 0{\cdot}44$, $\lambda_\pi = 100$ g cm^{-2})
Integral Density (m^{-2})
10^{-1}
10^{-2}
10^{-3}
10^{-4}
10^{-5}
1
10
100
Momentum (GeV/c)

FIGURE 6.7 The integral momentum spectrum of muons falling within the core distance interval 250 m to 350 m obtained from the Mk. 1 spectrograph data. Also shown is that predicted by the 1971 model for muons falling at a core distance of 300 m, normalised to the observed density at 1 GeV/c.

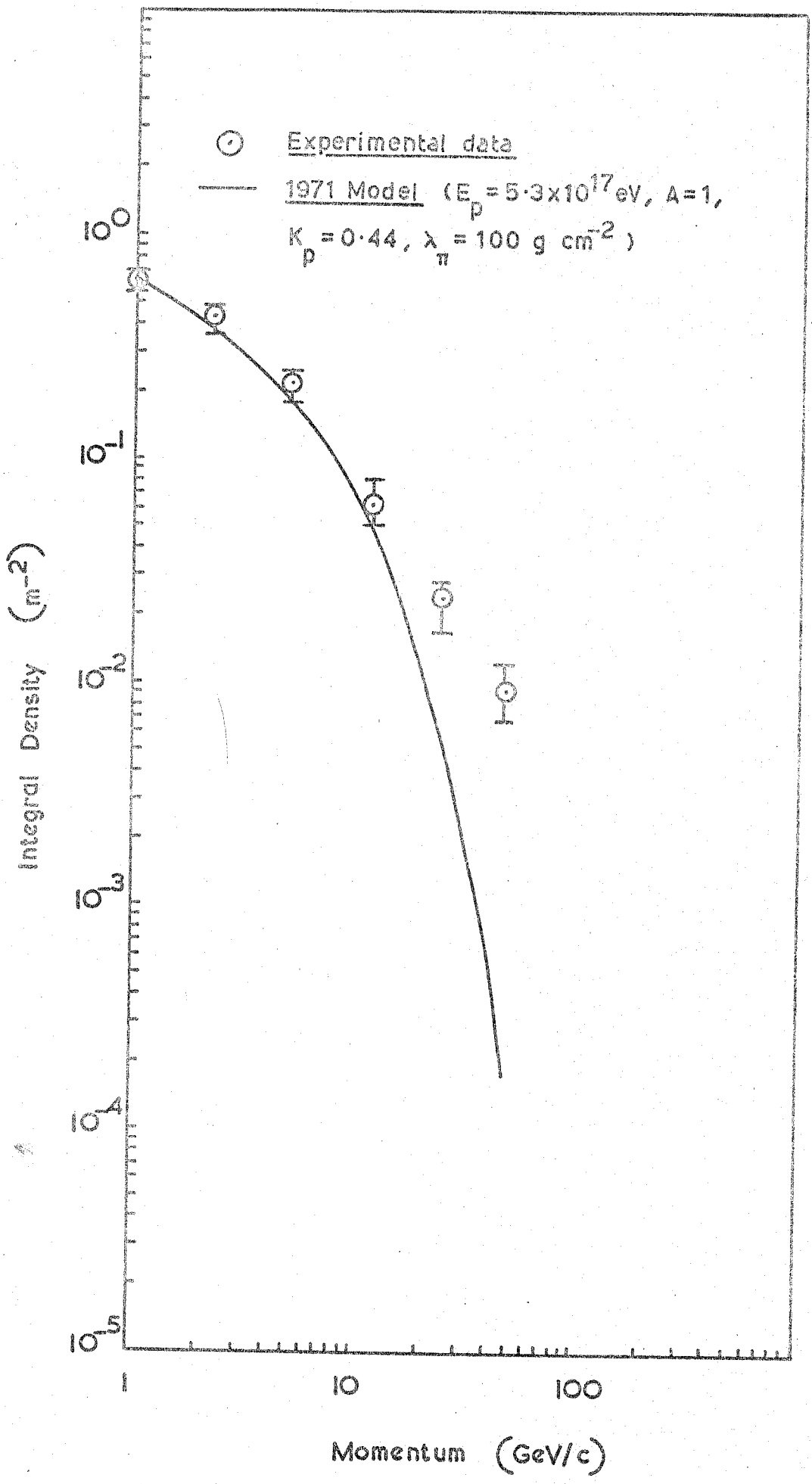
Experimental data
1971 Model ($E_p = 5{\cdot}3 \times 10^{17}$ eV, A = 1, $K_p = 0{\cdot}44$, $\lambda_\pi = 100$ g cm^{-2})
Integral Density (m^{-2})
10^{0}
10^{-1}
10^{-2}
10^{-3}
10^{-4}
10^{-5}
1
10
100
Momentum (GeV/c)

FIGURE 6.8 The integral momentum spectrum of muons falling within the core distance interval 450 m to 600 m obtained from the Mk. 1 spectrograph data. Also shown is that predicted by the 1971 model for muons falling at a core distance of 380 m, normalised to the observed density at 1 GeV/c.

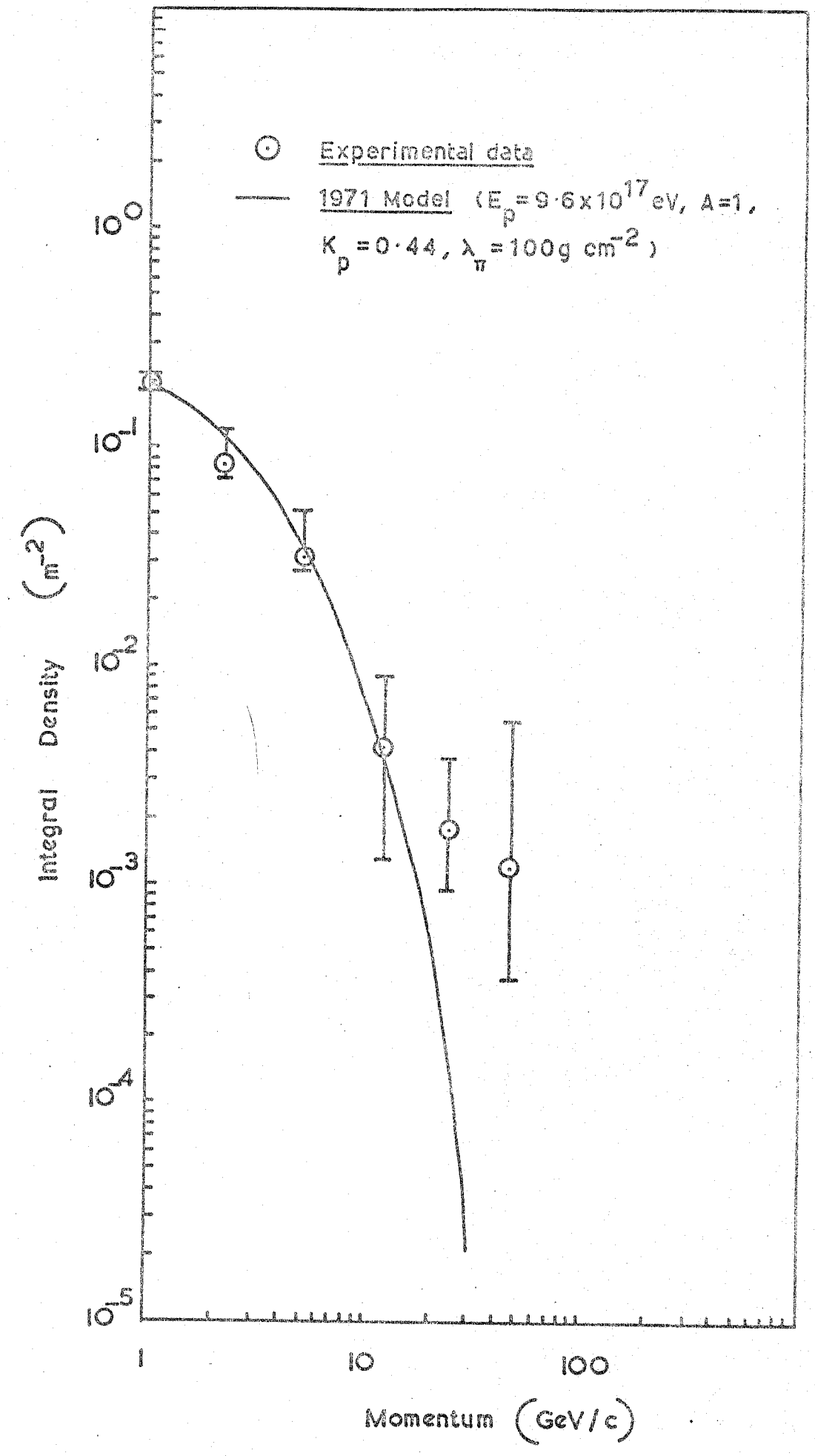
Experimental data
1971 Model ($E_p = 9{\cdot}6 \times 10^{17}$ eV, A=1, $K_p = 0{\cdot}44$, $\lambda_\pi = 100$ g cm^{-2})
Integral Density (m^{-2})
10^0
10^{-1}
10^{-2}
10^{-3}
10^{-4}
10^{-5}
1
10
100
Momentum (GeV/c)

and (ii) the mean muon number as a function of shower primary energy, E_p, derived by de Beer et al.,(1968), assuming a proton primary.

Because of the uncertainty in the relationship between shower size and primary energy, an accurate comparison between the Greisen result and the model predictions is difficult. In terms of shape, however, the curves representing the results of all the models are in good agreement with the Greisen relationship above 10 GeV.

6.3.3 Comparison of the Mk1 results and the model predictions

The integral momentum spectra for different core distances obtained from the Mk1 spectrograph and predicted by the 1971 model are shown in Figures 6.6, 6.7 and 6.8. The primary energy in each case was that required to give predicted densities in agreement with observed muon densities at 1 GeV/c and is obtained by assuming that the densities obtained for a primary proton of energy 10^{17} eV may be scaled as $E_p^{1.0}$. It may be seen that (i) for increasing core distance the required mean primary energy also increases, and (ii) for those groups of showers having mean core distances greater than 200 m the predicted momentum spectra beyond a momentum of approximately 10 GeV/c are steeper than those observed. Similar discrepancies were reported by Orford and Turver (1969), and it was suggested that agreement with the observed densities could only be obtained for a primary of acceptable energy if it was heavier than a proton. Similarly, agreement on the basis of spectral shapes could only be brought about by suggesting that, for a proton primary, the energy degredation should be greater than that produced by a multiplicity rising as $(K.E_p)^{\frac{1}{4}}$.

6.4 Conclusions and future work

The primary aim of the work described in this chapter was to investigate the validity of the analytical model of Orford and Turver (1969). It is

FIGURE 6.9 The lateral distribution of muons of energy greater than 1 GeV predicted by : (a) the 1971 model and (b) four typical runs of a Monte-Carlo model. Both (a) and (b) relate to a proton primary of energy 10^{15} eV.

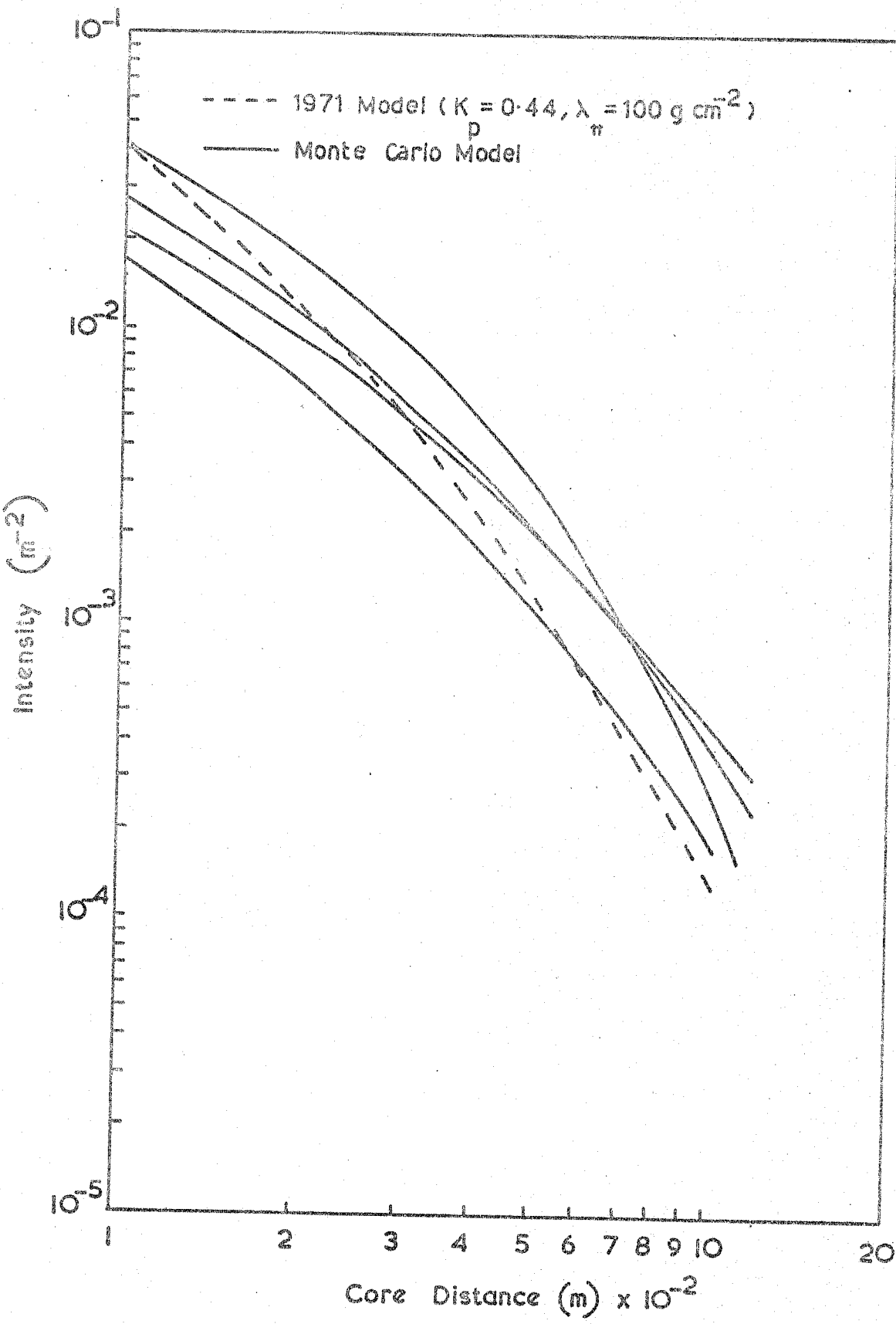
1971 Model (K = 0·44, λπ = 100 g cm⁻²)
p
Monte Carlo Model
Intensity (m⁻²)
10⁻¹
10⁻²
10⁻³
10⁻⁴
10⁻⁵
1
2
3
4
5
6
7
8
9
10
20
Core Distance (m) x 10⁻²

shown in Section 6.3.1 that if similar assumptions are made concerning the nuclear physics, then termination of the method of successive collisions at a height of 10 km and the use of fixed interaction heights thereafter, gives muon densities, at all momenta, similar to those obtained by continuing the method of successive collisions throughout the development of the shower. In the 1969 model,as described at the Budapest Conference, this simplification was made with the object of reducing the computing time, but it has been found that, by suitable choice of the computing method (see Appendix C), the computation time of the 1971 model is comparable with that of the 1969 model.

Comparison of the two models has been made assuming that the primary particle is a proton and on the basis of revised nuclear physics data and a more consistent method of treating the energy distribution among the created particles. Under these conditions it is found that both the 1969 and 1971 models give muon densities for the mean primary energy of showers detected at Haverah Park lower than observed, but in better agreement than those predicted by the Budapest version of the 1969 model. Similarly, both the 1971 model and the revised 1969 model, in common with Hillas' model "E", give lower muon intensities at high momenta and core distances of 300 m and beyond, than observed. In connection with the problem of the observed excess of high energy momentum muons at large core distances over predictions, recent simulations by Earnshaw, J.C., and Turver, K.E.,(Private Communication) using a Monte-Carlo technique, indicate a mean lateral distribution for a primary energy of 10^{15} eV, which is somewhat flatter than the scaled predictions of the 1971 model, (see Figure 6.9). This serves to highlight the effect of fluctuations on the lateral distribution function, as pointed out by de Beer et al.,(1967), and to show that a study based solely upon the results of analytical models may be insufficient to enable any conclusions to be reached regarding the validity of model parameters used here.

A complete Monte-Carlo type model at a primary energy of 10^{17}eV makes excessive demands insofar as computing time is concerned, so that a hybrid model is envisaged in which particular chosen parameters are varied. Hillas (1971) points out that the development of the shower is most sensitive to fluctuations in the distance travelled between collisions of the most energetic particle in the nucleon cascade. Recent work by Dixon, H.E., and Turver, K.E., (Private Communication) has shown that this free path may be fluctuated,together with a small number of other quantities such as inelasticity, multiplicity, and decay probabilities,without a significant increase in the computing time.

Chapter 7

Conclusions and future work

7.1 The Mk1 experiment

7.1.1 General checks on the data

In part, the work reported in this thesis has been concerned with a repetition, in the light of an increased number of events, of checks on the Mk1 spectrograph data originally reported by both Earnshaw (1968) and Orford (1968). From this standpoint of improved statistics it is concluded that:

(i) The expected dependence of the muon momentum spectrum on shower zenith angle is confirmed.

(ii) For muons falling in the core distance interval 200 m to 600 m there is no apparent variation in the momentum spectra with primary energy in the range considered, namely: 10^{16} eV - 10^{18} eV.

(iii) The charge ratio of muons falling between 200 m and 600 m from the shower core and detected by the Mk1 spectrograph is close to unity at all momenta up to the highest detectable by the instrument. That this is so for those high momentum muons originating early in the shower development lends little support to the possibility of charge asymmetric muon production at high momenta.

Turning now to consider checks for biasses in the data, not having been undertaken previously, the work reported here has shown that:

(a) The effect on the momentum spectra of inaccuracy in core location is small for uncertainties of less than 30 m.

(b) In comparison with the effect of core location errors, the degree to which the earth's magnetic field distorts the lateral distribution of muons is negligible for vertical showers. It is important to note, however, that for zenith angles greater than 40° the geomagnetic distortion of the lateral distribution increases rapidly.

(c) A comparison of the distribution of high momentum muons in core distance

with the corresponding distribution for all muons of momentum greater than 1 GeV/c shows that the distributions are related in a manner consistent with the absence of possible selection biasses. It had been supposed that such biasses could have stemmed from the difficulties in selecting high momentum muons in the dense events found at small core distances.

7.1.2 The derived momentum spectra

Notwithstanding an increase in the number of events and improved EAS data the final momentum spectra obtained for core distances greater than 300 m persistently show an excess of high momentum muons (> 50 GeV/c), over accepted model predictions for a shower initiated by a proton. In addition to the design and operation of a spectrograph having increased momentum resolution, other work which has gained impetus as a result of the above mentioned discrepancy has been concerned with: (a) examination of the validity of the model of Orford and Turver (1969) and (b) attempting to provide an independent experimental means of differentiating between possible model variants by measurements of the heights of origin of muons.

7.2 Model calculations

The model described in this thesis uses the method of successive collisions continued to sea level and gives results essentially similar, as regards shapes, to the model of Orford and Turver (1969). The predicted densities are slightly in excess of those given by the latter authors but in better agreement with the model "E" of Hillas. In this context it is interesting to note the results of recent work by Dixon and Turver (Private communication), in which fluctuations of a limited number of variables are introduced into the model. Sensibly complete agreement with model "E" is produced. Such independent agreement can only decrease the likelihood of the existence of gross errors in the model framework. Any conclusions regarding the validity of the nuclear physics, however, is precluded by the similarity between all the models in this respect.

7.3 The height of origin of muons

The effect of the earth's magnetic field on the charge ratio of muons in EAS has been investigated in detail. For momenta up to the highest detectable by the Mk1 spectrograph it is concluded that the difference between the charge ratio of muons, of a given momentum, in a shower developing early and in a shower developing more slowly, is minimal. The earlier development in the former is compensated for, in its effect on the charge ratio, by a lateral distribution function which is flatter than for the later developing shower.

A more promising technique for measuring heights of origin is the measurement of the angular deviation of muons from the shower core as described by Machin (1972) and outlined in Chapter 5.

7.4 The Mk2 spectrograph

Using the deflection of EAS muons passing through the central hole in the magnet, the r.m.s. angular uncertainty in the measurement of deflection using the Mk2 instrument has been assessed as $0.16 \pm 0.01^{\circ}$. It is concluded that this is larger than the target r.m.s. angular uncertainty for two possible reasons:

(i) the approximate nature of the theory of track location in a flash tube array used in the design study, and

(ii) the use of twenty layers of small diameter flash tubes in each arm has reduced the mean corridor width, as defined in Chapter 2, to such an extent that the uncertainty in tube location is no longer negligible by comparison.

During a period of nine months operation, 493 muons in EAS falling at core distances between 150 m and 350 m have been detected and their deflections in the spectrograph magnet measured. Although there is no significant disparity between this spectrum of angular deflections and that predicted on the basis of the momentum spectrum derived from the Mk1 data, the number of events is not yet sufficient to allow of any firm verdict.

7.5 Future work

In due course a statistically accurate value for the density of muons of momentum greater than 100 GeV/c falling in a core distance interval of 250 m to 350 m will be available from the Mk2 spectrograph data. The importance of such a measurement is considerable in view of the present difficulty in reconciling the value obtained from the Mk1 experiment with the predictions of rigorously tested models in which a conventional interaction model is used and the primary is a proton.

The possibility of an independent test of the suitability of the last mentioned type of model, using other detectable features of EAS, seems remote in view of recent work by Dixon and Turver (Private communication). This work has shown that, in general, the analytical or "averaged" Monte-Carlo type of models predict only relatively small changes in the majority of the measurable characteristics of showers, for large changes in the input parameters of interest such as primary mass or multiplicity. In the light of this difficulty, a method of seemingly greater potential could be the use of a Monte-Carlo, or Monte-Carlo/analytical hybrid model to predict, for a particular change in the primary mass or other feature of the interaction, the type and frequency of the fluctuations in those characteristics of showers most easily measured at Haverah Park. Simultaneous measurement of the rate at which a certain sized fluctuation occurs in all the measured quantities and subsequent comparison with predictions appears especially attractive for the Haverah Park array because of the near independence of the method of measuring the shower primary energy of changes in the primary mass. Characteristics which might be simultaneously measured in this way are radio signal, atmospheric cerenkov light, muon height of origin and muon density for a given momentum. Insofar as a muon spectrograph might be concerned, ultra high momentum resolution would not, necessarily be needed; the requirement would be for an

increase in the data collection rate and hence an increase in magnet area.

Figure A1

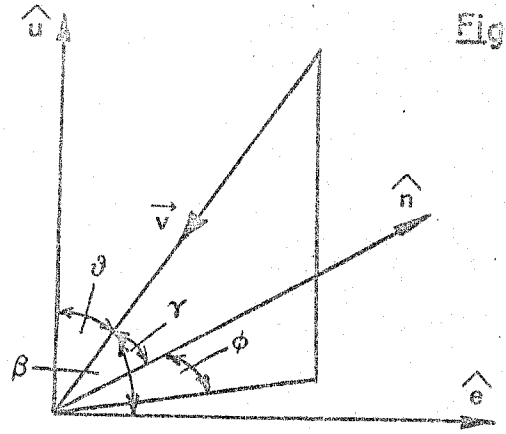

Figure A2

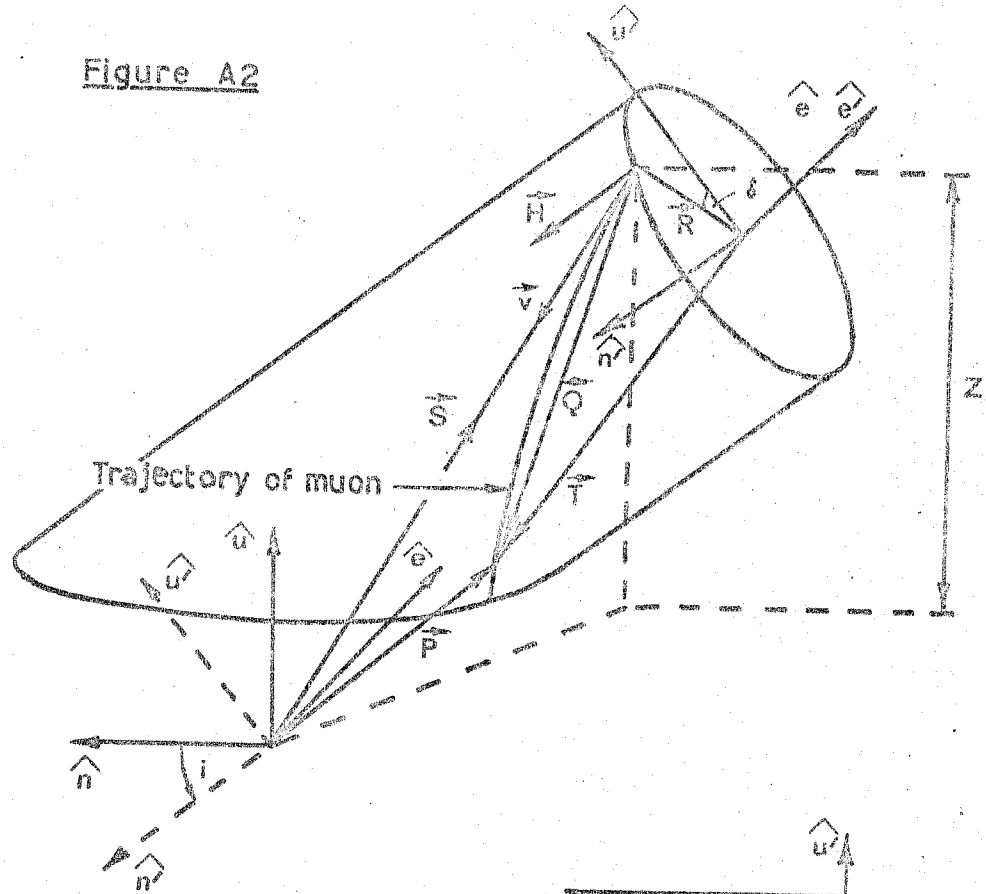

Figure A3

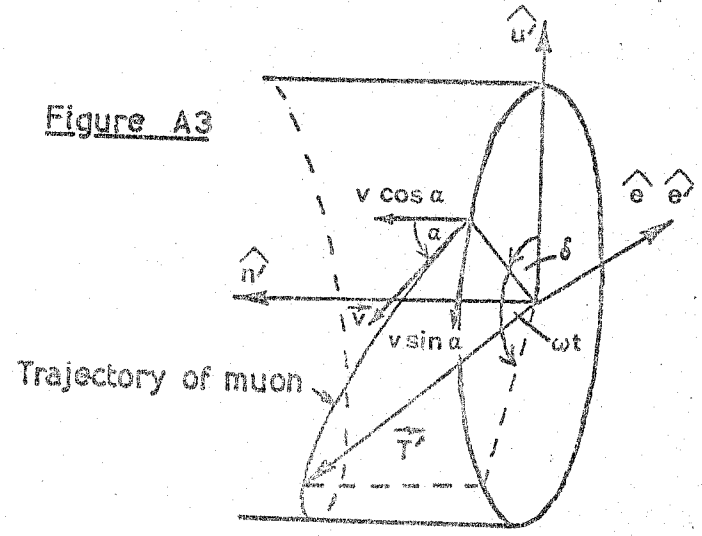

Appendix A

The Geomagnetic Deflection of Muons in EAS

It is assumed that at production a muon has a velocity $\vec{V}$ along the shower axis. The vector $\vec{V}$ may be written as follows: (see Figure A.1)

$$\vec{V} = -V(\cos\beta\hat{e} + \cos\gamma\hat{n} + \cos\theta\hat{u})$$

$$= -V(\sin\theta.\sin\phi\hat{e} + \sin\theta.\cos\phi\hat{n} + \cos\theta\hat{u})$$

where V is the absolute magnitude of $\vec{V}$.

Representing the earth's magnetic field by the vector $\vec{H}$, we may write:

$$\vec{H} = H(\cos i\,\hat{n} - \sin i\,\hat{u})$$

where H is the absolute magnitude of $\vec{H}$ and i is the angle of dip.

The unit vector $\hat{R}$ in the direction of the force acting on the muon at the point of production, due to its motion in the magnetic field, is given by:

$$\hat{R} = \frac{\vec{V} \times \vec{H}}{V.H.\sin\alpha}$$

$$= \frac{1}{\sin\alpha}\left[(\sin\theta.\cos\phi.\sin i + \cos\theta.\cos i)\hat{e} - (\sin\theta.\sin\phi.\sin i)\hat{n} - (\sin\theta.\sin\phi.\cos i)\hat{u}\right]$$

If the original coordinate system is rotated by an angle i about the unit vector $\hat{e}$ to obtain the primed coordinate system, then, assuming that energy loss is negligible, the path of the muon will be a helix along the surface of a cylinder of radius R, the axis of which lies along $\hat{n}'$, (see Figure A.2). R is given by the expression $R = p\sin\alpha/H.e$, where p is the momentum of the muon and e is the electronic charge. We may now write:

$$\vec{R} = R\hat{R} = \frac{R}{\sin\alpha}\left[(\sin\theta.\cos\phi.\sin i + \cos\theta.\cos i)\hat{e} - (\sin\theta.\sin\phi.\sin i)\hat{n} - (\sin\theta.\sin\phi.\cos i)\hat{u}\right]$$

Now, if the point of production is such that $\vec{R}$ makes an angle δ with $\hat{u}'$ (see Figure A.3) and thereafter the position vector of the muon, $\vec{r}'$, rotates

about $\hat{n}'$ with an angular velocity ω, then at time t after production the vector $\vec{T}'$ may be written:

$$\vec{T}' = -R\sin(\delta + \omega t)\hat{e} + V.t.\cos\alpha\,\hat{n}' + R.\cos(\delta + \omega t)\hat{u}'$$

Transforming to the unprimed system we obtain:

$$\vec{T} = -R.\sin(\delta + \omega t)\hat{e} + (R.\cos(\delta + \omega t).\sin i + V.t.\cos\alpha.\cos i)\hat{n}$$
$$+ (R.\cos(\delta + \omega t).\cos i - V.t.\cos\alpha.\sin i)\hat{u}$$

Now $\vec{Q} = \vec{R} + \vec{T}$

$$= R\left[\frac{\sin\theta.\cos\phi.\sin i + \cos\theta.\cos i}{\sin\alpha} - \sin(\delta + \omega t)\right]\hat{e}$$
$$+\left[R(\cos(\delta + \omega t).\sin i - \frac{\sin\theta.\sin\phi.\sin i}{\sin\alpha}) + V.t.\cos\alpha.\cos i\right]\hat{n}$$
$$+\left[R(\cos(\delta + \omega t).\cos i - \frac{\sin\theta.\sin\phi.\cos i}{\sin\alpha}) - V.t.\cos\alpha.\sin i\right]\hat{u}$$

Also, if the height of production is Z then we may write:

$$\vec{S} = Z.\tan\theta.\sin\phi\,\hat{e} + Z.\tan\theta.\cos\phi\,\hat{n} + Z\,\hat{u}$$

Thus:

$$\vec{P} = \vec{Q} + \vec{S}$$

$$= R\left[\left(\frac{\sin\theta.\cos\phi.\sin i + \cos\theta.\cos i}{\sin\alpha} - \sin(\delta + \omega t)\right) + Z.\tan\theta.\sin\phi\right]\hat{e}$$
$$+\left[R(\cos(\delta + \omega t).\sin i - \frac{\sin\theta.\sin\phi.\sin i}{\sin\alpha}) + V.t.\cos\alpha.\cos i + Z.\tan\theta.\cos\phi\right]\hat{n}$$
$$+\left[R(\cos(\delta + \omega t).\cos i - \frac{\sin\theta.\sin\phi.\cos i}{\sin\alpha}) - V.t.\cos\alpha.\sin i + Z\right]\hat{u}$$

The muon passes through the plane containing $\hat{n}$ and $\hat{e}$ when the $\hat{u}$ component of $\vec{P}$ is zero, that is:

$$R\left[\cos(\delta + \omega t).\cos i - \frac{\sin\theta.\sin\phi.\cos i}{\sin\alpha}\right] - V.t.\cos\alpha.\sin i + Z = 0.$$

This equation may be solved by an iterative method for t if δ and ω are known. δ may be found from the equation which gives the direction cosine of $\hat{R}$ with respect to e, namely:

$$\cos(\delta - \pi/2) = \sin\delta = \frac{\sin\theta \cdot \cos\phi \cdot \sin i + \cos\theta \cdot \cos i}{\sin\alpha}$$

Taking V to be equal to the speed of light then ω may be found from:

$$\omega = \frac{V \cdot \sin\alpha}{R}$$

Appendix B

The mean momentum of muons between production and observation

The relationship between atmospheric depth, t, in gm cm^{-2} and the height above sea level, Z, in km, of an isothermal atmosphere is assumed as, $t = t_o \exp - Z/Z_o$ (Wolfendale (1964), where Z_o is the "scale height" of the atmosphere and t_o the total atmospheric depth.

For a muon observed with a momentum p_o GeV/c produced at an altitude Z km above sea level in an air shower of zenith angle θ, the mean momentum between production and observation used in the work reported here is defined as:

$$\bar{p} = p_o + \frac{\varepsilon}{2 \cos\theta} \text{ to } \{1 - \exp - Z/Z_o\}$$

where ε is the mean specific loss in momentum due to ionisation in GeV/c/gm cm^{-2}.

Taking ε as 2.2×10^{-3} GeV/c/gm cm^{-2}, t_o as 1030 gm cm^{-2} and Z_o as 7.5 km we obtain

$$\bar{p} = p_o + \frac{2.23}{2 \cos\theta} \{1 - \exp (- Z/7.5)\}$$

Appendix C

The method of successive collisions used in the model

Let the probability that a proton of energy E_i will interact in the interval dx at a depth in the atmosphere x be $P(E_i,x)dx$. The probability, $N(E_i, x, E_\pi)\, dE_\pi\, dx$ of a pion being produced as a result of this interaction with an energy in the range E_π to $E_\pi + dE_\pi$ is then

$$N(E_i, x, E_\pi)dE_\pi\, dx = f(E_\pi, E_i).\ P(E_i, x).\ n_s(E_i)\, dE_\pi\, dx \quad \ldots\ldots\ldots\ldots C.1$$

where $n_s(E_i)$ is the multiplicity of secondary pions in a nucleon-nucleus collision of primary energy E_i and $f(E_\pi, E_i)dE_\pi$ is the differential energy spectrum of the pions produced.

The total probability, $\rho_1(E_\pi, x)\ \Delta E_\pi \Delta x$, of a pion having energy in the range E_π to $E_\pi + \Delta E_\pi$ being produced in depth interval x to $x + \Delta x$, in this first generation is:

$$\rho_1(E_\pi, x)\ \Delta E_\pi \Delta x = \sum_i N(E_i, x, E_\pi)\ \Delta E_\pi \Delta x \quad \ldots\ldots\ldots\ldots\ldots\ldots\ldots\ldots C.2$$

This may be represented by a matrix of probabilities for discrete values of E_π and x, say $E_{\pi k}$ and x_j, provided intervals of E_π and x are chosen which are small such that all functions are sensibly constant throughout the interval. Each element of this matrix represents the probability defined in Equation C.2 and is represented by ρ_{kj}.

If $n_s(E_{\pi k})$ now refers to pion-nucleus collisions and we define the functions $\rho_{\text{dec } k_{jj'}}$, as the probability that no decay will occur and $\rho_{\text{int } k_{jj'}}$ as the probability of an interaction occurring for a pion of energy $E_{\pi k}$ travelling from a depth x_j to a new depth $x_{j'}$, we may write for the probability, $\rho_{2\ k'j'}$ of the production of a second generation pion of energy $E_{\pi k'}$ at a depth $x_{j'}$ by a pion of the first generation interacting with a nucleus.

$$\rho_{2k'j'} = \sum_{k} \sum_{j} \rho_{1kj} \; p_{dec\ kjj'} \; p_{int\ kjj'} \; f(E_{\pi k'}, E_{\pi k}) \; n_s(E_{\pi k})$$

where $k' = 1, 2, \ldots \ldots k_{max} - 1$

and $j' = 1, 2, \ldots \ldots j_{max} - 1$

Similarly for the third generation

$$\rho_{3\ k'j'} = \sum_{k} \sum_{j} \rho_{2\ kj} \; p_{dec\ kjj'} \; p_{int\ kjj'} \; f(E_{\pi k'}, E_{\pi k}) \; n_s(E_{\pi k})$$

where $k' = 1, 2, \ldots \ldots k_{max} - 2$

and $j' = 1, 2, \ldots \ldots j_{max} - 2$

Generally for the nth generation

$$\rho_{n\ k'j'} = \sum_{k} \sum_{j} \rho_{(n-1)kj} \; p_{dec\ kjj'} \; p_{int\ kjj'} \; f(E_{\pi k'}, E_{\pi k}) \; n_s(E_{\pi k}) \ldots\ldots \text{C.3}$$

where $k' = 1, 2, \ldots \ldots (k_{max} + 1 - n)$

and $j' = 1, 2, \ldots \ldots (j_{max} + 1 - n)$

It will be apparent that the matrices p_{dec}, p_{int}, f and n_s need not be computed afresh for each generation so that the calculation of the pion height-energy matrix for a sufficient number of generations to follow the shower development to sea-level is simplified and computing time saved. In the development to sea-level the probability of more than thirteen generations is small and in the analytical model described in this thesis $\rho_{13\ k\ j}$ was taken as the height-energy distribution of pions from which the probability distribution in energy, height of origin and direction of muons were derived.

References

The following abbreviations are used for the proceedings of Cosmic Ray conferences:

Proc. Jaipur Conf. Proceedings of the 8th International Conference on Cosmic Rays, Jaipur, 1963 (Bombay: Commercial Printing Press, 1964).

Proc. London Conf. Proceedings of the 9th International Conference on Cosmic Rays, London, 1965 (London: Institute of Physics and the Physical Society, 1966).

Proc. Calgary Conf. Proceedings of the 10th International Conference on Cosmic Rays, Calgary, 1967 (Canadian Journal Phys., 46, No. 10, 1968).

Proc. Budapest Conf. Proceedings of the 11th International Conference on Cosmic Rays, Budapest, 1969 (Acta Physica Academiae Scientiarum Hungaricae 29, 1970).

Proc. Hobart Conf. Proceedings of the 12th International Conference on Cosmic Rays, Hobart, 1971.

ABRAHAM, F., GIERULA, J., LEVI SETTI, R., RYBZCKI, K., TSAO, C.H., WOLTER, W., FRICKEN, R.L., and HUGGETT, R.W., 1967, Phys. Rev., 159, 1110.

AKIMOV, V.V., GRIGOROV, N.L., MAMANTOVA, N.L., NESTEROV, V.E., PROKHIN, V.L., RAPOPORT, I.D., and SAVENKO, I.A., 1969, Proc. Budapest Conf., 3, 211.

ALAKOV, A.V., BOLOTOV, V.N., DEVISHEV, M.I., KLIMANOVA, L.F., and SHEMELEVA, A.P., 1967, Proc. Calgary Conf., S694.

AMATI,D., STRANGHELLINI, A., and FUBINI, S., 1962, Nuovo Cimento, 26, 896.

ANDREWS, D., EVANS, A.C., REID, R.J.O., TENNENT, R.M., WATSON, A.A., and WILSON, J.G., 1969(a), Proc. Budapest Conf., 3, 343.

ANDREWS, D., EVANS, A.C., HOLLOWS, J.D., REID, R.J.O., WATSON, A.A., and WILSON, J.G., 1969(b), Proc. Budapest Conf., 3, 349.

ANDREWS, D., EDGE, D.M., EVANS, A.C., REID, R.J.O., TENNENT, R.M., WATSON, A.A., WILSON, J.G., and WRAY, A.M., 1971, Proc. Hobart Conf., EAS 17.

ANDRONIKASHVILI, E.L., CHIKOVANI, G.E., GARIBASHVILI, D.I., GABUNIA, L.L., KAKAURIDZE, D.B., KOTLYAREVSKI, D.M., MANJAVIDZE, Z. SH., ROINISHVILI, N.N., RAZDOLSKAYA, L.A., and SHERER, E.N., 1967, Proc. Calgary Conf., S689.

APPLETON, E.V., 1934, Nature 133, 793.

AURELA, A.M., and WOLFENDALE, A.W., 1967, Ann. Acad. Sci. Fennicae, Series A, VI, 227.

AZIMOV, S.A., 1964, Bull. Acad. of Sci. U.S.S.R., 28, 11, 1664.

BAKICH, A.M., MELLEY, D., McCUSKER, C.B.A., NELSON, D., PEAK, L.S., RATHGEBER, M.H., and WINN, MM., 1967, Proc. Calgary Conf., S30.

BARNAVELI, T.T., BINILASVILI, M.F., GRUBELASHVILI, G.A., JAVRISHVILI, A.K., KAZAROV, R.E., KURIOZE, R.V., and KHALDEEVA, I.V., 1964, Proc. Jaipur Conf., 4, 273.

BARRETT, P.H., BOLLINGER, L.M., COCCONI, G., EISENBERG, Y., and GREISEN, K., 1952, Rev. Mod. Phys., 24, 133.

BELENKY, S. Z., and LANDAU, L.D., 1954, Uspekhi Fizicheskikh Nauk, 56, 309.

BENNETT, S., and GREISEN, K., 1961, Phys. Rev., 124, 1982.

BHABHA, H.J., and HEITLER, W., 1937, Proc. Roy. Soc., A159, 432.

BLAKE, P.R., FERGUSON, H., NASH, W.F., and THOMAS, D.W.E., 1971, Proc. Hobart Conf., EAS 32.

BÖHM, E., BÜSCHER, W., FRITZE, R., ROOSE, U.J., SAMORSKI, M., STAUBERT, R., and TRÜMPER, J., 1967, Proc. Calgary Conf., S50.

BOLOTOV, V.N., DEVISHEV, M.I., KLIMANOVA, L.F., and SHMELEVA, A.P., 1965, Proc. London Conf., 2, 863.

BOWEN, W.A., MAPLE, E., and SINGER, S.F., 1950, J. Geophys. Res., 115.

BOZOKI, G., FENYVES, E., CHRISTOV, C., AHABABIAN, N., BETEV, B., and KAVLAKOV, S., 1967, Proc. Calgary Conf. S742.

BRADT, H.V., and RAPPAPORT, S.A., 1967, Phys. Rev., 164, 1567.

BROWNLEE, R.G., CHAPMAN, G.J., DAVID, S.A., FISHER, A.J., HORTON, L., GODREVICH, L., KOHN, P.E., McCUSKER, C.B.A., OUTHRED, A., PARKINSON, A.F., PEAK, L.S., RATHGEBER, M.H., RYAN, M.J., and WINN, M.M., 1969(a), Proc. Budapest Conf., 3, 377.

BROWNLEE, R.G., DAVID, S.A., FISHER, A.J., HORTON, L., GOOREVICH, L., KOHN, P.C., McCUSKER, C.B.A., OUTHRED, A., PAGE, D.E., PARKINSON, A.F., PEAK, L.S., RATHGEBER, M.H., REID, R.J.O., RYAN, M.J., and WINN, M.M., 1969(b), Proc. Budapest Conf., 3, 383.

BURBIDGE, E.M., and BURBIDGE, G.R., 1965, Proc. London Conf., 1, 92.

CIOK, P., COQHEN, T., GIERULA, J., HOLYNSKI, R., JURAK, A., MIESOWICZ, M., SANIEWSKI, T., and STANISZ, O., 1958, Nuovo Cimento, 8, 166.

CLARK, G., EARL, J., KRAUSHAAR, W., LINSLEY, J., ROSSI, B., and SHERB, F., 1958, Nuovo Cimento, 8, 623.

COCCONI, G., KOESTER, L.G., and PERKINS, D.H., 1961, (Unpublished: Lawrence Radiation Lab. Seminar 28, part 2, UCID - 1444).

COLGATE, S.A., 1966, Proc. London Conf., 1, 112.

CONVERSI, M., and GOZZINI, A., 1955, Nuovo Cimento, 2, 189.

COXELL, H., and WOLFENDALE, A.W., 1960, Proc. Phys. Soc., 75, 378.

de BEER, J.F., CRANSHAW, T.E., and PARHAM, A.G., 1962, Phil. Mag., 7, 499.

de BEER, J.F., HOLYOAK, B., WDOWCZYK, J., and WOLFENDALE, A.W., 1966, Proc. Phys. Soc., 89, 567.

de BEER, J.F., HOLYOAK, B., ODA, H., WDOWCZYK, J., and WOLFENDALE, A.W., 1967, Proc. Calgary Conf., S737.

de BEER, J.F., HOLYOAK, B., ODA, H., WDOWCZYK, J., and WOLFENDALE, A.W., 1968, Proc. Phys. Soc., Ser. 2, 1, 72.

de BEER, J.F., de VILLIERS, E.J., KEINECKE, J.P.L., and VEWTER , F.A., 1969, Proc. Budapest Conf., EAS 56.

DIGGORY, I.S., EARNSHAW, J.C., HOOK, J.R., and TURVER, K.E., 1971, Proc. Hobart Conf., TECH 11.

DOVZHENKO, O.I., NELEPO, B.A., NIKOLSKII, S.I., 1957, Jor. Exp. Teor. Phiz., 32, 463.

EARNSHAW, J.C., ORFORD, K.J., ROCHESTER, G.D., SOMOGYI, A.J., TURVER, K.E., and WALTON, A.B., 1967, Proc. Phys. Soc., 90, 91.

EARNSHAW, J.C., 1968, Ph.D. Thesis, University of Durham.

EARNSHAW, J.C., MACHIN, A.C., ORFORD, K.J., PICKERSGILL, D.R., TURVER, K.E., 1971(a), Proc. Hobart Conf. EAS 44.

EARNSHAW, J.C., MACHIN, A.C., ORFORD, K.J., PICKERSGILL, D.R., and TURVER, K.E., 1971(b), Proc. Hobart Conf., EAS 45.

ELBERT, J.W., ERWIN, A.R., MIKAMO, S., REEDER, D., CHEN, Y.Y., WALKER, W.D., and WEINBERG, A., 1968, Phys. Rev. Letters, 20, 124.

EYGES, L., 1948, Phys. Rev., 74, 1534.

FEINBERG, E.L., and IVANENKO, I.P., 1969, Proc. Budapest Conf., Rapporteur paper.

FELTEN, J.E., and MORRISON, P., 1966, Astrophys. J., 146, 686.

FERMI, E., 1950, Prog. Theor. Phys., 5, 570.

FEYNMANN, R.P., 1969, Phys. Rev. Letters, 23, 1415.

FOWLER, P.H., and PERKINS, D.H., 1964, Proc. Roy. Soc., A278, 401.

GIERULA, J., and KRZYWDZINSKI, S., 1968, Nuovo Cimento, A55, 370.

GINZBURG, V.L., and SYROVATSKII, S.I., 1964, "The Origin of Cosmic Rays", (Oxford: Pergamon Press, 1964).

GOLD, T., 1968, Nature, 218, 731.

GOLD, T., 1969, Nature, 221, 25.

GREISEN, K., 1960, Ann. Rev. Nucl. Sci., 10,63.

GREISEN, K., 1966, Phys. Rev. Letters, 16, 748.

GRIEDER, P.K.F., 1969, Proc. Budapest Conf., EAS 43.

GRIEDER, P.K.F., 1971(a), Proc. Hobart Conf., EAS 11.

GRIEDER, P.K.F., 1971(b), Proc. Hobart Conf., HE 50.

GRIGOROV, N.L., SOBINYAKOV, V.A., TRETYAKOVA, Ch. A., SHESTAPEROV, V.Ya., BABAIAN, Kh.P., and DULYAN, G.G., 1965, Proc. London Conf., 2, 860.

GURWITZ, S.A., DAIBOG, E.I., and ROSENTAL, I.L., 1971, Proc. Hobart Conf., HE27.

HARA, T., KAWAGUCHI, S., MIKAMO, S., NAGANO, M., SUGA, K., TANAHASHI, G., UCHINO, K., and AKIYAMA, H., 1969, Proc. Budapest Conf., 3, 361.

HEISENBERG, W., 1952, Zeit. Phys., 133, 65.

HILLAS, A.M., 1965, Proc. London Conf., 2, 758.

HILLAS, A.M., HOLLOWS, J.D., HUNTER, H.W., and MARSDEN, D.J., 1969, Proc. Budapest Conf., 3, 533.

HILLAS, A.M., HOLLOWS, J.D., HUNTER, J.W., and MARSDEN, D.J., 1971, Proc. Hobart Conf., EAS 19.

HOLYOAK, B., 1967, Ph.D. Thesis, University of Durham.

JONES, L.W., BUSSIAN, A.E., de MUSTER, G.D., LOO, B.W., LYON, D.E., RAMANA MURTHY, P.V., ROTH, R.F., VISHWANATH, P.R., ERICKSON, K.N., LEARNED, J.G., REEDER, D.D., WILKES, J., CORK, B., and MILLS, R.E., 1971, Proc. Hobart Conf., 3, 1194.

KAMIYA, Y., 1962, J. Phys. Soc., Japan, 17, Supp. A-III, 315.

KANEKO, T., YOKOYAMA, C., AGUIRRE, C., TREPP, A., MEJIA, G.R., MURAKAMI, K., KAMATA, K., TOYODA, Y., MAEDA, T., SUGA, K., UCHINO, K., LAPOINTE, M., and MacKEOWN, P.K., 1971, Proc. Hobart Conf., EAS 2.

KAYE, G.W.C., and LABY, T.H., 1960, "Tables of Physical and Chemical Constants", (London: Longmans Green and Co. Ltd.).

KAZUNO, M., 1967, Ph.D. Thesis, Institute of Advanced Studies, Dublin.

KHRENOV, B.A., 1962, Soviet Physics (JETP), 14, 1001.

KOSHIBA, M., NOZAKI, T., TOTSUKA, Y., and YAMADA, S., 1967, Proc. Calgary Conf., S671.

KRAUSHAAR, W.L., and MARKS, L., 1954, Phys. Rev., 93, 326.

KRIEGER, A.S., and BRADT, H.V., 1969, Phys. Rev., 185, 1629.

KRISTIANSEN, G.B., 1958, Nuovo Cimento, 8, Ser. 10, 598.

LANDAU, L.D., 1953, Dok. Akad. Nauk. SSSR., 12, 51.

LAPIKENS, J., MARTIN, R., REID, R.J.O., ROBINSON, P.D., TENNENT, R.M., WATSON, A.A., and WILSON, J.G., 1971, Proc. Hobart Conf., OG88.

MACHIN, A.C., ORFORD, K.J., PICKERSGILL, D.R., and TURVER, K.E., 1969, Proc. Budapest Conf., 3, 579.

MACHIN, A.C., 1972, Ph.D. Thesis, University of Durham.

MATANO, T., MIURA, I., NAGANO, M., ODA, M., SHIBATA, S., TANAKA, Y., TANAHASHI, G.E., and HASEGAWA, H., 1963, Proc. Jaipur Conf., 4, 129.

MATANO, T., NAGANO, M., SHIBATA, K., SUGA, K., TANAHASHI, G., and HASEGAWA, H., 1967, Proc. Calgary Conf., S56.

McCUSKER, C.B.A., PEAK, L.S., and RATHGEBER, M.H., 1969, Phys. Rev., 177, 1902.

MIYAKE, S., HINOSTANI, K., ITO, N., KINO, S., SASAKI, H., YOSHII, H., SAKUYAMA, H., and KATO, E., 1967, Proc. Calgary Conf., S25.

MURTHY, G.T., SIVAPRASED, K. SRINIVASA RAO, M.V., TONWAR, S.C., VATCHA, R.H., and VISHWANATH, P.R., 1967, Proc. Calgary Conf., S147.

ODA, M., 1957, Nuovo Cimento, 5, 615.

OREN, Y., 1959, Bull. Res. Coun. Israel, 8F, 103.

ORFORD, K.J., TURVER, K.E., and WALTON, A.B., 1967, Proc. Calgary Conf., S122.

ORFORD, K.J., 1968, Ph.D. Thesis, University of Durham.

ORFORD, K.J., and TURVER, K.E., 1969, Proc. Budapest Conf., 3, 585.

OSTRIKER, J.P., and GUNN, J.E., 1969, Astrophys. J., 157, 1395.

PAL, Y., and PETERS, B., 1964, Mat. Fys. Medd. Dan. Vid. Selsk., 33, No. 15.

PARKER, E.N., 1969, Space Sci. Rev., 9, 651.

PETERS, B., 1962, Proc. Conf. High Energy Phys., (CERN), 623.

PETERS, B., 1966, CERN Report 66-22.

PETERS, B., 1970, Preprint Manuscript for Encyclopaedia Universalis.

RAND, R.E., 1962, Nuc. Inst. and Methods, 17, 65.

RAPPAPORT, S.A., and BRADT, H.V., 1969, Phys. Rev. Lett., 22, 960.

RASTIN, B.C., 1964, Ph.D. Thesis, University of Nottingham.

ROCHESTER, G.D., SOMOGYI, A.J., TURVER, K.E., and WALTON, A.B., 1965, Proc. London Conf., 2, 765.

ROSEN, L.C., 1969, Astrophys. Space Sci., 1182.

ROSSI, B., 1952, "High Energy Particles", (Prentice Hall Inc.).

RUNCORN, S.K., 1956, Handbuch der Physik, 67, 515.

SALZMAN, F., and SALZMAN, G., 1960, Phys. Rev. 120, 599.

SCHMIDT, M., 1967, Astrophys. J., 149, L39.

SHAPIRO, M.M., 1962, Science, 135, 175.

SOMOGYI, A.J., 1966, Ann. Physik, 17, 221.

STERNHEIMER, R.M.1959, Phys. Rev., 115, 137.

STUBBS, R.J., and BREARE, J.M., 1969, Proc. Budapest Conf., 4, 473.

SUGA, K., SHIBATA, S., MIKAMO, S., TOYODA, Y., MURAKAMI, K., LaPOINTE, M., KAMATA, K., and DOMINGO, V., 1969, Proc. Budapest Conf., 3, 423.

SURI, A.N., 1966, Ph.D. Thesis, University of Leeds.

TENNENT, R.M., 1967, Proc. Phys. Soc., 92, 622.

THOMPSON, M.G., TURNER, M.J.L., WOLFENDALE, A.W., and WDOWCZYK, J., 1969, Proc. Budapest Conf., 3, 615.

TONWAR, S.C., and SREEKANTAN, B.V., 1971, Proc. Hobart Conf., HE14.

TRÜMPER, J., 1969, Proc. Budapest Conf., Rapporteur paper.

WALTON, A.B., 1966, M.Sc. Thesis, University of Durham.

WANG, C.P., 1969, Phys. Rev., 180, 1463.

WILSON, J.G., ALLAN, H.R., LILLICRAP, S.C., REID, R.J.O., and TURVER, K.E., 1963, Proc. Jaipur Conf., 4, 27.

WINN, M.M., WAND, R.H., ULRICHS, J., RATHGEBER, M.H., POOLE, P.C., NELSON, D., McCUSKER, C.B.A., JAUNCEY, D.L., CRAWFORD, D.F., and BRAY, A.D., 1965, Nuovo Cimento, 36, 701.

YAMEDA, S., and KOSHIBA, M., 1967, Proc. Calgary Conf., S671.

YODH, G.B., and PAL, Y., 1971, Proc. Hobart Conf., HE20.

ACKNOWLEDGEMENTS

I wish to express my deep thanks to Professor G. D. Rochester, F.R.S., for providing the facilities which made this study possible and for his unfailing interest in the work. It is also a pleasure to record my gratitude to my supervisor, Dr. K. E. Turver, for his continual encouragement, advice and guidance.

Professor J. G. Wilson and his colleagues in the University of Leeds are thanked for their cooperation and for the provision of the results of their EAS analysis.

My colleagues, Dr. A. C. Machin, Dr. K. J. Orford and Dr. J. C. Earnshaw have been very helpful in the collection and analysis of data. This help is gratefully acknowledged.

I am indebted to those many members of the technical staff of the Physics Department of the University of Durham who willingly and generously gave me help and advice on countless occasions. In particular, Miss A. M. Bevils is thanked for her help in track reconstruction and in the preparation of this thesis. Special thanks are also due to Mr. W. Leslie and Mr. H. Davison for their help in construction work.

Finally, for her patience and perception, Mrs. J. Moore, who typed this thesis, is sincerely thanked.